LBL-10021

Lawrence Berkeley Laboratory
UNIVERSITY OF CALIFORNIA

Materials & Molecular
Research Division

LASER INDUCED FLUORESCENCE OF TRAPPED MOLECULAR IONS

Frederick Joseph Grieman
(Ph. D. thesis)

October 1979

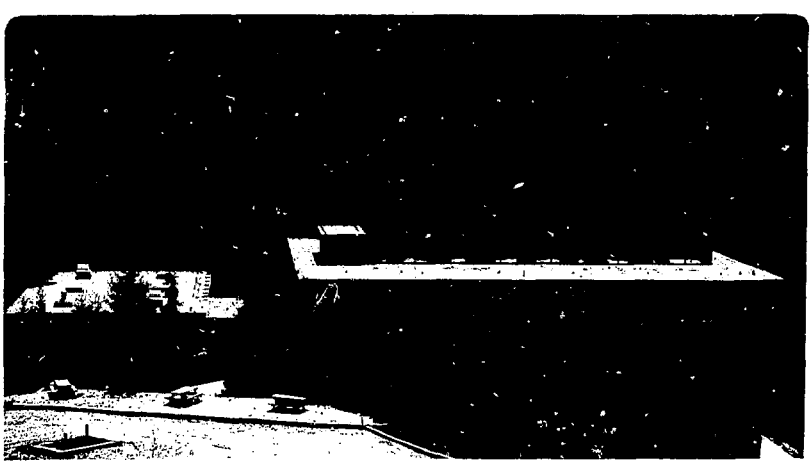

Prepared for the U.S. Department of Energy under Contract W-7405-ENG-48

LASER INDUCED FLUORESCENCE OF TRAPPED MOLECULAR IONS

Frederick Joseph Grieman

Lawrence Berkeley Laboratory
University of California
Berkeley, California

This work was prepared with the support of the
U. S. Department of Energy under Contract W-7405-ENG-48.

Laser Induced Fluorescence of Trapped Molecular Ions

Frederick Joseph Grieman

Abstract

An experimental apparatus for obtaining the optical spectra of molecular ions is described. The experimental technique includes the use of three dimensional ion trapping, laser induced fluorescence, and gated photon counting methods.

The ions, which are produced by electron impact, are confined in a radio-frequency quadrupole ion trap of cylindrical design. Because the quadrupole ion trap allows mass selection of the molecular ion desired for study, the analysis of the spectra obtained is greatly simplified. The ion trap also confines the ions to a region easily probed by a laser beam.

In the laser induced fluorescence technique employed in this experiment the ions, after being stored and mass selected, are interrogated by an intense, narrow bandwidth dye laser pulse ten nanoseconds in duration. Any subsequent fluorescence is not dispersed, but is detected by a bare photomultiplier tube. A gated photon counting system is utilized to increase the signal-to-noise ratio. The signal is further enhanced by signal averaging which is accomplished using an on-line minicomputer. The computer also controls the progress of the experiment and normalizes the fluorescence signal with respect to laser power and ion density which are

monitored throughout the experiment. The result is a fluorescence excitation spectrum which in many instances contains the same information as an absorption spectrum.

The spectra of the molecular ions studied thus far by this experimental technique are presented. The first two systems studied, the $^2\Sigma_u^+ - {}^2\Sigma_g^+$ transition of N_2^+ and the $^2\Pi_i - {}^2\Sigma_g^+$ transition of CO^+, were used to determine many of the capabilities and characteristics of our apparatus. The $^2\Sigma_u^+$ state of N_2^+ has a short radiative lifetime which served to test our experiment in the nanosecond time regime. The $^2\Pi_i$ state of CO^+, on the other hand, has a long radiative lifetime and was used to test the operation of our experiment when dealing with low signal levels.

The third spectrum obtained was the $^2A_2'' - {}^2E''$ band system of the 1,3,5-trifluorobenzene cation. This spectrum provides an excellent example of how a laser induced fluorescence spectrum can yield information which supplements that obtained from emission spectroscopy. A Jahn-Teller interaction also occurs in the degenerate ground electronic state and its effect on the observed spectrum is discussed.

The final spectrum observed is the $^2\Pi - {}^2\Pi$ band system of the BrCN cation. The spectrum was found to be very complicated allowing only approximate values for the bending vibrational frequency, the C-Br stretching frequency, and the spin-orbit splitting constant to be determined. The complications observed are believed to be due to a Fermi resonance

interaction. The plausibility of such an interaction occurring and its effect on the spectrum is discussed.

ACKNOWLEDGEMENTS

There are a number of people to whom I owe a great deal of thanks for their help, guidance, and encouragement during my years as a graduate student. Above all, I extend my greatest appreciation to Professor Bruce H. Mahan under whose direction this research was carried out. From the original conception of this experiment to its completion, his creative ideas and scientific intuition were invaluable. His suggestions and advice during the course of this work, while necessary for its successful completion, still allowed me to make my own decisions and, therefore, to develop my own independence as a researcher.

Next in line for thanks are the members, both past and present, of the "awesome" Mahan group (recently christened as such by the newest member of our group, Tom Turner). I wish to thank each of these guys for their contributions not only in the laboratory, but also in real life and on the playing field. Steve Hansen, who was always easy to talk with, would often clear up my confused thoughts in a few minutes of discussion. Tony O'Keefe, who also worked on the project presented in this thesis, contributed numerous ideas which were instrumental to its success. His constant energy and eagerness to "get the job done" will always be remembered. I would also like to thank Richard Davis for his help in the design and construction of this experiment and Ralph Terkowitz who originally began the work on this apparatus. Learning how

to interface the computer to the experiment would have been much more difficult without the help of Jim Kleckner.

The bulk of the experimental apparatus construction was performed by Frank Lopez in the Chemistry department machine shop. His skill and enthusiasm made it fun to work with him and also taught me a great deal about machining. Tom Merrick, who built the computer interface was very helpful in its design and in dealing with problems associated with it. Phil Eggers was of tremendous help in the electrical maintenance and problem solving in the early stages of this work.

I would next like to thank Professor John S. Winn who read my entire thesis and whose comments and help made the whole process of finishing much easier. The combination of his research group with ours for group discussions was a very valuable and pleasurable experience. I would also like to acknowledge Professors Herbert L. Strauss and Yuan T. Lee for their consultation.

Cordelle Yoder who skillfully typed my entire thesis (both the rough draft and final version) was always ready to answer any of my questions about procedural matters. Her competence and cheerfulness made it a real pleasure to work with her. I would also like to thank Nancy Monroe for her excellent drafting of many of the drawings in this thesis.

Of course, I would be nowhere without the support of my family. The encouragement offered by my parents in all aspects of my life has given me the confidence necessary to proceed onward. Finally, I would like to express my deepest

appreciation and love to my wife Janet. Not only did she contribute to the completion of this thesis (the drawings in Chapter V are hers), but more importantly her love and encouragement have always given me the support I so desperately need.

TABLE OF CONTENTS

TABLE OF CONTENTS (continued)

TABLE OF CONTENTS (continued)

TABLE OF CONTENTS (continued)

LIST OF TABLES

LIST OF FIGURES

LIST OF FIGURES (continued)

CHAPTER I

INTRODUCTION

The underlying theme of the research performed by the Mahan group in the past and at present is the understanding of chemical reactions on a microscopic level. To accomplish this goal, studies of ion-molecule reactions under single collision conditions have been carried out using various beam techniques. In order to interpret and explain many of these reactions, information concerning the available electronic states, the relative energies of these states, and the geometry of the molecules involved in the reactions is required.

Optical and ultraviolet spectroscopy have been very instrumental in obtaining this information for a great many molecules. However, these spectroscopic techniques have been primarily limited to the study of neutral species. The reason for this is the difficulty in attaining a sufficient concentration of molecular ions in a chemically uncomplicated environment. The motivation behind the research effort presented in this thesis was to overcome this problem and develop a reliable and widely applicable experimental technique for obtaining optical spectra of molecular ions. With such a method, a large amount of data for several molecular ions could be procured and eventually used to help interpret, systemize, and predict ion-molecule reactions. In addition to providing quantum mechanical and structural information

about molecular ions, a knowledge of their electronic structure can provide a greater understanding of chemical bonding in their neutral counterparts as well.

The primary techniques employed to obtain spectra of molecular ions up to 1971 were outlined by Herzberg in a Faraday Lecture.[1] The techniques included electric and flash discharges, electron impact, flash radiolysis, photoionization, and photoelectron spectroscopy. Most of these methods rely on analysis of emission spectra to identify the fluorescing species. Because the violent nature by which these techniques produce the ions leads to complicated situations, the identification can be quite ambiguous. Several different excited species can be produced by the ion creation mechanism invoked and by subsequent reactions making assignment and identification of the emission lines produced difficult. In photoelectron spectroscopy, this complication usually does not exist. However, because it entails measurement of the kinetic energy of electrons emitted from a neutral gas irradiated by monochromatic light, the resolution is poorer than that usually obtained in optical spectroscopy.

Since 1971, several research efforts have been put forth to increase the amount of molecular ion spectra. Lew has used a large hot cathode discharge source to obtain the relatively weak emission spectrum of H_2O^+.[2] The research groups of both Maier[3] and Leach[4] have used controlled electron impact techniques to observe the emission spectra of a wide variety of molecular ions.

Many new experimental techniques have also been developed which try to avoid the complications inherent in the methods mentioned above. Carrington's technique depends on the variance of reaction cross section with respect to the internal state of the molecular ion.[5] The measurement of photofragment ions produced by irradiation of a fast ion beam with laser light has been developed by Moseley and co-workers[6] into a method which has yielded high resolution spectra for several ions. In both of these experimental systems, mass spectrometric techniques are used to isolate and identify the molecular ion being studied. However, both of these methods also involve indirect detection of light absorption which somewhat limits their applicability.

Other research groups[7-10] have used the laser induced fluorescence technique[11] (LIF) with varying degrees of success to obtain fluorescence excitation spectra of molecular ions. Miller, Bondybey, and co-workers use LIF to excite ions created by rare gas metastables in a flowing after glow[7] or ions created in Ne and Ar matrices[8] to obtain their spectra. In both of these methods, the molecular ions are in thermal equilibrium with their environment resulting in the investigation of a relaxed ion sample. The only means by which the fluorescing species is identified in these methods is by spectroscopic analysis and comparison with results from photoelectron and emission spectra. In cases where identification is not straight-forward, mass selection of the desired ion (as was utilized by Carrington and Moseley) simplifies matters.

Brown et al.[10] have recently accomplished this by obtaining the CO^+ $\tilde{A}$-$\tilde{X}$ spectrum by laser induced fluorescence of a mass selected ion beam.

The experimental apparatus we developed also combines the techniques of mass selection and laser induced fluorescence. However, the isolation and mass selection of our molecular ions are accomplished with the use of a three dimensional ion trapping technique rather than with a two dimensional quadrupole mass filter as is used in ion beams. A considerable amount of research concerning the theory and characteristics of three dimensional trapping has been carried out over the last twenty years.[12] From this wealth of information the best trapping configuration and operating conditions for our purposes was determined. The resulting cylindrical radio-frequency (r.f.) ion trap used in the experiments described in this thesis presented several advantages. In addition to mass selection, a relatively high concentration of ions can be obtained. Another advantage is that the ion sample is confined to a small localized region (~10 ml) which can be conveniently probed by a laser beam.

The concentration of ions produced is still small enough to require a sensitive detection technique. Laser induced fluorescence was selected for several reasons. Zare and co-workers[11,13] have already demonstrated that this technique allows spectroscopic measurement of a small sample concentration in the case of a neutral molecule. In this method, a narrowband light source (the laser) excites the molecules

in the sample while a broadband detection system measures any subsequent fluorescence photons over a wide range of energies. Because the resulting signal consists of a small number of fluorescence photons mixed with some background radiation, highly developed photon counting and signal averaging techniques are employed. The result is a fluorescence excitation spectrum which in many instances contains information very similar to that of an absorption spectrum. Because this information is frequently quite different from that obtained in an emission spectrum, it can be used to supplement that obtained for an ion already observed in emission. The wavelength region available in our experiment is limited only by the lasers and detectors available. The entire visible region is presently accessible and with the continued research efforts in the laser field, tunable ultraviolet lasers will surely be developed in the near future.

In the next chapter, a description of the ion spectroscopy apparatus developed in our laboratory is given. The different components involved in the ion trapping, laser excitation, and fluorescence detection will be described separately. A discussion of the experimental timing organization and the computer interfacing is then presented to demonstrate how these different components are united together to form one experiment.

Following the experimental apparatus description, the results which we have obtained thus far are given. The first two systems studied, the $\tilde{B}$-$\tilde{X}$ transition of N_2^+ and the $\tilde{A}$-$\tilde{X}$

transition of CO^+, were used to determine many of the capabilities and characteristics of our apparatus. The $\tilde{B}$ state of N_2^+ has a short radiative lifetime (~60 nanoseconds) and served to test our experiment in the nanosecond time regime. On the other hand, the $\tilde{A}$ state of CO^+ has a relatively long radiative lifetime (~3 microseconds) and was used to test the operation of our experiment when dealing with low counting rates. For both of these systems, rotational structure was observed which allowed the determination of our wavelength resolution.

The next fluorescence excitation spectrum we obtained was the $\tilde{B}\ ^2A_2'' - \tilde{X}\ ^2E''$ band system of the 1,3,5-trifuloro-benzene cation. This transition has been observed in emission spectroscopy[3b,4b] and by another laser induced fluorescence technique.[7] A comparison of these results with those that we have obtained is given to demonstrate how our technique can yield information which will supplement that obtained by other methods. The degenerate ground electronic state is split by a Jahn-Teller interaction. Its effect on the spectrum we observe is also discussed.

The final spectrum described in this thesis is the $\tilde{B}\ ^2\Pi - \tilde{X}\ ^2\Sigma$ band system of $BrCN^+$. An approximation to the Br-C stretching frequency, the bending frequency and the spin-orbit coupling constant of the $\tilde{B}$ state of $BrCN^+$ were obtained. Only an approximation to these values is possible because of a vibrational perturbation observed in the spectrum believed to be due to a Fermi resonance between the Br-C stretch and

even quanta of the bending frequency. Although no definite proof can be given, the probability of such a resonance effect occurring is discussed.

The systems described in this thesis are hoped to be just the beginning of many to be studied by this experimental technique. The mass selection aspect offers an advantage over many other experimental techniques and will be especially useful in the study of fragment ions which must be isolated from other ionic species. The laser induced fluorescence technique, as mentioned before, allows one to obtain spectra which can provide information supplemental to that obtained for molecular ions already observed in emission. The combination of the methods of ion trapping and LIF yields what we feel to be a versatile experimental technique for the study of molecular ion optical spectra.

References, Introduction

1. G. Herzberg, Quarterly Review Chem. Society, 25, 201 (1971).

2. H. Lew, Can. J. Phys., 54, 2028 (1976).

3. a) J. P. Maier, O. Marthaler, and F. Thommen, Chem. Phys. Lett., 60, 193 (1979) and references therein; M. Allan and J. P. Maier, Chem. Phys. Lett., 34, 442 (1975); M. Allan and J. P. Maier, Chem. Phys. Lett., 43, 94 (1976); M. Allan, J. P. Maier, and O. Marthaler, Chem. Phys., 26, 131 (1977); J. P. Maier and O. Marthaler, Chem. Phys., 32, 419 (1978); M. Allan, J. P. Maier, O. Marthaler, and J. Stadelmann, J. Chem. Phys., 70, 5271 (1979).

   b) M. Allan and J. P. Maier, Chem. Phys. Lett., 41, 231 (1976).

4. a) C. Cossart-Magos, D. Cossart, and S. Leach, J. Chem. Phys., 69, 4313 (1978); M. Horani, S. Leach, and J. Rostas, J. Chem. Phys. 63, 1015 (1966); J. H. D. Eland, M. Devoret, and S. Leach, Chem. Phys. Lett., 43, 96 (1976).

   b) C. Cossart-Magos, D. Cossart, and S. Leach, Molec. Phys., 37, 793 (1979).

5. A. Carrington, D. R. J. Milverton, and P. J. Sarre, Mol. Phys. 35, 1505; A. Carrington, D. R. J. Milverton, P. G. Roberts, and P. J. Sarre, J. Chem. Phys., 68, 5659 (1978).

6. For example: J. T. Moseley, P. C. Cosby, and J. R. Peterson, J. Chem. Phys., 65, 2512 (1976); A. Tabche-Fouhaille, J. Durup, J. T. Moseley, J. B. Ozenne, C. Pernot, and M. Tadjeddine, Chem. Phys., 17, 81 (1976); J. T. Moseley, M. Tadjeddine, J. Durup, J. B. Ozenne, C. Pernot, and A. Tabche-Fouhaille, Phys. Rev. Lett., 37, 891 (1976); J. T. Moseley, R. P. Saxon, B. A. Huber, P. C. Cosby, R. Abouaf, and M. Tadjeddine, J. Chem. Phys., 67, 1695 (1977); R. Abouaf, B. A. Huber, P. C. Cosby, R. P. Saxon, and J. T. Moseley, J. Chem. Phys., 68, 2406 (1978).

7. T. A. Miller, V. E. Bondybey, and J. H. English, J. Chem. Phys., 70, 2919 (1979); V. E. Bondybey and T. A. Miller, J. Chem. Phys., 69, 3597 (1978); T. A. Miller and V. E. Bondybey, Chem. Phys. Lett., 58, 454 (1978); V. E. Bondybey and T. A. Miller, J. Chem. Phys., 70, 138 (1979); V. E. Bondybey and T. A. Miller, J. Chem. Phys., 69, 3597 (1978); V. E. Bondybey and T. A. Miller, J. Chem. Phys., 67, 1790 (1977).

8. V. E. Bondybey, J. H. English, and T. A. Miller, J. Am. Chem. Soc., 100, 5251 (1978); V. E. Bondybey, J. H. English, and T. A. Miller, J. Chem. Phys., 70, 1621 (1979); V. E. Bondybey, J. H. English, and T. A. Miller, J. Chem. Phys., 70, 1765 (1979); V. E. Bondybey, T. A. Miller, and J. H. English, J. Am. Chem. Soc., 101, 1248 (1979).

9. P. C. Engelking and A. L. Smith, Chem. Phys. Lett., 36, 21 (1975); J. Allison, T. Kondow and R. N. Zare, Chem. Phys. Lett., 64, 202 (1979).

10. R. D. Brown, P. D. Godfrey, J. G. Crofts, Z. Ninkov, and S. Vaccani, Chem. Phys. Lett., 62, 195 (1979).

11. R. N. Zare and P. J. Dagdigian, Science, 185, 739 (1974).

12. See Chapter II, Section C of this thesis.

13. A. Schultz, H. W. Cruse, and R. N. Zare, J. Chem. Phys., 57, 1354 (1972).

CHAPTER II

EXPERIMENTAL APPARATUS

A. Introduction

The ion spectroscopy experimental apparatus developed in our laboratory evolved over a few years. This evolution resulted in an apparatus which combines many experimental techniques to accomplish the final goal. Because this thesis primarily deals with the development of this apparatus, a fairly thorough description of it is given in this chapter. To clarify the discussion it is divided into six sections, each dealing with a particular aspect of the experiment.

The first section describes the vacuum chamber configuration and the vacuum system. Although the vacuum system is not very sophisticated, it produces a pressure low enough to minimize the influence of ion-neutral collisions on our experimental results. The vacuum chamber, however, did require some elaborate design and machining to ensure correct alignment of the various experimental components.

The basis of our experiment, laser induced fluorescence of confined molecular ions, divides neatly into three sections. The first of these deals with three dimensional trapping of molecular ions. Theoretical and empirical results obtained by other research groups concerning ion trapping are used to derive the particular trapping techniques we employ. The technique which measures the density of

these confined ions and determines our trapping characteristics is also described. The laser induced fluorescence technique is presented in the following two sections which deal with the excitation source and the fluorescence detection system, respectively. The laser section includes a description of its properties, the techniques used to measure its power and calibrate its wavelength, and the baffle system utilized to minimize the effect of scattered laser light. In the fluorescence detection section, the expected signal level is calculated and used to determine the type of detection systems which must be employed. The specific detection systems decided upon and the means by which they increase the signal-to-noise ratio are described.

To demonstrate how these three separate functions combine to form one experiment, the timing of the different experimental events is presented in the fifth section. The experimental components which synchronize the four different measurements required are also described. The last section describes the computer system, the interface, and the program which control the apparatus throughout a complete experiment.

B. Vacuum System and Vacuum Chamber Configuration

The vacuum chamber consists simply of a main chamber to house the ion trap apparatus, a flange to which the ion trap apparatus is attached, two baffle arm assemblies, and laser entry and exit window assemblies. As can be seen in Figure II-1, the entire chamber is pumped by an N.R.C. 162 6"

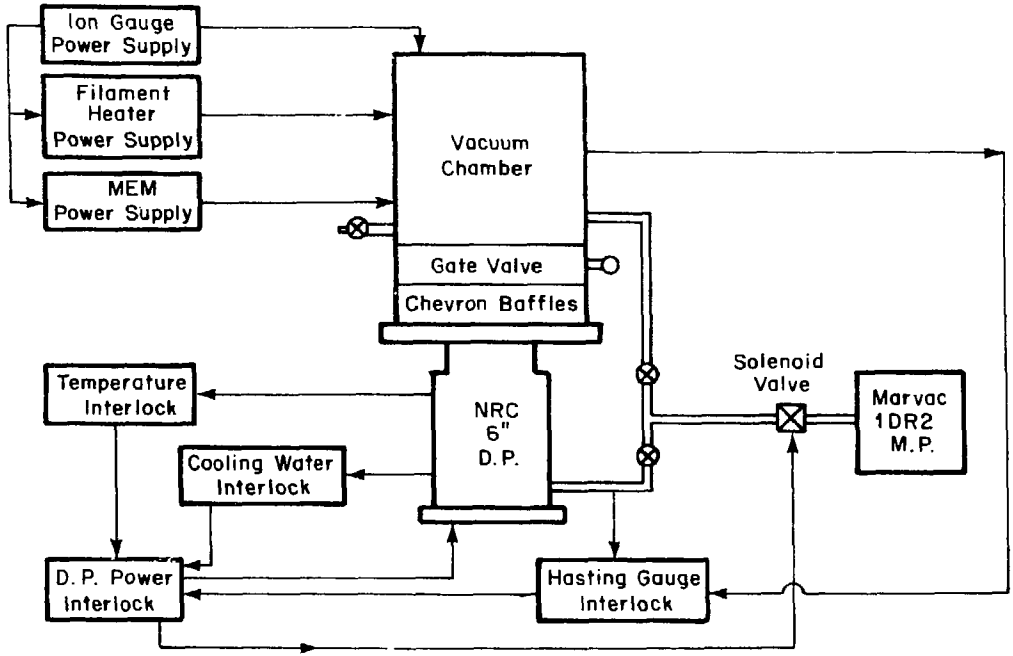

Figure II-1. Vacuum System.

XBL 798-11083

diffusion pump (d.p.) backed by a Marvac 1 DRZ mechanical pump. Liquid nitrogen cooled Chevron baffles are placed between the chamber and the diffusion pump. The vacuum system is a standard three valve system which allows the diffusion pump to remain on when the chamber is vented to atmosphere. The three valves include a gate valve between the chamber and the diffusion pump, a valve between the diffusion pump and mechanical pump, and a valve between the chamber and the mechanical pump. Another valve, located just above the gate valve, is used when venting the chamber to atmosphere.

With this vacuum system, a background pressure of 6 x 10^{-7} torr can be obtained after heating the chamber with heating tape for a period of 24 hours. The pressure in the vacuum chamber is measured by a Hastings thermocouple gauge and a Phillips VG1A or VG1B ionization gauge. The pressure in the foreline is measured by another Hastings thermocouple gauge. A standard L.B.L. interlock protection system (see Appendix 2 for L.B.L. drawing numbers) is used which will turn off the diffusion pump and isolate the mechanical pump via a solenoid valve if too high a pressure is reached in either the chamber or foreline as measured by the thermocouple gauges. The protection system also includes devices to turn off the diffusion pump and isolate the mechanical pump if the d.p. cooling water flow rate is too slow or if the d.p. becomes too hot. In addition, protection for components which can be damaged by high pressure (the electron gun

filament or the magnetic electron multiplier) is incorporated by linking their respective power supplies to the ionization gauge. If the ionization gauge turns off, the power supplies for the electron gun filament current and for the magnetic electron multiplier would be turned off. This protection can be overridden by a switch on the main control power rack.

The vacuum chamber configuration is shown in Figure II-2. The main chamber consists of 4 ports, the bottom port being connected to the vacuum pump system with an O ring seal. The ion trap apparatus which is shown in Figure II-3 is lowered into the top port with an O ring seal being made between the main chamber top port flange and the ion trap flange. The two side ports are used for mounting of the baffle arms again with an O ring seal being made between the two flange surfaces. The two side flanges were designed and constructed to be concentric to 0.001" in order to allow precise mounting of the baffle arms upon reassembly of the vacuum chamber system.

Each baffle arm flange has an interlocking surface which mounts in a main arm flange making alignment of baffle arms automatic and easy. Because the two main chamber side arms are of different lengths, the entry and exit baffle arms are not symmetrical. Both baffle arms extend into the main chamber the length of their respective main chamber side arm. Baffles and spacers are placed inside the baffle arms and held in place by a threaded end piece. The laser entry and exit window flanges are mounted to the end flanges of the baffle arms. No critical alignment is necessary here because

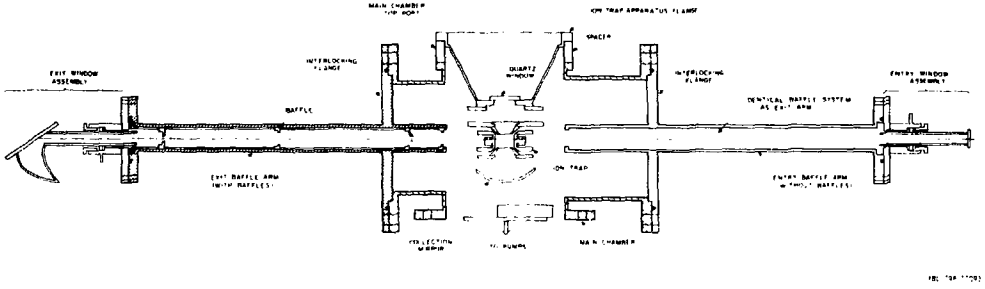

Figure II-2. Vacuum Chamber Configuration.

Figure II-3. Ion Trap Apparatus Assembly

1. Adjustment Plate
2. Top Electrode
3. Center Electrode
4. Faraday Cup
5. Bottom Electrode
6. Ion Focusing Plate
7. Teflon Insulator
8. Mirror Bracket
9. Collection Mirror
10. Magnetic Plate
11. Bottom Plate
12. Vertical Adjustment Screw
13. Electron Gun
14. Quartz Window
15. Magnetic Electron Multiplier
16. Interlocking Dowel Pin
17. Fresnel Lens

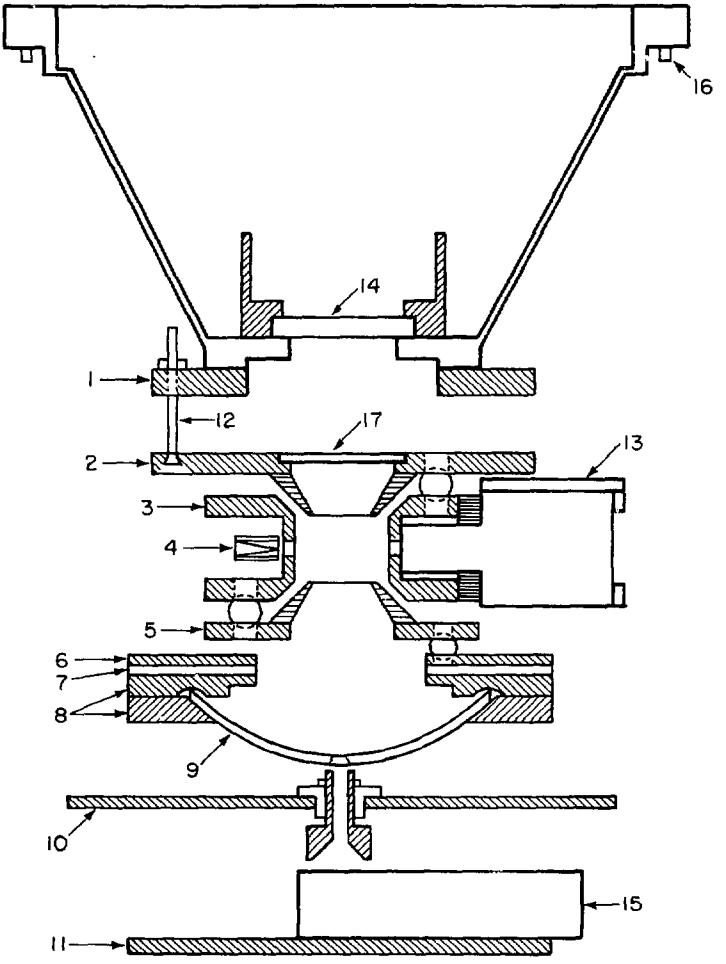

XBL 798-11091

the window sizes (1 inch) are much larger than the laser beam diameter (0.2 inch). The entry and exit windows are mounted on glass tubes which are in turn attached to metal tubes with Kovar seals. The metal tubes are placed in Wilson seals which are soldered to the entry and exit flanges. The Wilson seals allow rotation of the entry and exit windows without disturbing the vacuum. The wilson seals are differentially pumped by a small Welch 1400 Mechanical Pump. Descriptions of the baffling system and the entry and exit windows are given in the Laser and Light Entry section.

The ion trap apparatus and its flange are shown in Figure II-3. In addition to the O ring surface on this flange, there are two metal dowel pins placed 180 degrees apart. These two pins fit into two precision mounting holes in the main chamber top port flange. This insures alignment between the ion trap and the baffle arm axis (or laser beam axis) with respect to rotation about the trap's vertical axis. The ion trap apparatus is attached to its flange via a sliding adjustment plate. The adjustment plate allows alignment of the ion trap in the direction horizontal and perpendicular to the baffle arms. The ion trap is mounted to the adjustment plate with 3 threaded rods. Nuts on these rods allow adjustment of the trap along the vertical axis perpendicular to the baffle arm axis and also allow leveling of the trap. All of these adjustments have locking nuts or screws to secure the trap into position after alignment has been accomplished.

Also shown in Figure II-3 are the electron gun and the ion detection components situated below the ion trap. Both of these items are discussed in the Three Dimensional R.F. Trap and Ion Detection section. The fluorescence mirror and fluorescence detection window are discussed in the Fluorescence Detection section. A list of the mechanical drawings and their LBL numbers of all the parts described in the preceding paragraphs is given in Appendix 1.

Electrical connections are made through several electrical feedthroughs. The following have single pin electrical feedthroughs mounted in the main chamber: r.f. voltage with d.c. bias for ion trap center electrode, high voltage connections to magnetic electron multiplier, and the output signal line from the magnetic electron multiplier. The rest of the electrical connections are made via a 19 pin Cannon connector through two electrical feedthroughs mounted in the ion trap apparatus flange. A list of all electrical connections to the ion trap apparatus is given in Table II-1.

The gas inlet system consists of one stainless steel gas inlet line which is welded to the ion trap apparatus flange. Two Granville-Phillips leak valves are used in parallel as gas inlet ports. Usually, just one inlet port is used to leak in the parent gas desired. In some cases, mixing of the parent gas with a buffer gas is warranted in which case both inlet ports are used. With the vacuum system and inlet system just described, a static pressure between 10^{-6} and 10^{-3} torr is easily obtained.

Table II-1

Electrical Connections to Apparatus

1. Nineteen Pin Cannon Connector

Connector Pin No.	Feedthrough Pin No.	Connected to
1	1	Faraday cup
2	2	MEM field step output (ground)
3	3	filament shield
4	4	pulse plate
5	2	ground
6	6	bottom electrode
7	7	top electrode (ground)
8	8	N.C.
9	9	N.C.
10	10	ion focusing plate
11	11	mirror bracket
12	12	MEM dynode strip output
13	5	final focusing stage
14	14	grid
15-18	15-18	filament
19	19	N.C.

pins 2, 5, 7 are tied together

2. Individual Connectors in Main Chamber

Connector	Connected to
Mass Filter High Voltage	center electrode
MEM High Voltage Connector 7	MEM dynode strip input
MEM High Voltage Connector 4	MEM field strip input
MEM Output	MEM anode

C. Three Dimensional R.F. Ion Trap and Ion Detection System

1. History of 3-Dimensional Trap Development[1]

Quadrupole mass spectrometry had its beginnings in the early 1950's when Wolfgang Paul[2] and his co-workers and independently R. F. Post[3] proposed the use of r.f. electric fields to produce a quadrupole mass filter. Paul[4] was also the first to describe the three dimensional quadrupole ion trap and its feasibility was first demonstrated by Berkling[5] and Fischer.[6] Since that time, many workers have contributed to the development of the three dimensional quadrupole trap and the study of its properties and characteristics. Most notable among these are Dawson et al.[7,13,14,17,21,24,26,27] and Todd et al.[8,20,21,23] who have carried out extensive investigations on many aspects of three dimensional quadrupole trapping. These investigations have not only greatly aided in the understanding of ion trapping, but have also helped in the design and day-to-day use of the ion trap in the laboratory. Theoretical investigations of ion trapping under many different conditions have also been carried out and these will be mentioned where appropriate in the following sections.

The studies mentioned above concentrated on the hyperbolic three dimensional ion trap. In 1973, Benilan and Audoin[9] presented the theoretical description of a cylindrical ion trap. This work was the basis for the design of the ion trap used in our experiments. The cylindrical ion trap was chosen because it was felt that the various holes that had to be cut into the trap electrodes would disturb the

electric fields to a smaller degree in the cylindrical trap than in the hyperbolic trap. After we began the operation of our cylindrical trap, Bonner et al.[10] presented a thorough theoretical treatment and some experimental results for the cylindrical ion trap. These two works form the theoretical foundation for the cylindrical trap used in our experiments.

2. Brief Outline of Theory

An oscillating inhomogeneous electric field generated by applying an r.f. electric field to electrodes of a particular shape produces a pseudopotential in which ions can be confined. A good explanation of this effect is found in an article by Dehmelt[11] which is based on the fundamental theory presented by Landau and Lifshitz.[12] The purpose of this section is to outline the theory of the three dimensional hyperbolic trap in order to establish the equations necessary for its design and operation and to obtain an understanding of the principles of ion trapping. The results of the theory of the cylindrical trap are also discussed to show the similarity between the two types of traps which enables the use of results from many of the hyperbolic studies in designing and operation of the cylindrical trap.

Many theoretical discussions of three dimensional ion trapping have been given. The trap used in these experiments is operated in a mode first demonstrated by Dawson and Whetten[13] where the end caps are grounded and the trapping field is applied just to the center electrode. The outline of the theory presented here will therefore follow those given for a trap used in the mode.[14,15]

The potential ϕ for a quadrupole field is given by

$$\phi\ (x,y,z) = \phi_o\ (\lambda x + \sigma y + \gamma z). \qquad \text{(II-1)}$$

where ϕ_o is not a function of the coordinates but may be a function of time. With no ions present, the Laplace condition $\nabla^2\phi = 0$ must be satisfied yielding the equation

$$\lambda + \sigma + \gamma = 0. \qquad \text{(II-2)}$$

Many solutions exist for this equation. For the quadrupole mass filter the coefficients are chosen such that $\lambda = -\sigma$ and $\gamma = 0$. Thus, in the mass filter ions are confined in the x and y direction but not in the z direction. For the three dimensional trap, the coefficients are chosen such that $\lambda = \sigma = -2\gamma$. The potential then becomes

$$\phi\ (x,y,z) = \phi_o\lambda\ (x^2 + y^2 - 2z^2) \qquad \text{(II-3)}$$

or in polar coordinates (r,z,θ)

$$\phi\ (r,z) = \phi_o\lambda\ (r^2 - 2z^2). \qquad \text{(II-4)}$$

In the rz plane, the equipotential lines are, therefore, complimentary hyperbolas. Because there is no dependence on the angle θ, the electrode structure is then determined by revolving these hyperbolas around the z axis resulting in a ring electrode and two cap electrodes, shown in Figure II-4 where r_o and z_o are defined. Applying the potential to the 3 electrodes in a similar manner as in the mass filter case, the ring electrode is at ϕ_o and the end caps are at $-\phi_o$.

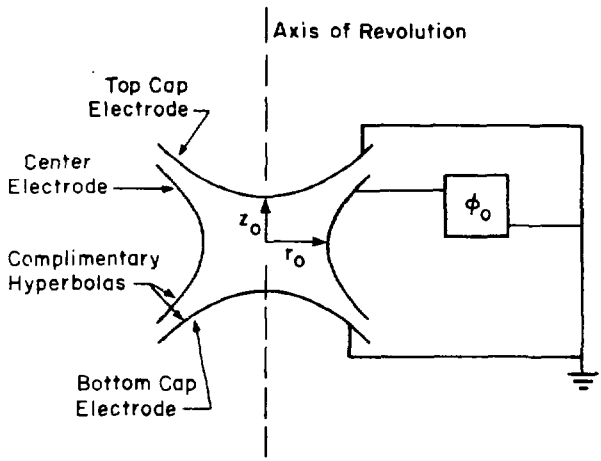

XBL 798-11075

Figure 1I-4. Hyperbolic Ion Trap, rz plane.

Then, at the coordinates $z = 0$ and $r = r_o$

$$\phi\ (r_o,0) = \phi_o = \phi_o \lambda r_o^2 \qquad \text{(II-5)}$$

and at $r = 0$ and $z = z_o$

$$\phi\ (0,z_o) = -\phi_o = -\phi_o \lambda 2z^2. \qquad \text{(II-6)}$$

Then from Eqs. (II-5) and (II-6)

$$r_o^2 = 2z_o^2 \qquad \text{(II-7)}$$

which more specifically defines the structure of the trap. Although the structure of the trap we use is defined by Eq. (II-7), we ground the end caps and apply the potential ϕ_o only to the center electrode. In this case the potential changes to an alternate form,[15]

$$\phi\ (r,z) = \phi_o \lambda\ (r^2 - 2z^2) + c \qquad \text{(II-8)}$$

Then at the ring electrode

$$\phi\ (r_o,0) = \phi_o = \phi_o \lambda r_o^2 + c \qquad \text{(II-9)}$$

and at the end cap electrodes

$$\phi\ (0,z_o) = 0 = -\phi_o\ 2\lambda z_o^2 + c \qquad \text{(II-10)}$$

Subtracting Eq. (II-10) from Eq. (II-9) and using Eq. (II-7) one obtains

$$\lambda = \frac{1}{2r_o^2}. \qquad \text{(II-11)}$$

Substituting Eq. (II-11) in Eq. (II-9) results in c = 1/2 giving

$$\phi\ (r,z) = \frac{\phi_o}{2r_o^2}\ (r^2-2z^2) + \frac{\phi_o}{2} \qquad \text{(II-12)}$$

for the trapping potential.

The potential ϕ_o applied to the center electrode is of the form U + V cosΩt where U is a d.c. potential and V is the peak r.f. voltage with frequency Ω. Because there are no cross terms, r and z can be treated independently. The equations of motion in cylindrical coordinates are then

$$\begin{aligned} \ddot{r} + \frac{e}{mr_o^2}\ (U + V\cos\Omega t)\ r &= 0 \\ \ddot{z} - \frac{2e}{mr_o^2}\ (U + V\cos\Omega t)\ z &= 0 \qquad \text{(II-13)} \\ \ddot{\theta} &= 0. \end{aligned}$$

From these equations, one can see that, in cylindrical coordinates, confinement is accomplished in just two dimensions with the angular velocity unaffected by the electric fields.

If the substitution $\Omega t = 2\xi$ is made, the equations of motion become

$$\frac{d^2u}{d\xi^2} + (a_u + 2q_u\cos 2\xi)\ u = 0 \qquad \text{(II-14)}$$

where u is either r or z and

$$a_r = \frac{4eU}{mr_o^2\Omega^2} : a_z = -\frac{8eU}{mr_o^2\Omega^2} = -2a_r \qquad \text{(II-15)}$$

$$q_r = \frac{2eV}{mr_o^2\Omega^2} : q_z = -\frac{4eV}{mr_o^2\Omega^2} = -2q_r. \qquad \text{(II-16)}$$

Equation (II-14) is the Mathieu differential equation and has two different types of solutions with respect to increasing ζ: stable and unstable. For a detailed discussion of the solutions to the Mathieu equation see reference 14. The a and q variables in Eqs. (II-15) and (II-16) are termed the stability parameters.

To determine the conditions under which ions are stable in the trap, a plot of the stable solutions for both the r and z directions is made in terms of the stability parameters. A stability region in which ions are stable in both the r and z directions is determined by where the r and z stability regions overlap. This results in a stability diagram or an "a, q diagram" shown in Figure II-5. If the values of the different variables in Eqs. (II-15) and (II-16) result in a and q values such that the (a,q) point lies inside the stability region, the ions will execute stable trajectories and, in principle, the ions will be trapped. In actuality, the stable trajectories divide into two classes: bound and quasibound trajectories. Where as the bound trajectories represent ions stable in the ion trap, quasibound trajectories represent ions that would be stable but are not due to the finite dimensions of the trap.

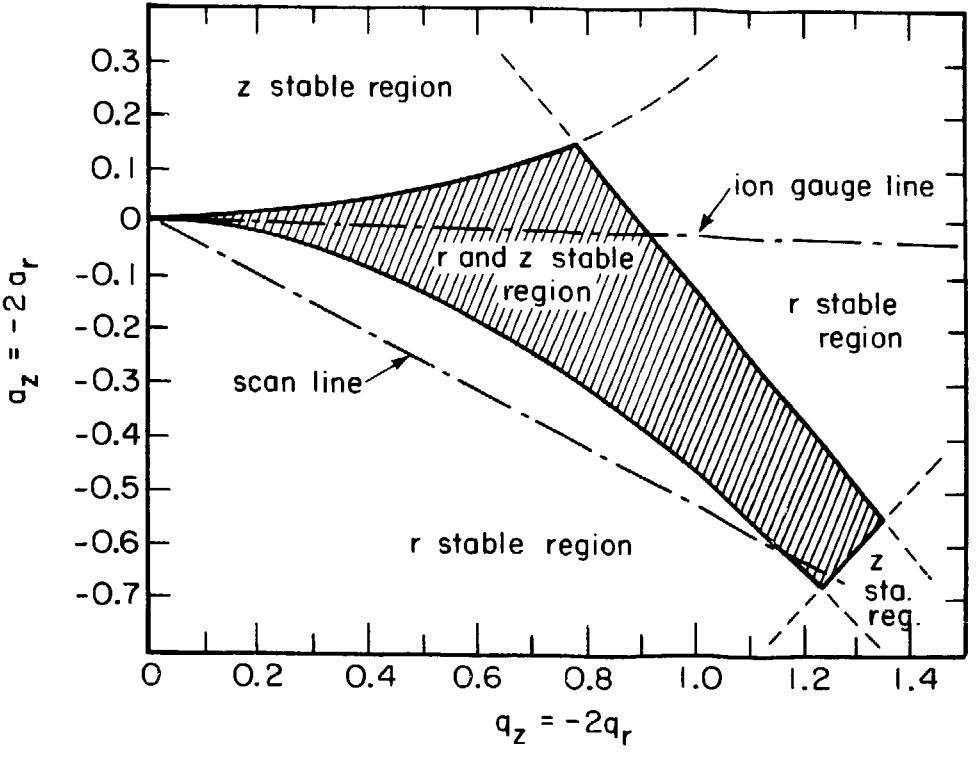

XBL 798-11076

Figure II-5. Hyperbolic Trap Stability Diagram.

When the voltages U and V and the frequency Ω are given, the a,q diagram determines the range of mass-to-charge ratios that are stable. Two examples are shown in Figure II-5 by dashed lines drawn through the stability region. The top line (ion gauge line) depicts a situation where the value of a is near zero. This is accomplished by setting U, the d.c. bias voltage, near zero volts. The result is a low mass resolution mode in which a wide range of mass-to-charge ratios are stable for a particular value of V and Ω. This mode of operation has been termed the "ion gauge mode" or the "total pressure mode". The lower dashed line (scan line) represents a high mass resolution mode. Here, the ratio a/q = 2U/V is chosen so that only a small portion of the stability region is intersected. Then, for a fixed Ω, only a small mass-to-charge ratio is stable in the ion trap. The masses which are stable are selected by varying U and V while maintaining a constant ratio a/q = 2U/V. The mass resolution can then be varied by changing the a/q ratio. This high mass resolution mode allows the ion trap to be utilized as a mass spectrometer, and this mode of operation is termed the mass selective mode.

As mentioned above, the ion trap used in this work is the cylindrical ion trap which was first proposed by Langmuir et al.[16] Unlike the hyperbolic trap, there is no simple solution for the potential distribution. Solutions for the potential distribution include zero-order modified Bessel functions of the first and second kind.[9,10] The resulting equations

for the electric fields and for motion in the r and z directions are coupled. The solutions to these equations require numerical integration. Benalin and Audoin[9] have shown that, under certain assumptions, the trapping conditions for the cylindrical trap are very similar to that of the hyperbolic trap. The configuration of the cylindrical trap is shown in Figure II-6. In the cylindrical trap used in these experiments, the dimensions were chosen so $r_1^2 = 2z_1^2$ where r_1 and z_1 are defined in Figure II-6. Trapping in this configuration closely approximates that of the hyperbolic trap, and the comparison made by Benalin and Audoin of the stability diagrams for the cylindrical trap and the hyperbolic trap is shown in Figure II-7. In this comparison, $z_0 = z_1$ which inscribes the cylindrical trap inside the hyperbolic trap. For this cylindrical trap the stability parameters are the same as those for the hyperbolic trap and the stability regions in Figure II-7 are seen to be very much alike. Benalin and Audoin also treated the case of $r_1 = z_1$ for the cylindrical trap and provisions were made in our apparatus design to allow for this configuration.

Benalin and Audoin's treatment differs from the trap used in our experiments in that the center electrode in their case was grounded and the potential was applied to the end caps. Bonner et al.[10] have treated the operation mode utilized in our experiments where the cap electrodes are grounded and the potential is applied to the center ring electrode. Their treatment is very complete and contains

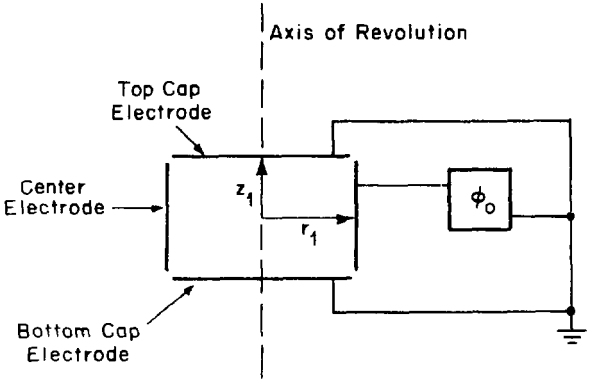

Figure II-6. Cylindrical Trap, rz plane.

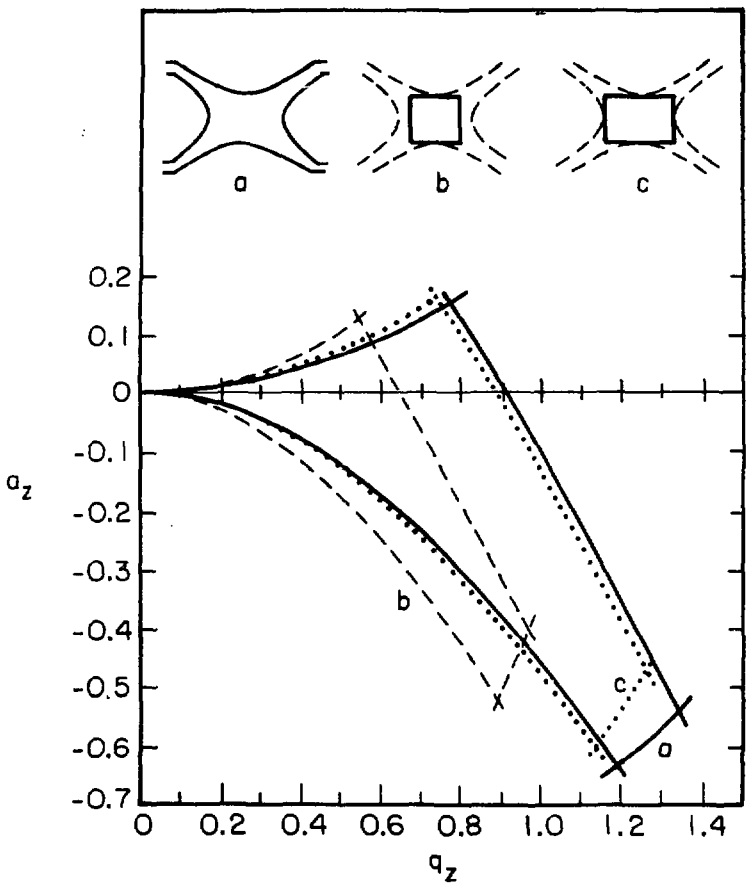

Figure II-7. Comparison of Hyperbolic and Cylindrical Trap Stability Diagrams.

some experimental results verifying the ion trapping by the cylindrical trap. They have also determined equipotential curves for both the hyperbolic and cylindrical traps. The similarity of the equipotential curves for these two cases explains the nearly identical trapping conditions predicted by Audoin and Benalin. Because of the similarity between the two traps, the vast amount of information obtained for hyperbolic traps was used in the design of the cylindrical trap.

3. Ion Trap Design Considerations

As seen in the previous section, the ion trap consists of three electrodes, a center electrode and two cap electrodes. First, the dimensions of these electrodes need to be determined. This is accomplished by using Eqs. (II-7), (II-15), and (II-16) derived in the previous section. By examining Eqs. (II-15) and (II-16) it is seen that the trap dimensions are limited by the maximum mass which is desired to be trapped and the maximum voltage which is applied. By further examining Eqs. (II-15) and (II-16) and by examining the stability diagram in Figure II-7 for possible values of a and q, it is seen that the d.c. voltage U is always some fraction of the r.f. voltage V. Therefore, to determine the trap's dimensions, we need only consider Eq (II-16) which is rearranged here,

$$r_1^2 \cong r_0^2 = \frac{-4eV}{q_z m\Omega^2} \,. \qquad \text{(II-17)}$$

The r.f. voltage is, in turn, limited by the maximum voltage available from the r.f. supply and by the desire to

keep the voltage low enough to minimize arcing problems. The r.f. supply used in our experiments is a modified version of the mass filter supply for the quadrupole mass filters which have been used in the Mahan research group for a number of years. The supply was modified for single phase operation and the L.B.L. number of the modification is given in Appendix 2. The maximum voltage from this supply is on the order of 1000 volts which is a reasonable voltage with which to work. Another important variable in Eq. (II-17) is the frequency Ω. The frequencies available from the mass filter supply which are useful for the ion trap are ($\nu = \Omega/2\pi$) 0.622 MHz and 1.077 MHz. As will be seen in Section II-C6 of this chapter the expression for the pseudo-potential well for the ions contains ν^2 in the denominator. For this reason the lower frequency 0.622 MHz will be used in Eq. (II-17) to determine the trap dimensions.

It is left to decide the values for q_z and m. From the stability diagram in Figure II-7 q_z is derived when the trap is operated in the mass selective mode yielding a value of $q_z \cong 1.2$. To obtain good mass resolution over the 1000 volt range, a mass of 100 a.m.u. was selected as the maximum mass desired to be trapped. Substituting the values chosen above (V = 1000 volts, q_z = 1.2, m = 100 a.m.u., ν = .622 MHz) in Eq. (II-17), a value of 1.45 cm is calculated for r_1. The actual value of r_1 used in the ion trap is 1.43 cm or 9/16 inch. The center electrode is then a cylinder with a radius of 1.43 cm.

The heighth of the cylinder is yet to be determined. As mentioned in the previous section, we use two different ion trap configurations, one with $r_1^2 = 2z_1^2$ and one with $r_1 = z_1$. For this reason, both the top and bottom electrodes consist of two pieces, a mounting plate and an electrode cone. Electrode cones were constructed for both trapping configurations. The center electrode height is determined by the $r_1 = z_1$ case and was constructed so as to allow for this configuration. Switching between the two configurations becomes just a matter of changing electrode cones on the cap electrode mounting plates. A diagram of the cylindrical ion trap is shown in Figure II-8. The electrodes are made of 304 stainless steel and are insulated and accurately separated from one another by ceramic balls. The remaining modifications to the electrodes arise from mounting the trap to the flange, the electron and laser beam path, fluorescence detection, and ion detection. The modifications of each electrode is described separately below.

As can be seen in Figure II-8, the top cap electrode mounting plate is of larger diameter than that of the bottom cap electrode. This is to allow mounting of the top electrode to the adjustment plate (which is connected to the top flange) via the vertical adjustment screws. A hole is cut in the top electrode mounting plate to allow for the passage of fluorescence and a slot is cut out of the top of this plate to hold a Fresnel lens. A hole is also cut in the electrode cone to allow for the passage of fluorescence and stainless steel wire mesh is spot-welded across the surface closest to the

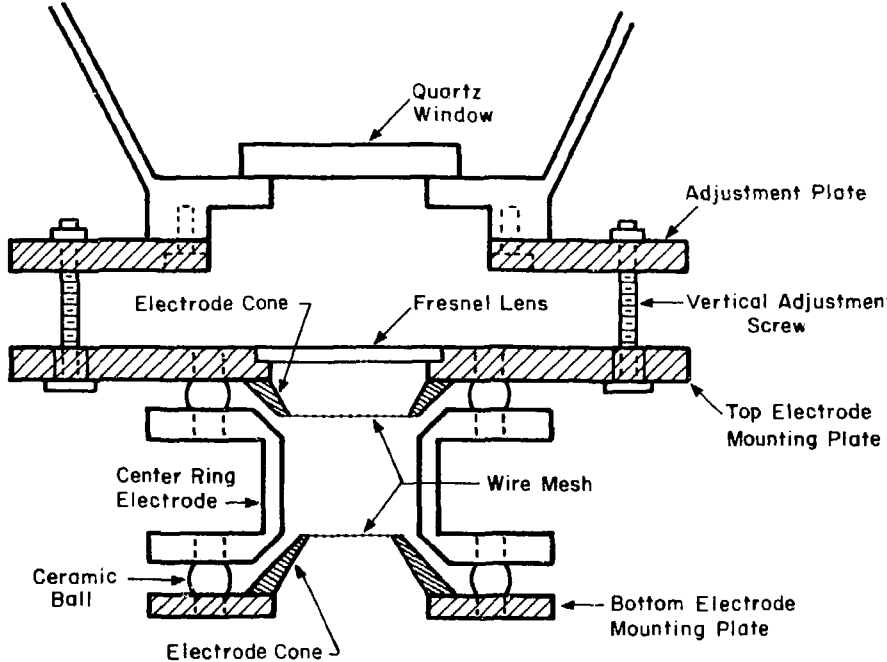

Figure II-8. Cylindrical Ion Trap Configuration.

center electrode to create the flat cap electrode. The bottom electrode's design is very similar to that of the top electrode with the exception of the smaller diameter of the mounting plate. Wire mesh is again spot-welded across the cone. The hole in the bottom electrode allows both the passage of the fluorescent light down to a mirror below the trap and the passage of ions down to a detector situated below the trap.

The laser beam passes radially through the center electrode. To minimize the amount of scattered light it is very important that the laser beam not be allowed to strike any of the center electrode surfaces. The laser beam is on the order of 1/4 inch in diameter necessitating holes larger than this size to be cut into the center electrode. Because of the large size of these holes, steps were taken to minimize the perturbation of the desired electric field by any penetrating fields. This was accomplished by adding cylinder extensions or "ears" to the holes in the electrode as can be seen in Figure II-9. Several sizes of cylinder extensions were made allowing the hole size to vary between 1/4 and 7/16 inch in diameter. The alignment of the laser beam holes in the trap to the laser beam axis has already been described in Section B and will be more completely described in the Laser and Light Entry System, section II-D2.

The electron beam also passes through the center electrode in a radial direction perpendicular to the laser beam. The ions are then created in the trapping region. Dawson and

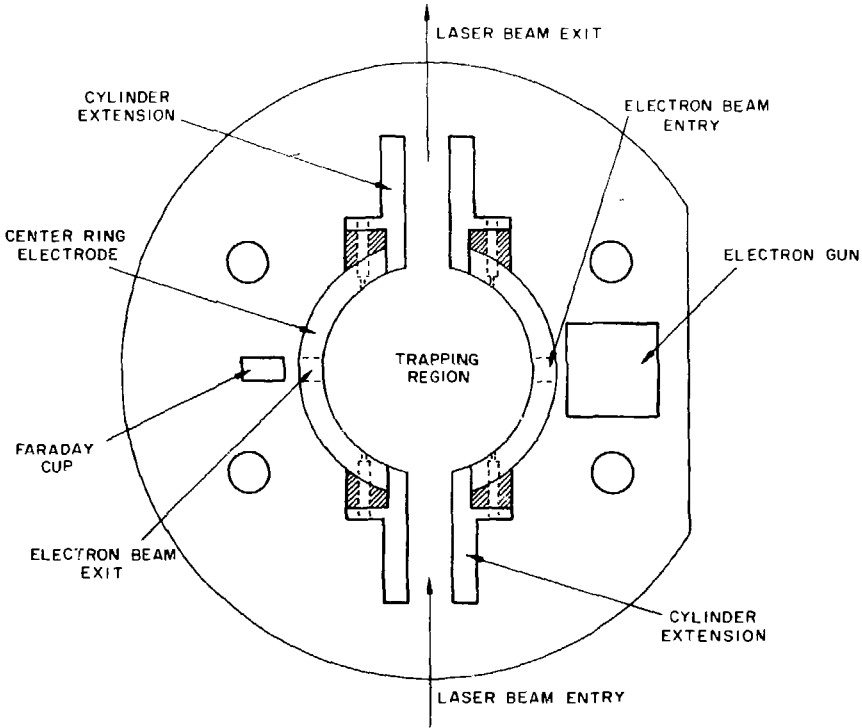

Figure II-9. Cross Section of Center Ring Electrode, Top View.

Lambert[17] have demonstrated that ions are trapped more efficiently when the electron beams are directed radially (along r) than with beams directed axially (along z). Holes, 3/16 inch in diameter, were cut in the center electrode to allow for electron beam entry and exit. As can be seen in Figure II-9, a Faraday Cup was placed at the exit hole opening and connected to a Keithly 610B electrometer to measure the electron beam current. On the opposite side, the electron gun is mounted as a unit to the center electrode. The outside shroud of the electron gun is connected directly to the electrode via a light tight shield. The electron gun components are electrically isolated from the electrode by a lava ring. The electron gun design and performance is discussed in the next section. The L.B.L. mechanical drawing numbers for all the ion trap components is given in Appendix 1.

4. The Electron Gun

The electron gun generates an electron beam which passes through the entry aperture in the center electrode and creates ions from the background gas in the trapping region. The electron beam then passes through the opposite side of the center electrode into a Faraday Cup where the electron current is measured. The electron gun consists of a heated 1% thoriated tungsten filament and associated focusing electrodes. Design considerations for the electron gun included high and stable electron current (at least 1 μamp), pulsed electron current operation, and low light levels in the trapping region.

These considerations led to a modified Pierce design[18] for the electron gun which is shown in Figure II-10. The electron gun is cylindrically symmetric about the electron beam axis. Also shown in Figure II-10 is the center electrode and the position of the Faraday cup.

The electron gun is attached (and can be detached) as a unit from the center electrode with four screws through the light tight shield. The rest of the electron gun is held together by the pressure exerted by four threaded rods which attach to the front plate and to the back plate. All of the elements in the electron gun are electrically insulated and accurately spaced by 3/16 inch ceramic balls. The electron gun elements are surrounded on 3 sides by a blackened brass shroud which serves to absorb much of the light generated by the filament. The shroud is insulated from the gun by ceramic balls and a light tight lava ring. A blackened ceramic plate covers the fourth side of the electron gun. The electrical connections are made through this plate via nickel pins and brass fittings which rest against each of the elements. Each electron gun element and its function are described below.

The 0.010 inch thick thoriated tungsten filament is spot-welded to two molybdenum pins which are mounted in a ceramic cap. The pins extended through the ceramic cap to allow electrical connection to be made to the filament. Two supplies are connected to the filament. A current regulated supply (designed by Phil Eggers) is used to heat the filament.

Figure II-10. Electron Gun.

1. Center Electrode
2. Faraday Cup
3. Light Tight Shield
4. Front Plate
5. Light Tight Lava Ring
6. Final Focusing Stage
7. Grid
8. Pulse Plate
9. Filament Shield
10. Ceramic Plate
11. Ceramic Filament Holder
12. Back Plate
13. Molybdenum Pins
14. Thoriated Tungsten Filament
15. Brass Shroud

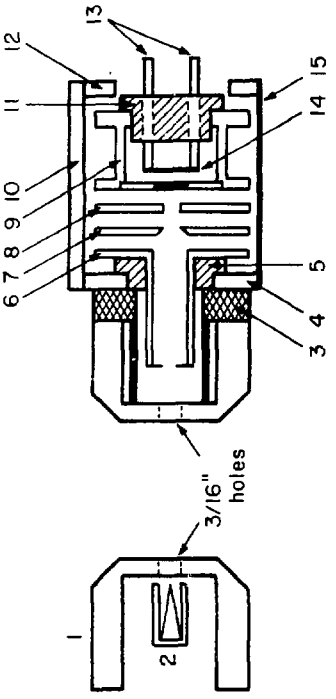

XBL 798-11081

A voltage regulated supply biases the filament to a negative voltage. Using four screws the ceramic cap mounts into a filament shield which completely surrounds the filament. A hole was cut in the center of the ceramic cap to allow filament light to escape out the rear of the electron gun.

In addition to electrons, light is also produced when the filament is heated. The filament shield serves to block this light and to draw electrons from the filament. A molybdenum plate with a 1/4 inch hole was welded on the filament shield and a tantalum strip which lines up with the filament was spot-welded to the plate. While the electric fields on the various elements are used to bend the electrons around this strip, it effectively keeps direct light given off by the filament from reaching the trapping region. The filament shield is kept at a positive voltage relative to the filament potential and draws off electrons emitted by the heated filament.

The next element in line is the molybdenum pulse plate. The potential on this plate is kept more positive than that of the fialment shield when it is desired to draw electrons around the tantalum strip. The number of electrons drawn into the trapping region is very sensitive to this voltage. When it is desired to stop the electron beam, a variable negative high voltage pulse (~-200 V) is applied to the pulse plate by the experimental timing pulse control box which is discussed in Section II-F. Thus, the pulse plate has two functions: to draw the electrons around the blocking strip and to accomplish the pulse mode operation.

The final two electron gun elements serve to focus the electron beam into the trapping region. After the pulse plate, a variable potential is applied to the stainless steel electron grid. On some occasions it was found necessary to change the polarity of the voltage applied to the grid from positive to negative in order to maximize the electron current at the Faraday cup. The electrons then pass through the 1/8 inch hole in the electron grid and enter the final focusing stage. The final focusing stage consists of a plate to draw the electrons and a 15/16 inch long tube which forms a constant potential region for the electrons before entering the trap. The final focusing tube also serves to minimize filament light from reaching the trapping region. A baffle system (not shown in Figure 10) very similar to the design presented in Section II-D2 is inserted into the tube with a minimum baffle hole diameter of 1/8 inch. The last aperture in the final focusing stage is 3/16 inch in diameter. The combination of this baffling system, the tantulum strip, the light tight lava ring, the light tight shield, and the hole in the ceramic filament cap successfully meet the low light level criterion.

The other two criteria are also met by this design. Typical operating voltages and currents are shown in Table II-2. It is important to realize that each of the voltage supplies is floated on the d.c. bias potential which is applied to the ion trap. The conditions listed in Table II-2 are all variable and day-to-day adjustment is required

Table II-2

Typical Operating Conditions for the Electron Gun

E Gun Element	Voltage	Current	Power Supply
Filament	-150 V	5 mamps	Kepco ABC* 200 m
Filament	~2 V	6 amps	Filament Current Supply
Filament Shield	0 V	-	Lambda 29 m*
Pulse Plate	10 V - -180 V	-	External Timing Pulse Control Box* (Lambda 29 m supplies high voltage)
Grid	100 V	-	Kepco HB-6m*
Final Focus	200 V	-	Lambda 29 m*
Faraday Cup	-	3-50 amp	-

* These voltage supplies are floated on the ion trap d.c. bias.

to optimize the electron beam current. After a few hours of breaking in a new filament, an electron current at the Faraday cup of between 3 and 50 μamps is easily obtained which exceeds the minimum current requirement. This value is, of course, lower (usually by a factor of 10) when the r.f. potential is applied to the center electrode due to the deviation of the electron beam from the Faraday cup and the fact that the electrons only enter on half of each r.f. cycle.

The pulsed operation of the electron gun was confirmed by both the measurement of ions and the measurement of electron impact fluorescence. Ions and electron impact fluorescence were measured by their respective detectors only during the electron gun "on" time and not during the "off" time when the high negative voltage pulse was applied to the pluse plate. The measurement of fluorescence is discussed in Section II-E and the measurement of ions is discussed in the next section.

5. Ion Measurement Technique

The ion detector is a continuous dynode magnetic electron multiplier (MEM) made by the Bendix Corporation (Model #306) and is thoroughly discussed in reference 19. The MEM consists of an ion entry region, a dynode strip (DS), a field strip (FS), and an electron collector (anode). Four voltages required for the operation of the MEM were applied to the FS input and output and the DS input and output. The ion entry region of the MEM consists of a grid kept at the FS input voltage and a cathode kept at the DS input voltage. A potential of about 1800 volts is applied between the input and

output of both strips with the FS being floated about 350 volts more positive than the DS. The necessary voltages are produced by a John Fluke 405 power supply which is connected to a voltage divider circuit. The voltages that are actually used are determined by setting the potentials to the approximate conditions mentioned above and then adjusting the voltage divider potentiometers until the maximum ion signal is obtained. In the 2000 volt operating range, the MEM responds linearly with a gain between 10^6 and 10^7.

The electrons are collected at the anode of the MEM and sent to a voltage follower. The voltage follower allows impedance matching between the MEM and the two measuring devices. The ion signal measurement devices include an oscilloscope for observation and an integrator for accurate measurement. Whereas ions were observed on the oscilloscope during the electron gun "on" time, no ions are observed during the electron gun "off" time confirming the pulsed operation of the electron gun.

The observation of the trapped ions takes place during the electron gun "off" time. In order to observe the ions which are confined in the ion trap, a high negative voltage pulse (~-200 V) must be applied to the bottom electrode of the trap. The ions are then driven out of the trap, through the wire mesh in the bottom electrode, and to the MEM which is placed below the ion trap as seen in Figure II-11. The high voltage drive-out pulse is generated by the experimental timing pulse control box (discussed in Section II-F) and is

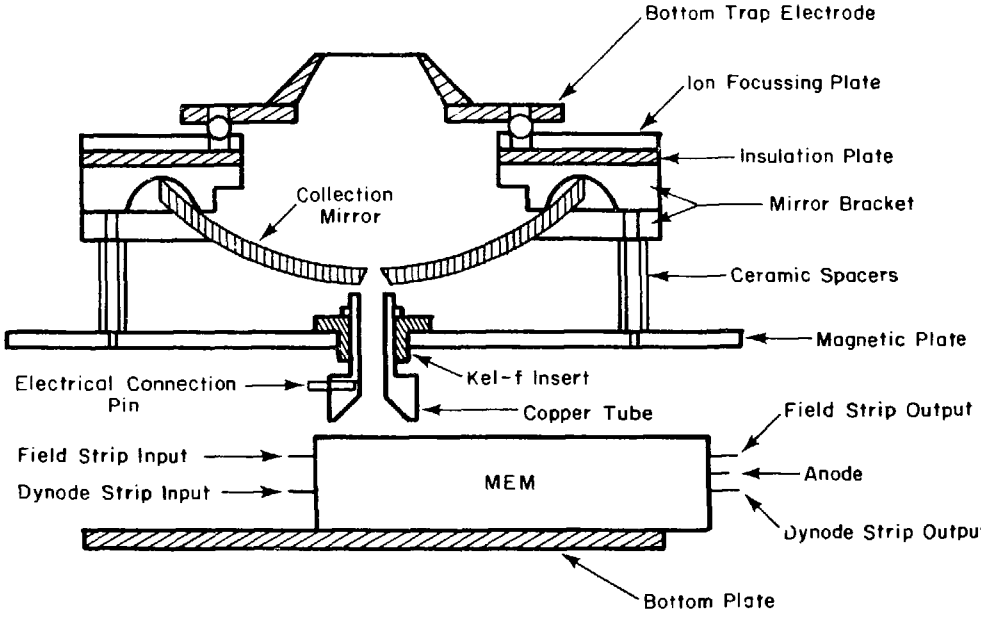

Figure II-11. Ion Measurement Apparatus.

variable in magnitude and duration. Although the ion signal is found to be sensitive to the magnitude of the drive-out pulse, the pulse length has no effect. This is because the drive-out pulse duration is at all ti s longer than one rf cycle.[20]

As can be seen in Figure II-11, several plates are situated between the ion trap and the MEM. The stainless steel ion focusing plate is the first element located below the bottom trap electrode. This plate is insulated from the bottom electrode by ceramic balls and a potential varying between 100 and -200 volts is applied to it. It is found, however, that the potential on this plate has little effect on the ion signal seen at the MEM. The voltage was usually kept at ~0 V. The next surface encountered by the ions is the spherical collection mirror. A 1/16 inch diameter hole in the center of the mirror allows the ions to pass through to the MEM. The mirror is insulated from the ion focusing plate by a teflon spacer and a potential varying between 100 and -220 V is applied to the mirror and the bracket holding the mirror. The ion signal is found to be very sensitive to the mirror potential and the maximum ion signal occurs when the potential is kept at -220 V. The voltages for the ion focusing plate and the mirror are produced by two Lambda 29 power supplies which are connected to a voltage divider circuit.

The magnetic shield, constructed from magnetic steel, is the final plate between the trap and the MEM. The MEM is

placed 2.75 inches below the trap with the magnetic shield placed between them in order to negate the effects of the magnetic field of the MEM on the trap and electron gun. No electrical connection is made to the magnetic shield. A hole in the center of the magnetic shield allows passage of the ions to the MEM. A copper tube is placed in this hole and is insulated from the magnetic shield by a Kel-F insert. The copper tube extends from close to bottom of the spherical collection mirror through the magnetic shield to the ion entry region of the MEM. The potential on the copper tube is kept at the same potential as the entry grid of the MEM. The typical operating conditions for each of the components described above is given in Table II-3. Under these conditions an ion signal is clearly observed on the oscilloscope 5 to 10 microseconds after the leading edge of the high voltage pulse. The signal, however, is observed to be very erratic because of the random application of the high voltage drive-out pulse with respect to the phase of the r.f. voltage applied to the ion trap.

Several people[21] have investigated the detection of trapped molecular ions by the high voltage drive-out pulse technique and discovered the importance of synchronization of the pulse with the r.f. phase. The synchronization is accomplished in our experiment with two electronic circuits. The first circuit (designed by Phil Eggers) produces a ttl signal with the same period as the r.f. voltage. This circuit exists in the modified mass filter supply and its circuit

Table II-3

Typical Ion Detection System Operating Conditions

Component	Voltage (Volts)
1. Magnetic Electron Multiplier	
field strip input	1650
field strip output	0
dynode strip input	2000
dynode strip output	250
2. Ion Focusing Plate	0
3. Collection Mirror	-220
4. Magnetic Plate	N.C.
5. Drive Out Pulse (bottom electrode)	-200

diagram is given on the mass filter electrical drawing. The ttl signal from this circuit (termed the R.F. ttl) along with the pulse indicating when it is time to detect the ions (termed the Experimental ttl) is input into the circuit shown in Figure II-12, where the synchronization occurs. The circuit uses a series of J-K flip-flops to obtain the synchronization. A dual one-shot in the circuit allows one to vary the initiation time of the output pulse with respect to the r.f. phase. To complete the circuit, a line driver sends the synchronized pulse to the external timing pulse control box (PCB) where the drive-out pulse is triggered.

The stability of the ion signal as observed on the oscilloscope is dramatically improved by this synchronization. The most intense ion signal is produced when the leading edge of the high voltage drive-out pulse occurs roughly when the most negative r.f. voltage is applied. However, the exact point in the r.f. phase for maximum signal is very dependent on the mass-to-charge ratio. The ion signal is believed to be more representative of the actual ion concentration in the trap when it is synchronized with the r.f. potential.

When it is desired to measure the ion signal rather than observe it, the ion signal from the voltage follower is sent to an L.R.S. 333 amplifier and then to one of the channels of an L.R.S. 227-sg gated integrator. The 333 amplifier serves two functions. The first is, of course, to amplify the signal

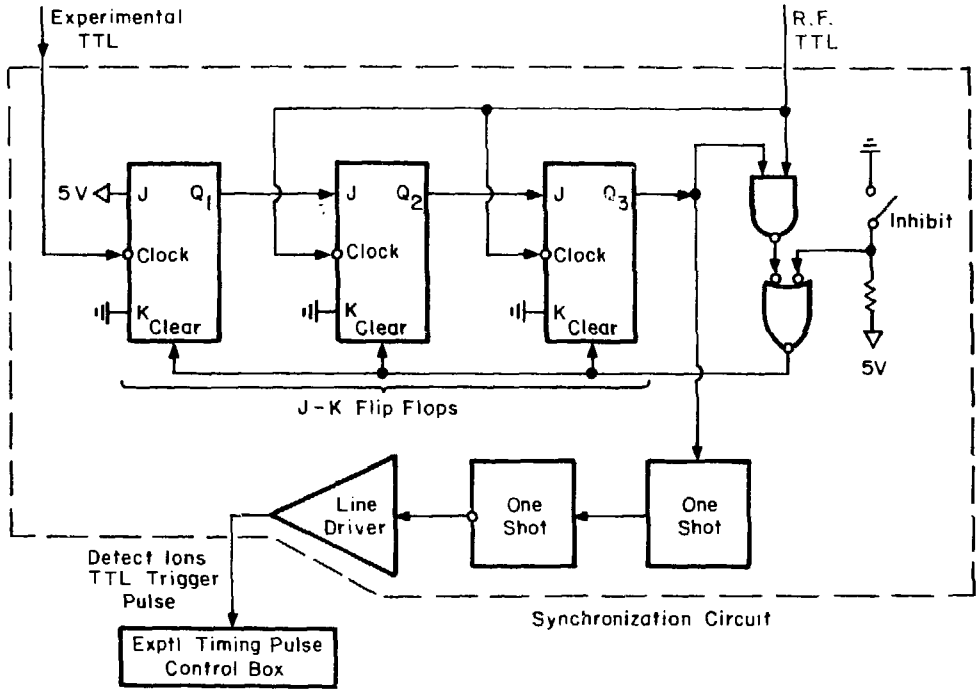

XBL 798-11085

Figure II-12. Drive-Out Pulse Synchronization Circuit.

before integration. Because the signal from the voltage follower is on top of a d.c. level, the amplifier also serves to a.c. couple the signal to the integrator. A more complete description of the 227-sg gated integrator is given in the Fluorescence Detection System section. The entire ion measurement system is shown in Figure II-13 and a description of this system is given below.

After receiving a trigger pulse from the syncrhonization circuit, the external timing pulse control box (PCB) generates a high voltage pulse to drive the ions out of the trap. Because the 227-sg gated integrator needs a detection gate signal to begin integration, the PCB also generates a ttl logic pulse simultaneous with the high voltage pulse. This pulse is sent to a Tektronix PG-501 pulse generator where a detection gate of correct magnitude and duration is produced. The detection gate spans the time of the ion signal seen at the MEM and is sent to the 227-sg gated integrator. During the duration time of the detection gate, the 227-sg integrates the ion signal and holds an output voltage proportional to the magnitude of the ion signal until a ttl pulse to clear the 227-sg gated integrator is received.

Two modes of ion measurement occur in our experiments. When it is desired to obtain a mass spectrum, the output signal from the 227-sg is sent directly to the y axis of a recorder and the clear pulse for the 227-sg is generated by the PCB. The x-axis is driven by a voltage proportional to the mass number. When the ion measurement is used to normalize the fluorescence signal, the output of the 227-sg is sent

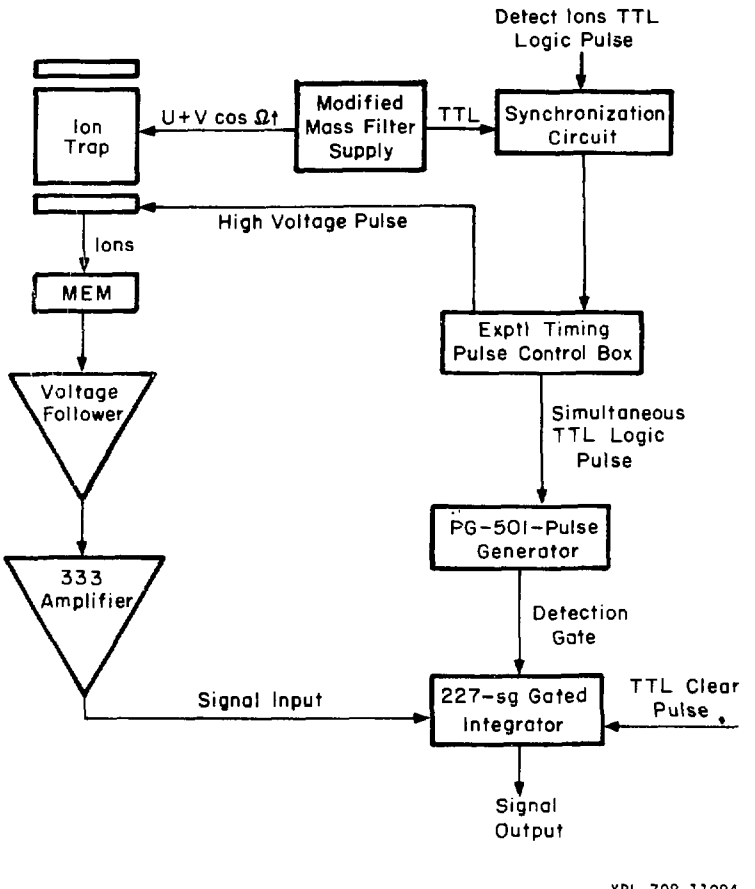

Figure II-13. Ion Signal Detection System.

to the PDP-8f computer and the clear pulse is generated by the computer. The interface between the 227-sg integrator and the PDP-8f computer is discussed in Section II-G. The next section discusses the ion trap operating conditions and the resulting ion trap characteristics as determined from the ion measurement.

6. Ion Trap Operating Conditions and Characteristics

Using the ion measurement technique just discussed, the characteristics of the ion trap were determined. The point here was to determine the conditions under which the laser induced fluorescence experiments can best be run. The conditions desired for the spectroscopy experiment includes high concentration of molecular ions, low number of ion molecule reactions, mass identification of the molecular ions, isolation of the ions desired for study, and little or no interference from electron impact fluorescence. These conditions are controlled by several experimental variables including pressure, mass resolution, electron beam intensity, and timing of the experiment. The determination of these variables, their effect, and the range over which they are operated is discussed below.

The first variable to be determined is the duration of the ionization period (electron beam "on" time). This requires knowledge of the ionization rate and the total number of ions to be created. To determine the number of ions produced in one second, the following equation is used

$$R = in\sigma\ell \qquad \text{(II-18)}$$

where R is the number of ions produced per second, i is the electron beam current, n is the neutral parent gas number density, σ is the ionization cross section, and ℓ is the path length of the electrons. The electron beam current easily obtained in the experiment is between 3 and 50 μamps (10 μamps = 6.2×10^{13} e^-/sec) as measured at the Faraday cup. The cross sections for electron impact ionization are about 10^{-16} cm^2 for 100 V electrons[22] and the path length in our ion trap is about 3 cm. To limit the collisions of an ion to about one collision per millisecond, a pressure of 10^{-5} torr (3.2×10^{11} molecules cm^{-3}) is usually used. Substituting these values into Eq (II-18), it is found that 10^{10} ions are created in one second. The number of ions created per second is increased by increasing the pressure of the neutral parent gas or by increasing the electron beam current.

Obtaining a concentration of ions large enough to perform spectroscopic measurements has always been a problem. It is desired then to know the maximum number of ions that we are able to trap. Because no absolute measurement of the number of ions in the trap exists, equations developed by Dehmelt[11] are used to calculate the maximum number of ions expected. Although these equations are for the hyperbolic trap, it is assumed that they give reasonable estimates for the properties of the cylindrical trap because of the similar stability diagrams and trapping characteristics. The maximum concentration of ions confined in the trap is given by Dehmelt as

$$n_{max}(\text{ions cm}^{-3}) = 1.66 \times 10^{6}\ \bar{D}/z_o^{2}\ \left(\frac{\text{volts}}{\text{cm}^2}\right) \qquad \text{(II-19)}$$

where $\bar{D}$ is the pseudopotential created for the ions by the trapping fields and z_o is the half height of the trap defined previously in Section II-C2. Benalin and Audoin[9] give a much more complicated expression for n_{max} where they show that a slightly higher density is expected for the cylindrical trap. The pseudopotential, using Dehmelt's equations and our variables is given by

$$\bar{D} = 6.11 \times 10^{-3}\ \frac{V^2}{z_o^2 M\nu^2}\ \left(\frac{\text{volts}}{\text{cm}\cdot\text{amu}\cdot\text{MHz}}\right) \qquad \text{(II-20)}$$

where V and ν are the r.f. peak voltage and frequency respectively defined previously and M is the mass of ion desired to be confined. Substituting typical values found empirically (for $BrCN^+$) of V = 700 volts, ν = 0.622 MHz, M = 106 amu and z_o = 1.01 cm, into Eq. (II-20), we have $\bar{D} \cong 70$ volts. Using Eq. (II-19), it is found that $n_{max} = 10^8$ ions cm^{-3}. The ion trap volume is about 10 cm^3 which yielding 10^9 ions as the maximum total number of ions in the trap.

With an ion production of 10^{10} ions/sec, it would take 100 milliseconds to fill the trap. In the actual experiment, a 25 millisecond ionization period (electron gun "on" time) is used. From the measurement of the ions in the trap by the MEM it was found that only ~5 milliseconds of ionization period is required to fill the ion trap. This indicates that either the rate of ion production is faster than that estimated

in the preceding paragraphs or that the maximum number of ions calculated, n_{max}, is too high.

One reason that the ion production rate may have been underestimated is that the Faraday cup probably measures only a fraction of the electron beam current. It is estimated that the actual electron beam current is 5 to 20 times greater than that measured by the Faraday cup increasing the ionization rate by an equivalent amount. The ionization cross section for various ions can also be somewhat higher than the value of 10^{-16} cm^2 used which would also increase the ionization rate.

The n_{max} calculated represents the maximum ions expected with no mass selection and with no ion-molecule collisions, both of which would lower the value of n_{max}. Any mass selection would decrease the maximum number of ions in the trap by lowering the pseudopotential seen by the ions. The extent of this effect is difficult to determine. However, the number of ions observed at the MEM is found to depend on the degree of mass resolution. A resolution on the order of one a.m.u. decreased the ion signal to about 1% of the maximum ion signal obtained under low mass resolution. This is demonstrated in Figure II-14 where two mass spectra of N_2^+ with different mass resolution are displayed. (How the mass spectra are accomplished in our experiments is discussed in Section II-C5 and below. The splitting of the mass peaks is also discussed below.) The mass resolution ($\frac{m}{\Delta m}$) for the upper scan is approximately 3 whereas the mass resolution is

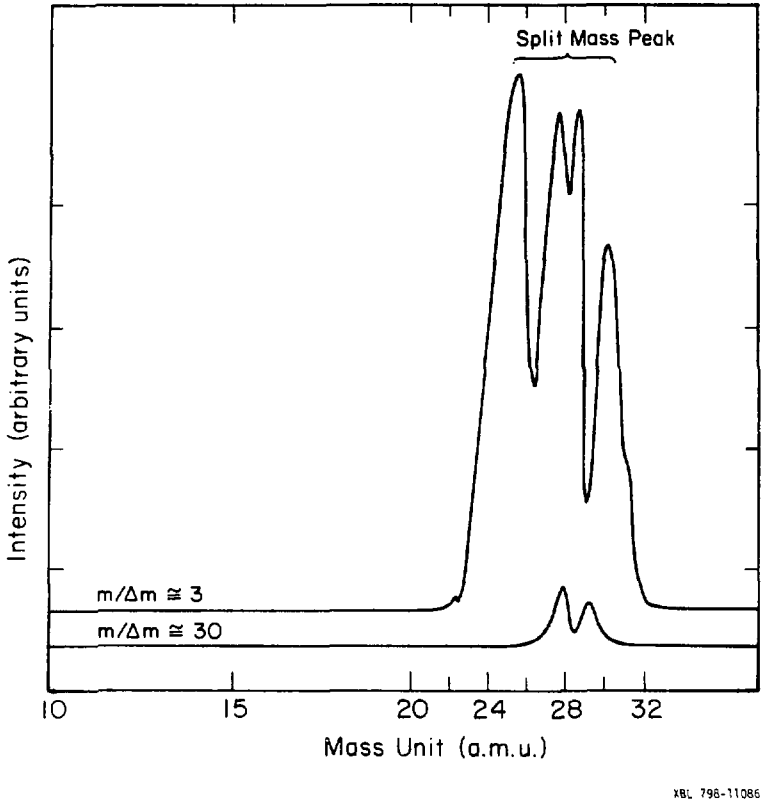

Figure II-14. N_2^+ Mass Spectra, Two Different Mass Resolutions.

about 30 in the lower scan. The dramatic decrease in ion signal under high mass resolution is clearly observed.

At a pressure of 10^{-5} torr, ions are primarily removed from the trap by ion-molecule collisions rather than ion-ion collisions. Operating under trapping conditions similar to those used in these experiments and using a hyperbolic trap, Lawson et al.[23] obtained a rate constant of 2×10^{6} $torr^{-1}$ sec^{-1} for removal of ions from the ion trap by ion-molecule collisions. (Pentane was the parent gas used in their experiments.) At 10^{-5} torr and with 10^{8} ion$\cdot cm^{-3}$, 2×10^{9} ions would be removed from the trap in one second. On a millisecond time scale, 2×10^{6} ions are expected to be removed by ion-molecule reaction which should only have had a small effect on n_{max}. Finally, the actual n_{max} obtained may be somewhat less than that calculated for the ideal trap due to imperfections in the electrodes and the electric fields applied and interferences from penetrating fields.

We have then an estimate of 10^{6}-10^{8} ions/cm^{3} in the trap which are created in a 5 millisecond ionization period. An ionization period of 25 milliseconds is used because of the maximum repetition rate allowed by the laser at 40 Hz. After the electron beam is gated off, a period of time is needed to allow excited molecules and ions to relax, to allow any mass selection to occur, and to allow the spectroscopic measurement to be made. A period of time on the order of one millisecond is required. Observing the ion signal at the MEM, it is seen to decrease less than one percent

from its maximum value in two milliseconds under the operating condition presented in the preceding paragraphs. Therefore, plenty of time exists for the spectroscopic experiment to be performed without the complication of a decreasing ion concentration.

Many of the criteria desired for the experiment are met by the experimental conditions described in the preceding discussion. A workable, although not very large, concentration of ions is obtained. The pressure is kept low enough to limit the influence of ion-molecule reactions and collisions. Enough trapping time exists after the electron beam is turned off to allow the electron impact fluorescence to disappear before performing the spectroscopic part of the experiment. The criteria left to satisfy are the isolation and identification of the molecular ions.

Isolation and identification of the molecular ions is tied up with the mass resolution where some difficulties are encountered. The problems are two-fold: difficulty in determining the actual mass resolution and the low concentration of ions trapped when in a high mass resolution mode. As was seen in Section II-C2, the mass resolution is increased by increasing the d.c. potential U while keeping the r.f. potential V fixed. Once the desired mass resolution is obtained, a mass spectrum is obtained by varying U and V while keeping their ratio constant.

As mentioned in Section II-C3, the r.f. potential $V\cos\Omega t$ that is applied to the trap is supplied by a modified version

of the mass filter supply used for quadrupole mass filters. The power for this supply is obtained from two external power supplies; a modified John Fluke 407 DR power supply and a Lamda 28 power supply. In addition to the r.f. voltage, the mass filter supply also produces the d.c. bias U on the which the r.f. voltage is floated. The magnitude of the d.c. voltage is controlled by two potentiometers on the front panel of the mass filter supply and can be measured at the d.c. voltage check point also on the front panel. The r.f. voltage can be determined by P.A. plate volt meter (on the front panel) and a graph of the r.f. peak voltage versus the P.A. plate voltage. (This graph is with the mass filter supply manual.) From the r.f. voltage and the d.c. voltage, the mass resolution can be approximated by calculating the stability parameters, a and q, and using the stability diagram (Figure II 7). The actual mass resolution is determined by running a mass spectrum. This is accomplished by using the ion measurement system described in Section II-C5 in the mode where the external timing control pulse box (PCB) provided all the logic signals needed for the 227-sg integrator. The output of the integrator is applied to the y-axis of a recorder and the d.c. voltage at the d.c. voltage test point is applied to the x-axis.

The difficulties in determining the mass resolution are many. The problems stem from both trapping characteristics and from ion measurement characteristics. First, the mass scale is not strictly linear with respect to the applied

voltage. The non-linearity also changes depending on the mass resolution invoked. In our experiments, a variety of mass resolutions are used. For this reason, the easiest method for determining the required trapping conditions is to achieve them empirically for each ionic species by observation of the ion signal and adjustment of the r.f. supply controls until the desired resolution and ion concentration is obtained.

Another problem in determining the mass resolution is the observation of split mass peaks (Figure II-14). This was also observed and explained by Dawson and Whetton.[13,24] The peak splitting seen in Figure II-14 is very complicated. The problem which arises here is the difficulty in identification of mass peaks differing by only one or two mass units. The split peaks can be made to disappear to some degree by going to higher mass resolution. However, the concentration of ions is then too small for any use except in mass spectra scans.

The problem arising in the measurement of the ions was mentioned before in Section II-C5: the point in the r.f. phase where the drive-out pulse produces the maximum ion signal is dependent on the mass/charge ratio. An example of this is shown in Figure II-15, for Ar^{+} and Ar^{++}. The solid-line spectrum shows the results when the drive-out synchronization is made for Ar^{+} where as the dashed line spectrum shows the results when it is made for Ar^{++}. The only problem that occurs here is the misrepresentation of the relative intensities of the mass peaks; the mass resolution is not effected.

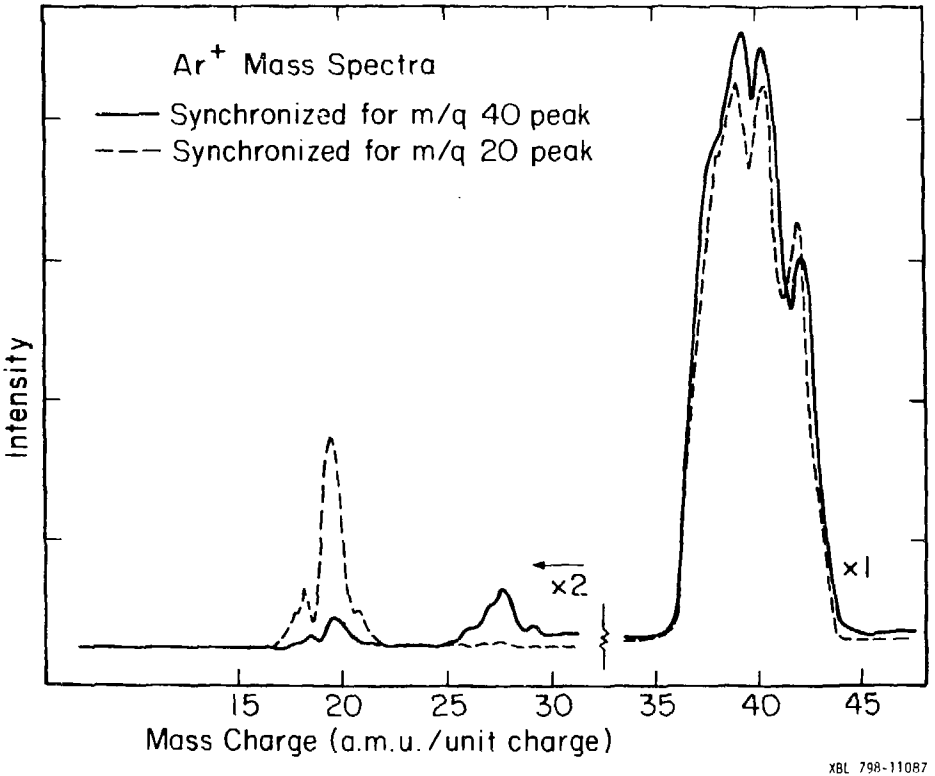

Figure II-15. Effects of Synchronization of Drive-out at Different Points in R.F. Phase.

Above all, the greatest problem with the high mass resolution mode is the low ion concentration. Most of the spectroscopic experiments are run, therefore, in the following manner. High mass resolution is used to identify the ions produced by electron impact and confined in the cylindrical trap. Then, the lowest mass resolution possible is used to exclude any interfering ions, but still maintain a high enough ion concentration. For all the ions dealt with in this work, isolation and high concentration were easily attained. In other cases, such as H_2O^+ vs OH^+, simultaneous isolation and high concentration would be difficult to obtain.

Three other characteristics of ion trapping should be mentioned. An estimate of the ion velocity in the trap is important for Doppler width considerations. Using the virial theorem and the pseudopotential $\bar{D}$, the mean velocity of the ion is deduced. The resulting expression is

$$v_{rms} = 1.39 \times 10^6 \left(\frac{\bar{D}}{m}\right)^{1/2} \left(\frac{\text{volts}}{\text{amu}}\right)^{1/2} \qquad \text{(II-21)}$$

With a pseudopotential of 70 volts and a mass of 106 a.m.u., a mean velocity of 10^6 cm/sec is obtained. This value is probably an upper limit because the pseudo-potential $\bar{D}$ is reduced to some degree by the potential created by the ions in the trap. The Doppler width of ions moving at 10^6 cm/sec varies between 0.2 and 0.5 Å (0.9 and 2 cm^{-1}) for the wavelength range 4000 to 7000 Å.

A knowledge of the distribution of ions in the trap is also of interest. Knight and Prior[25] have obtained the distribution of Li^+ in a hyperbolic trap using a laser scanning

technique. They have found the ion density to be consistent with a Gaussian distribution. Bonner, et al.,[10] have found that the potential distribution in the cylindrical trap to be very similar to that of the hyperbolic trap. The main deviations were found to occur in the corners of the cylinder where the end caps and center electrode nearly meet. The ion distribution in the cylindrical trap is expected, therefore, to be quite similar to that in the hyperbolic trap.

The final characteristic to be dealt with is the importance of initial ion velocity in determining trapping efficiency. Using computer simulation and matrix calculations, Dawson, et al.,[17] found that the trapping efficiency to be very dependent on the initial ion velocity. In fact, the trapping efficiency was found to be more dependent on initial ion velocity than on the initial position of the ions. In going from no initial ion velocity to an initial velocity of 2.22×10^3 m sec^{-1}, the trapping efficiency dropped by a factor of three. This decrease in trapping efficiency may explain the difficulty in obtaining a large concentration of fragment ions which we observed in our experiment and was also observed by Dawson, et al.,[26] when operating an ion trap in the mass selective mode. Lawson, et al.,[23] improved on the fragment ion concentration by operating the trap in a low mass resolution, total pressure mode and pulsing the ions through a quadrupole mass filter to determine the mass spectrum. They suggested that the low concentration of fragment ions observed by Dawson was a result of the trap discriminating against low mass ions.

In any case, no dramatic improvement in the concentration of fragment ions with respect to the parent ion concentration over that obtained with usual mass spectrometric techniques has ever been observed.

D. Laser and Light Entry System

1. The Laser and Its Characteristics

The laser used in our experiments is the Molectron DL-200 dye laser pumped by the Molectron UV-1000 nitrogen laser. The only modification of the nitrogen laser was the installation of the UV 1010 Retrofit Kit (supplied by Molectron) which replaced the 100 transmission cables with a metal sheet. The nitrogen laser delivers a laser pulse of between 0.8 and 1.0 megawatt in peak power at a rate of up to 40 Hz. The UV-1000 laser can be internally or externally triggered to fire. In our experiments, the laser is triggered externally by a ttl logic pulse generated by the experimental timing pulse control box (PCB) through an optical isolator circuit. The optical isolation is necessary to reduce RF interference of the other experimental electronic circuits caused by the firing of the laser.

The DL-200 dye laser consists of a U.V. focus lens, a dye cell, a dye reservoir and pump, a beam expander telescope, a grating, an output mirror, and a sine-drive motor and mechanism for moving the grating. No modifications of the dye laser were required. The alignment of the dye laser cavity is accomplished with a HeNe laser following instructions

which are included in the dye laser manual. Whenever the dye laser beam quality becomes poor (about every 3 months), the dye laser must be realigned. After alignment, the beam power and quality is maximized by adjustment of the U.V. focus lens, dye cell position, and output mirror position. The power output of the dye laser obtained closely resembles the wavelength characteristics given in the graph for the various laser dyes supplied by the Molectron Corporation, except that the overall power is lower by a factor of two. The maximum peak power of the dye laser is approximately 50 kilowatts. The usable power of the dye laser varies between 50 and 500 microjoules per pulse which corresponds to between 10^{14} and 10^{15} photons per pulse.

The bandwidth of the dye laser, controlled by the focus of the beam expander telescope, is 0.6 cm^{-1}. This bandwidth is slightly smaller than the expected 1 cm^{-1} Doppler width of our trapped molecular ions calculated in Section II-C6. Consequently, an etalon is not used to further reduce the bandwidth.

The wavelength region of the available laser dyes ranges from 3700 to 7400 Å. The short wavelength limit can be extended by doubling the frequency of the dye laser. However, because the power suffers greatly when the frequency doubler is used, no experiments described in this thesis were performed at wavelengths shorter than 3700 Å.

The wavelength scanning is controlled by the Molectron DL-040A scan control unit which operates the sine-drive

grating motor. Push buttons allow manual control of the laser wavelength. The scan control can also be operated by logic signals generated by the computer. Interfacing the computer to the scan control unit is discussed in Section II-G.

The length of the dye laser pulse is primarily determined by the duration of the nitrogen laser pulse resulting in a laser pulse approximately 5-10 nanoseconds in length. This short excitation time has several advantages. The first advantage is that the concentration of ions in the trap remains constant during the period of interrogation by the laser pulse. Secondly, the 10 nanosecond pulse length allows radiative lifetime measurements of most molecular ion excited states. The final advantage is that the effect of scattered laser light can be reduced by the use of gated detection techniques. These techniques are discussed in the Fluorescence Detection System section. The important characteristics of both the UV-1000 and the DL-200 lasers are listed in Table II-4.

2. Laser Light Entry System

To reduce the effects of scattered laser light, the laser beam is made parallel for a distance of one meter at a diameter of approximately 0.5 cm and passed through a baffle system similar to that of Zare and co-workers.[28] A diagram of the laser light path is given in Figure II-16. Two lenses are used to collimate the laser beam. A short focal length lens (11 cm) is placed a focal length distance from the dye cell. A mount for this lens was constructed and attached

Table II-4

Characteristics of UV-1000 Nitrogen Laser and DL-200 Dye Laser

UV-1000 Nitrogen Laser	
Peak Power	0.8-1.0 Mwatt
Average Power	250 mwatt
Usable Pulse Rate	1-40 Hz
Pulse Duration	10 nsec
Wavelength	3371 Å
DL-200 Dye Laser	
Peak Power	~30 kwatt
Average Power	2-20 mwatts
Power per Pulse	50-500 μjoules
Photons per Pulse	10^{14}-10^{15} photons
Pulse Duration	5-10 nsec
Bandwidth	0.6 cm^{-1}
Wavelength Tuning Range	370-740 nm
Frequency Doubled Wavelength Range	258-360 nm
Beam Divergence	2 mrad

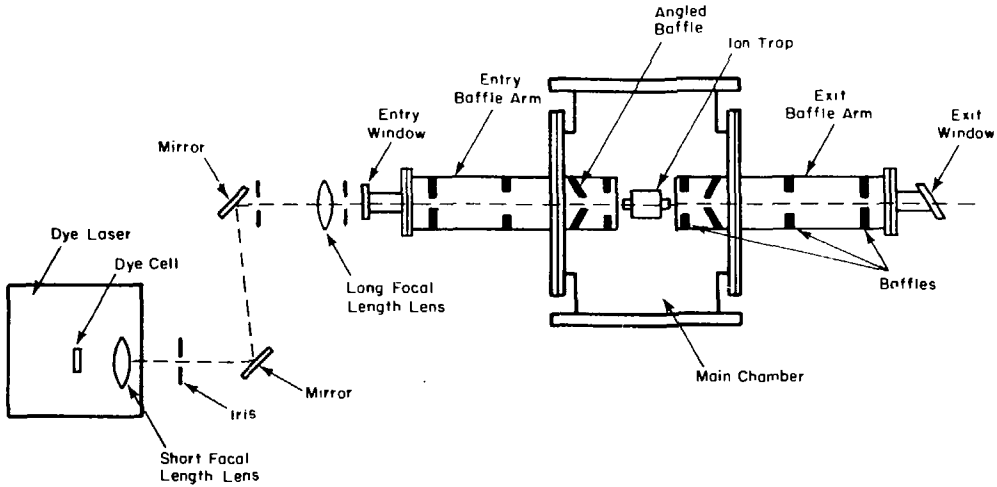

Figure II-16. Light Path and Baffle System.

to the dye laser cabinet. The design drawing numbers are given in Appendix 1.) A long focal length lens (800 cm) is placed approximately 800 cm from the first lens and just before the entry window in order to keep the beam collimated through the vacuum chamber. Two quartz mirrors and three irises are used to align the laser beam through the baffle arm system and the ion trap. The mirrors are of 90% reflectance in the visible region and were supplied by Optical Industries. The mirrors are placed in Lansing mounts which have micrometers for accurate adjustment.

The entry window is 1.5 inches in diameter and 1/8 inch thick. The front and back surfaces of the window are at an angle of 5' with respect to one another to negate etalon effects and are polished to a high surface quality to reduce scattered laser light. Because the laser light is not 100% polarized, the entry window is placed perpendicular to the laser beam instead of at the Brewster angle. When using a Brewster angle entry window, the polarized light for which the window is not at the Brewster angle causes many scattered light problems due to reflections in the window. The exit window is, however, at the Brewster angle with a Wood's horn below it to capture any light reflected by the window. The exit window is 2.0 inches in diameter, 1/8 inch thick, and polished to the same surface quality as the entry window.

As can be seen in Figure II-16, the baffle system is comprised of an entry and an exit baffle arm. Each baffle arm consists of a flange for mounting a window assembly, a

tube to hold the baffles, and a flange to mount the baffle arm to the main chamber. As discussed in Section II-B, the baffle arm mounting flanges of the main chamber are concentric to 0.001 inch. Interlocking surfaces are used on these flanges and the baffle arm flanges so that alignment of the baffle arms is accomplished just by mounting the arms to the chamber. Because the window assembly flanges require no critical alignment, they are simply bolted to their respective flanges on the ends of the baffle arms. Each baffle arm is approximately one-half meter in length placing the entry and exit windows (which scatter the laser light) well away from the light detection region. The total length of one meter over which the laser beam has to be collimated still allows a reasonable beam diameter (<0.25").

The baffles are used to further reduce the light scattered by the windows. The baffles also reduce the interference of fluorescence from the dye cell which follows the laser beam, but cannot be as well collimated. The baffles are made of blackened brass and fit tightly in the baffle arm tubes. The inner surface of the tube is smooth enough to allow the baffles to slide along the entire length of the tube. The baffles are kept in place by blackened aluminum locking rings which are placed between the baffles and lock into place by pressure exerted by a threaded end piece.

Three types of baffles are used all of which are 1/32 inch thick at the aperture. Two types have either 0.25 inch or 0.75 inch aperture diameters with surfaces perpendicular to the laser beam. The third type has the aperture surface

at a 60° angle with respect to the laser beam. As explained by Dare and co-workers,[28] the purpose of the angled surface is to reflect any scattered light that strikes this baffle (and is not absorbed) up to the tube surface. The baffles are placed in such a manner and the apertures are large enough in the ion trap that any scattered light which passes completely through one baffle arm also passes completely through the trap and strikes a baffle in the other arm.

The alignment of the ion trap with respect to the baffle arm axis is accomplished in the following manner. The baffle arm mounting flanges on the main chamber are designed and constructed so that the baffle arm axis intersects a line perpendicular to it and passing through the center of the top port flange. The ion trap which is connected to the ion trap apparatus flange, is then roughly aligned by simply placing it in the main chamber. As described in Section II-C3, the ion trap is mounted to a horizontal adjustment plate with three vertical adjustment screws. Slots in the adjustment plate allow alignment along the axis horizontal and perpendicular to the baffle arm axis. A holding plate slides in the adjustment plate by turning a screw on one side which moves the trap into position. The aligned position is secured by a screw on the opposite side of the adjustment plate. Nuts on the three vertical adjustment screws allow alignment along the axis vertical and perpendicular to the baffle arm axis and also allow leveling of the trap along the baffle arm axis. Locking nuts secure the trap into position.

Rotation around the vertical axis is prevented by two dowel pins in the ion trap apparatus flange which mount into two alignment holes in the top port flange.

The first alignment of the trap was accomplished using a cathotometer to align crosshairs on the entry and exit holes of the ion trap with crosshairs placed on the baffles. After this first alignment, the laser beam, once aligned through the baffle arms, is used to position the trap. Once the trap is locked into the correct position, realignment is usually not necessary even when the apparatus is removed from and then replaced in the chamber.

The baffle arm system was found to work reasonably well. Before the baffle arm system was incorporated, scattered light hindered experiments to a great degree. Many times the scattered light was so intense that severe afterpulsing in the photomultiplier tube was observed.[29] With the laser at peak power and using this baffle system, a signal corresponding to only 200 photoelectrons is observed at the time of the laser pulse and very few scattered photons (<1 count/laser pulse) are observed after this time. With the gated detection system and the baffle system no severe interference from scattered light occurs.

5. Laser Power Measurement

Two types of laser power measurement are required for our experiments. The first measurement determines the absolute laser power and is required to determine the dye laser's performance. An Eppley 16 junction thermopile is used to measure the absolute laser power.

Because the time constant is very long for the Eppley thermopile, an alternate measurement is needed for the shot-to-shot determination of laser power used to normalize the fluorescence signal. The laser power measurement scheme is shown in Figure II-17. After passing through the baffle arm system and exiting the vacuum chamber, the laser beam strikes a lens mounted at approximately 45 degrees. This lens acts as a beam splitter to allow the major part of the beam to enter the wavelength calibration device which is described in the next section. The 4% reflection from the front surface of the lens is used to determine the laser power. A lens is used instead of a glass slide to avoid any interference that might be caused by the reflection from the back surface.

The 4% reflection is directed through a 1% transmittance neutral density filter and into a PIN-8LC pin photodiode. The U.D.T. Model PIN-8LC photodiode is a low capacitance model with a fast time response. The photodiode is used in the standard reverse biased mode. The 1% neutral density is needed to reduce the signal to a level that does not saturate the measuring device, the 227-sg gated integrator. (The 227-sg integrator is described in the Fluorescence Detection System section.) To allow adjustment of the signal to a desired level, it is first sent through a variable voltage divider before being integrated.

Because the 227-sg integrator requires a detection gate in order to perform the integration, the signal from the laser

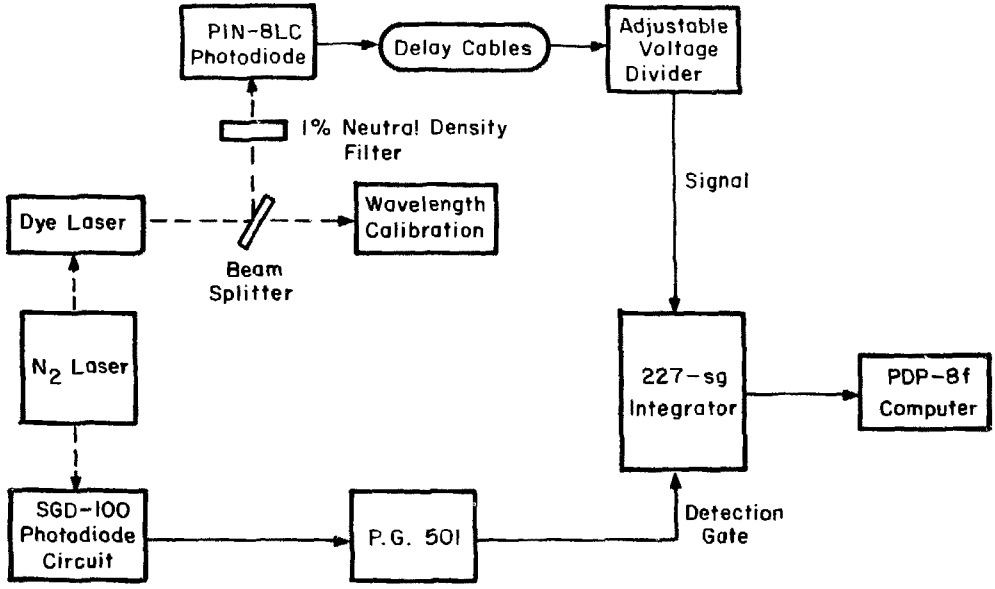

Figure II-17. Laser Power Measurement.

power photodiode cannot be input directly into the integrator. The laser power detection gate is triggered by a ttl logic pulse generated by another photodiode circuit discussed in Section II-E4. This photodiode (EG&G SGD-100) is placed behind the back mirror of the nitrogen laser. When the nitrogen laser is fired, the photodiode detects the laser light and its associated circuitry generates a ttl logic pulse. The logic pulse is used to trigger various components of the experiment including the detection gate for the laser power. Because of the delay time in generating this ttl logic pulse, the signal from the laser power photodiode has to be delayed before it is sent to the integrator. This delay is accomplished using long RG-58 signal cables which delay the signal approximately 1 nanosecond per foot. A delay of ~50 nanoseconds is necessary.

The ttl logic signal from the timing photodiode circuit is sent directly to a P.G. 501 pulse generator where a detection gate of the correct duration and magnitude is produced. The detection gate encompasses the time of the laser power signal and is applied to the 227-sg integrator. The signal from the integrator can be displayed on an oscilloscope and sent to the PDP-8f computer. The computer corrects the signal for the spectral response of the photodiode, stores the signal, and normalizes the fluorescence data with respect to the laser power. The spectral response of the photodiode is obtained from the Silicon Photodetector Design Manual supplied by U.D.T.

4. Wavelength Calibration

The wavelength calibration of the dye laser is obtained with the use of the optogalvanic effect (OGE). While several workers[30] have studied the various aspects of the OGE, it first came to our attention in an article published by King and Schenck.[31] The OGE provides a simple yet accurate method for wavelength calibration. It also provides a means of measuring the dye laser bandwidth.

A diagram of the wavelength calibration system is shown in Figure II 18. The laser light passed by the beam splitting lens is directed into a Westinghouse Cu hollow cathode lamp filled with Ne gas. The transitions observed are primarily Ne transitions which extend throughout the visible region. Because Ne atoms in excited states also exist in the lamp, transitions from these states also occur. In fact, most of the transitions observed populate high-lying metastable states. This increase in population leads to an increase in the collisional ionization rate causing a decrease in the voltage drop of the discharge in the lamp. The measurement of this change is discussed below.

The power to the lamp is supplied by a Power Designs Pacific H.V.-1556 d.c. power supply and is usually kept at 300-400 volts. A current limiting resistor is placed between the power supply and the lamp. A capacitor placed in parallel with the voltage line to the lamp's electrode eliminates the d.c. level of the electrode, but allows measurement of the fluctuations in the lamp's potential.

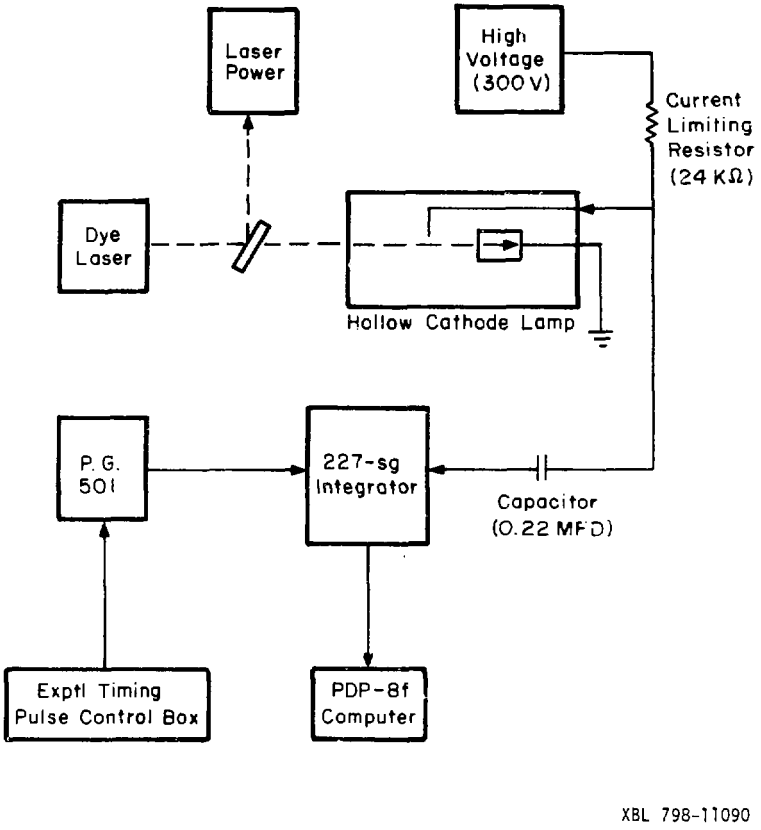

Figure II-18. Wavelength Calibration System.

The signal produced by the lamp can be observed on an oscilloscope or applied to the 227-sg gated integrator. Because the transitions primarily lower the potential drop across the lamp, a negative voltage signal pulse is produced when the laser light is resonant with a transition.

Again, a detection gate is required by the 227-sg in order to perform the integration. The signal from the lamp has a long time constant (a few milliseconds) due to the electronic circuit and also due to the migration time of the Ne ions to the electrodes. For this reason and because an accurate measurement of the signal intensity is not required, a variety of logic signals can be used to trigger the detection gate. The same logic signal produced by the external timing pulse control box to trigger the detection gate for the ion density measurement is used to trigger the detection gate for the optogalvanic signal. The detection gate is produced by a P.G. 501 pulse generator and is applied to the 227-sg integrator. In this case, the detection gate does not encompass the whole signal pulse resulting in integration of just part of the waveform. The wavelength calibration occurs concurrently with the laser induced fluorescence experiment, the optogalvanic signal from the integrator being gathered by the PDP-8f computer to be stored with the other experimental data.

Because the Ne linewidths in these lamps are on the order of 0.05 Å, the width of the bands observed in our optogalvanic spectra determine the dye laser bandwidth to at least 0.1 Å.

The bandwidth of the laser can be minimized by adjusting the beam expander telescope focus while observing an optogalvanic transition. Several transitions which exhibit the bandwidth of the laser are shown in Figure II-19. A typical optogalvanic spectrum covering one laser dye region is shown in Figure II-20. The lines were assigned by referring to the tables given in reference 32.

E. Fluorescence Detection System

1. Expected Signal Level

To derive an estimate of the signal level the fraction of light absorbed, I_a/I_o, must be calculated. In the weak absorption limit it is given by[33]

$$\frac{I_a}{I_o} = (8.83 \times 10^{-13})\ N_{mv''J''} \ell f F \qquad \text{(II-21)}$$

where $N_{mv''J''}$ is the number of molecules per cm^3 in the v'' J'' vibrational-rotational level of the m^{th} electronic state, ℓ is the absorption path length (cm), f is the oscillator strength of the transition and F is the Franck-Condon factor. From Section II-C, we found the path length to be ~3 cm and the concentration of ions was expected to vary between 10^6 and 10^8 ions cm^{-3}. Using rotational partition functions ranging from 10 to 10^3, f between 10^{-3} and 10^{-2}, and F to be between 3×10^{-2} and 3×10^{-1} in Eq. (II-21), it is found that the fraction of light absorbed will vary between 10^{-13} and 10^{-7}.

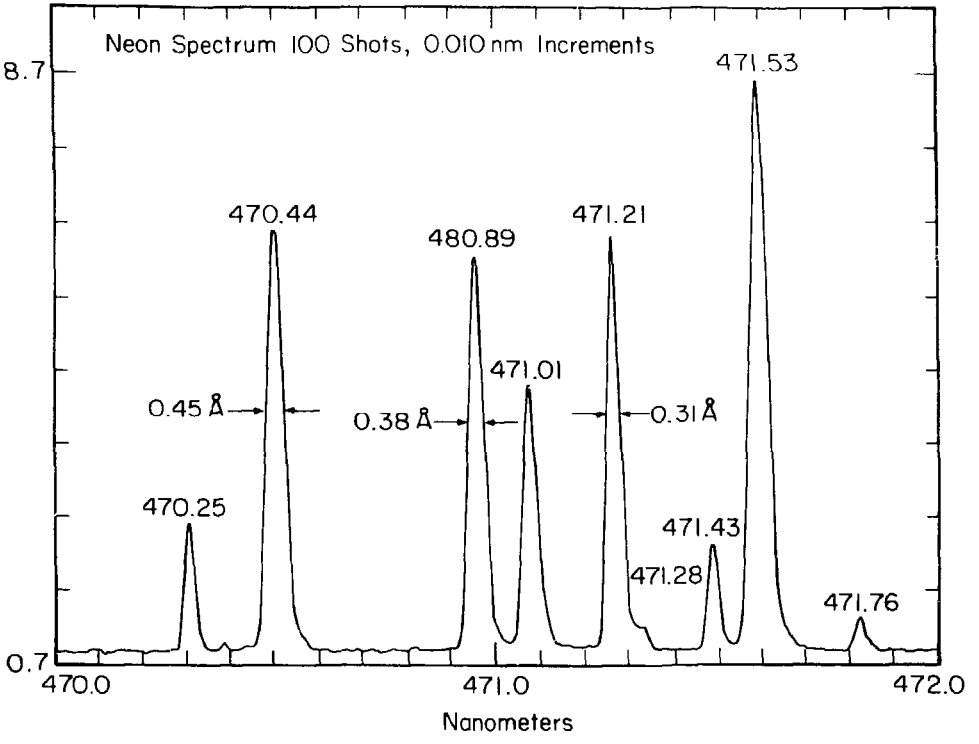

Figure II-19. Determination of Laser Bandwidth with Optogalvanic Technique.

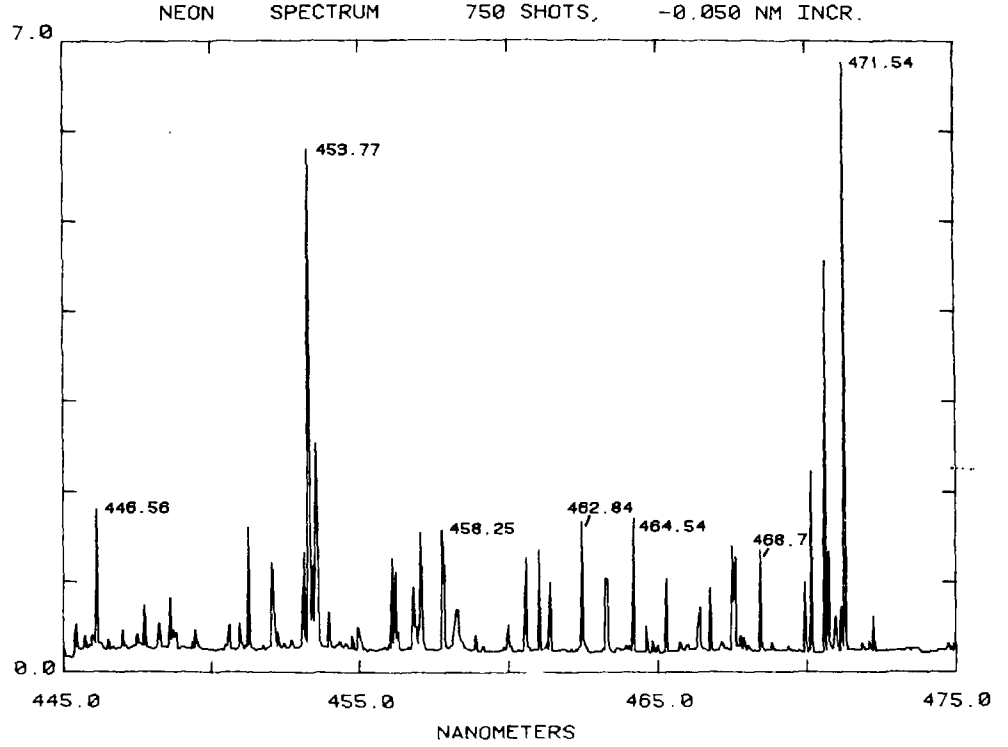

XBL 799-11262

Figure II-20. Typical Neon Spectrum Used to Calibrate Laser Induced Fluorescence Spectrum.

This model is used to calculate the MPD of SF_6. The algorithm is a simple time integration of Eq. 1, 2, 4, and 6 with the initial condition that all the population is initially in the lowest level. By varying the time step for integration around 10ps, it is ascertained that round off errors are negligible. The laser pulse profile, I(t), used in these calculations is shown in Fig. 11 and is representative of the pulse envelope from a Tachisto 215G laser ignoring the mode locking spikes of the pulse. The mode locking spikes in the 60ns multimode pulse were considered in our calculation by assuming that the mode locking doubles the peak intensity achieved by a single mode pulse. The limited time resolution of the detector and oscilloscope prevented us from measuring the actual peak intensity.

With the quasi-continuum absorption cross section assumed to have the form $\sigma_m = \sigma_0 e^{-\beta m}$, there are four independent parameters to be determined: γ and I_0 for excitation up the discrete vibrational ladder and σ_0 and β for excitation through the quasi-continuum. The parameters are chosen to fit the experimental results of Black et al.[12] on the average number of photons absorbed per molecule, <n>, versus energy fluence at 944 cm^{-1} using three different laser pulses: 0.6ns and 60ns single mode and 60ns multimode. We find that our calculation closely reproduces the experimental curves of Black et al.[12] with $\gamma = .5$, $I_0 = 20$ MW/cm^2, $\sigma_0 = 8\times10^{-19}$ cm^2, and $\beta = .042$. This is shown in Fig. 12. The fit to the 0.6 ns pulse is insensitive to the parameters γ and I_0 in the calculation because the maximum laser intensity is much larger than I_0. So, the 0.6 ns pulse result is used to find σ_0 and β and the 60ns single mode pulse result is used to find γ and I_0.

photomultiplier tube per laser pulse. The lower limit on the number of photons points out the importance of minimizing sources of background such as scattered laser light and electron impact fluorescence.

The photomultiplier tube we use has a quantum efficiency of 30% which yields 0.3 to 3 x 10^3 recordable events per laser pulse after a transition has occurred. This large range indicates a need for two different measurement schemes. In order to get an accurate measurement at high signal intensities, integration of the signal is necessary. At lower signal rates, photon counting techniques must be employed. The two different detection schemes are discussed in Section II-E3. The next section describes the photomultiplier tube and its associated electronics.

2. Photomultiplier Tube and Gated Dynode Chain

Besides increasing the collection efficiency, the Fresnel lens also allows the photomultiplier tube (PMT) to be moved further away from the trapping region. Using a point source approximation at the center of the trap, the one inch focal length lens focuses the light to a point 16 inches away. Because of the possible nonuniformity in the photocathode (2 inches in diameter), it is best not to sharply focus the fluorescence onto its surface. For this reason, the photocathode is placed about 10 inches from the Fresnel lens. Before the light reaches the PMT, it travels through a quartz window. When the wavelength of the fluorescence is less than

4000 Å, the acrylic Fresnel lens must be replaced with a quartz lens.

Due to its excellent sensitivity in the 300 to 500 nm wavelength region,[29] the RCA 8575 photomultiplier tube is used. It has a bialkali photocathode (K-Cs-Sb) and 12 BeO dynodes. Other excellent characteristics of the 8575 include high gain (over 10^7 at 2000 V), low dark noise, and fast rise and transit times (<10 nsec). The high voltage supply for the PMT is a John Fluke 408A power supply and is usually operated at 2200 V. Because the impedance of the anode transmission lines is 50 ohms, care should always be taken to terminate the PMT signal output into 50 ohms.

The dynode circuit for the PMT to which the high voltage is applied is designed for fast pulse response operation. To further reduce the effects of scattered light, the dynode chain is also designed for gated operation. At the time of the laser pulse, the scattered light signal can be large enough to interfere with the output signal of the PMT. The gated dynode circuit eliminates this problem by leaving the tube at low gain during the time of the laser pulse and then switching to high gain thereafter.

Most gated dynode chain designs require a long time for PMT "turn on" and also produce much "ringing" in the output signal. The design chosen for our dynode chain is that of Ramirez and Kruse[34] which eliminates these problems. With their design, they achieved a PMT turn on time of $\lesssim$30 nsec with less than 20 mV of ringing. Two other important

characteristics to note are that the time jitter between application of the gate signal and PMT turn on was much less than one nanosecond and the tube gain in the "on" mode is the same as that of the ungated dynode chain.

The strategy in their design is to lower the gain of the PMT by changing the resistances at two places in the dynode chain away from the important initial focusing dynodes. In their design (as well as in ours) a 10 MΩ resistor is placed between dynodes 3 and 4 and between dynodes 7 and 8 causing the gain to be lowered at these two points. An overall decrease of a factor of 100 is obtained. The circuit diagram for our gated dynode chain and its power supply is shown in Figure II-21. Two SCR circuits, triggered by a ~20 V pulse, switch the resistances between these dynodes back to their normal values (100 kΩ) restoring the PMT to its normal gain. After being triggered, the SCRs will conduct for several milliseconds leaving the tube at high gain for this amount of time.

In our experiment, the nitrogen laser light is detected by an EG&G SGD 100 photodiode. The photodiode's signal is sent to a Schmidt trigger and one shot circuit which generates a ttl logic pulse. This pulse, in turn, triggers the high voltage pulse in the gated dynode chain used to trigger the SCR's. Including all of these delay times, the PMT can be switched from low to high gain in ~60 nanoseconds from the time the laser fires. The ringing produced at PMT turn on was very small (<25 mV) and did not interfere with the

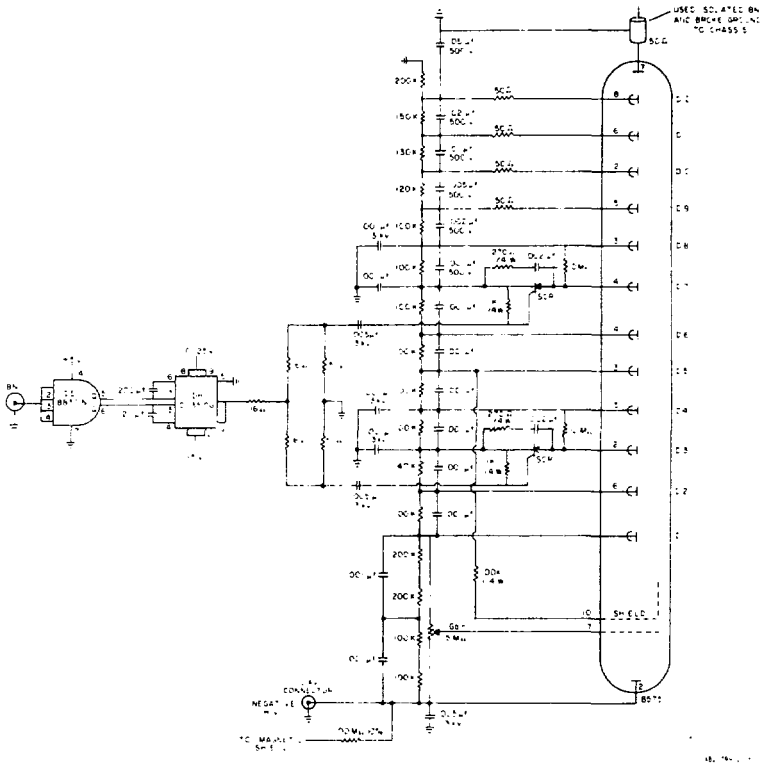

Figure II-21. Gated Dynode Chain Circuit.

fluorescence measurement. The drawing numbers of the circuit diagrams for the gated dynode chain and its power supply are given in Appendix 2.

The PMT and gated dynode chain are placed into a Pacific Photometrics Model 3463 water cooled PMT housing. The cooling of the PMT is quite important because of the heat generated by the gated dynode chain logic circuits. Without the cooler, the high temperature causes the PMT to become too noisy to be used. Using water to extract heat from the thermoelectric elements, the housing cools the tube to about -30°C. There is also a continuous ground cover for the entire housing unit to eliminate RF interference. The housing mounts on the main chamber top flange with 4 screws and forms a light-tight shield with the quartz window mount. There is room between the quartz window and the PMT to allow for the placement of filters in the event they are needed. This configuration can be seen in Figure II-22 where a schematic of the whole fluorescence detection system is shown. The rest of the components in this detection system are described in the next section.

3. PMT Signal Measurement System

As pointed out previously in Section II-D1, two detection systems are required to handle the wide range of expected signal levels. Although the signal is measured differently by the two systems, both signal measuring instruments are gated. The gated signal detection increases the signal-to-noise ratio by sampling the PMT output only when signal is

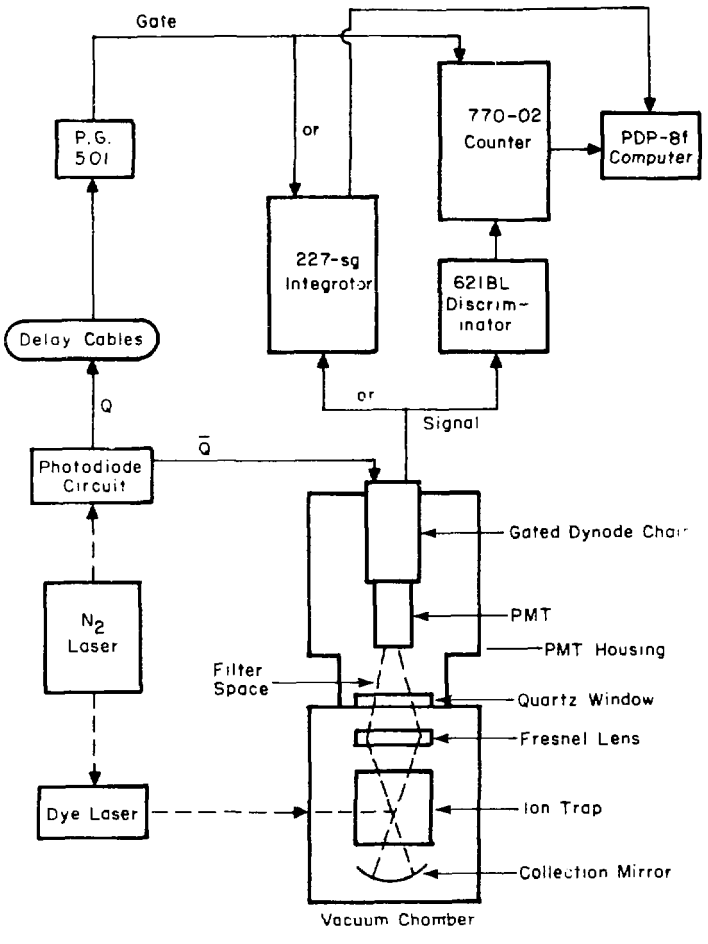

Figure II-22. Fluorescence Detection System.

expected to occur. The fluorescence detection gate is produced in both detection systems by a Tektronix P.G. 501 pulse generator.

The P.G. 501 is a very versatile pulse generator. It can be operated internally or triggered externally by a ttl logic pulse. Both positive and negative polarity pulses are available whose magnitudes can be varied up to 5 volts. The time duration of the pulses can also be varied from ten nanoseconds to tens of milliseconds. All of these features are put to use in the different detection systems.

All of the power for fluorescence measurement instruments is supplied by a NH-84A Nuclear Instrument Module (NIM) Bin. An overall view of the fluorescence detection system and its timing is described in Section II-E4. The integration and counting instruments will now be individually discussed.

a. L.R.S. 227-sg Quad Gated Integrator

For the higher signal levels, integration offers the most accurate measurement of the PMT signal. The 227-sg integrator was selected to perform the integration for several reasons, the most important of which is its high sensitivity. A signal of 100 picocoulombs is full scale for the integrator. At a PMT gain of 10^7 this amounts to 62 photoelectrons which indicates that no amplification of the PMT signal is necessary. The integrator also requires no prior pulse shaping, allowing the PMT output to be input directly with no preamplifier. For high signal intensities, the signal can be kept below full

scale by decreasing the PMT gain and by using a small detection gate.

The 227-sg was also selected because it provides four identical pulse integrator and storage channels with individual external gate inputs. The 227-sg can then be used to measure the four signals generated by this experiment; the fluorescence, the laser power, the laser calibration, and the ion density. Each channel has its own controls for input and output zeroing and for full-scale adjustment. After integration, an output amplitude for each channel is provided proportional to the area of the input pulses which were contained within its externally generated gate interval. The outputs are stored by each channel until a common clear pulse (which clears all channels) is received. The output of each channel is available at its own individual test point or at a multiplexed output. The test point outputs are used for observation of the individual channels on an oscilloscope. The multiplexed output is used for interfacing with the computer.

For control of the multiplexed output, a connector exists through which the necessary logic signals from the PDP-8f computer are transmitted. Each channel's output can be independently strobed onto the multiplexed line. The computer then measures the signal of a channel by strobing its output onto the multiplexed line which is, in turn, applied to an analog-to-digital converter. The converter, which is on the computer interface board, digitizes the signal for the

computer's use. After all the channels have been measured, the computer sends a ttl logic pulse to clear all the channels of the integrator.

The 227-sg integrator is packaged in an AEC #? width module which plugs directly into the NIM bin. The 227-sg integrator requires the external gates applied to be -0.5 volts in magnitude. The integration begins on the leading edge of the pulse and ends on the trailing edge. The 227-sg originally only allowed a maximum duration of 100 nanoseconds for the gate interval. Because many ions have radiative lifetimes on the order of microseconds, the 227-sg was modified to accept a gate duration of 2 microseconds.

The integrator is used primarily to obtain the spectra of molecular ions with short radiative lifetimes (<200 nanoseconds). Because the integrator is more insensitive than the counting system to the RFI noise generated by the nitrogen laser, its detection gate can be placed closer to the firing time of the laser. Therefore, the integrator performs better for short radiative lifetime ions than the counting system. For ions with long radiative lifetimes (>200 nsec), the counting system is found to be more reliable and provides better signal-to-noise statistics. When the counting system is used for the fluorescence measurement, the integrator is still used to measure the other experimental data signals.

b. The Counting System

The photon counting system consists of two components, a pulse discriminator and a pulse counter. The L.R.S. 621 BL Quad Discriminator used in our experiments has four channels

each with a variable threshold and output pulse width. (The 621 BL is packaged in an AEC #1 module). However, only one channel is utilized. The threshold level can be varied between -30 and -1000 mV and an output for measuring the magnitude of this level is provided. Because the threshold can be as low as -30 mV no amplification of the PMT signal is necessary. The 621 BL also accomplishes all the pulse shaping, requiring no preamplifier between it and the PMT. The output pulse width can be varied from 5 to 1000 nanoseconds which allows a maximum counting rate of 100 MHz. The 621 BL has 5 outputs and 1 complimented output. The output consists of 0.5 volt NIM logic pulses which are input into an Ortec 770 gated counter.

The 770 counter is a 6-decade scaler which has a maximum counting rate of 100 MHz and is packaged in an AEC #2 width module. The negative input accepts standard NIM logic pulses and has a fixed threshold at -250 mV. The counter gate input requires grounding to inhibit counting which is again accomplished by a P.G. 501. The output is displayed on a 6-digit LED visual readout. A signal indicating when an overflow of these 6 digits has occurred is also provided. The -02 option available from Ortec is used with the 770 counter to allow for parallel data output of the number count to the computer. The number count is stored in 24 binary-coded-decimal bits which can be strobed by the logic included in the 770-02 option. A modification in the logic (which is documented in the 770 manual) was made to allow just 12 of the 24 BCD bits to be strobed at a time. This is

required because the PDP-8f is a 12 bit word computer. Logic is also included for reseting the number count to zero (with a ttl logic pulse) after it has been read out.

4. Fluorescence Detection Scheme

In Figure II-22, a schematic diagram of the entire fluorescence detection system is given. With the aid of this figure the timing and interconnections involved in this measurement is described. When the laser fires, the SG-100 photodiode detects the light and its circuit (using a Schmidt trigger and a One Shot) generates two logic pulses denoted Q and $\bar{Q}$ in the diagram. The $\bar{Q}$ pulse triggers the gated dynode chain and turns the PMT on in ~60 nanoseconds. The signal from the PMT is sent to either the counting or integrating instruments.

The Q pulse is used to trigger the detection gate for either measurement system. The actual time for initiation of the detection gate with respect to the laser pulse varies depending upon the experimental conditions. When using the integrator for species with short radiative lifetime, it is usually desirable to have the detection gate as close as possible (~60 nsec) to the laser pulse. For longer lifetime species, a delay of between 100 and 300 nanoseconds is used to decrease the background while not affecting the fluorescence signal output to a great degree. Two main sources of noise in our experiment are scattered light from the laser and RFI noise at the time the laser fires. Both of these background sources are greatly reduced by delaying the

detection gate with respect to the laser pulse. The delay is accomplished by sending Q through RG-58 signal cables which delay the signal one nanosecond per foot of cable.

After Q is delayed, it is sent to a P.G. 501 pulse generator to produce a detection gate of the proper time duration. The time duration is primarily determined by the lifetime of the fluorescing species. Usually a period of several radiative lifetimes is used. However, the final time duration is decided upon by varying it until the best signal-to-noise ratio is obtained. The detection gate is applied to the measuring device being used. The signal is then measured during the gate interval and retrieved by the computer when needed. How the timing of the fluorescence measurement is synchronized with the other data measurements is described in the next section.

F. Experimental Timing Circuitry and Timing of Experiment

1. The Experimental Timing Pulse Control Box and the Timing of an Experimental Cycle

In the previous sections of this thesis, the various functions and measurements which make up the experiment were discussed separately. To understand how these pieces are integrated to form the whole experiment is best accomplished by describing the timing of the experiment. The experiment consists of the repetition of a number of cycles at a particular wavelength. After a preselected number of these cycles, the wavelength is advanced by a predetermined increment and another set of cycles is begun. A spectrum is completed when the entire wavelength region desired has been covered.

Each experimental cycle consists of: an ionization period, a waiting period, excitation of the ions, laser power measurement, fluorescence detection, ion density measurement, and wavelength calibration. The timing of one of these experimental cycles is shown in Figure II-23. As can be seen in this figure, the experiment begins with the ionization period which lasts for 20 milliseconds. The trapping of the ions occurs continuously throughout the experiment. The electron gun is then gated off and a waiting period ensues which allows for mass selection of the desired ion and the decay of electron impact fluorescence. The waiting period is variable, the extent being primarily determined by the radiative lifetime of the predominate excited state species created by electron impact. After the waiting period, the laser is triggered and a 10 nanosecond pulse of light excites the ions. The laser power is measured at this time. A delay of 60 to 300 nanoseconds follows the laser pulse before the fluorescence measurement takes place. The length of this delay is determined by the amount of background present following the laser pulse. The length of fluorescence detection time is usually set at 2 to 3 times the radiative lifetime of the ion being studied. Immediately after the fluorescence measurement, the ions are driven out of the trap for a density measurement. The drive-out pulse, as mentioned before, is synchronized with the r.f. potential applied to the ion trap. At the same time as the ion density measurement, the optogalvanic signal used for wavelength

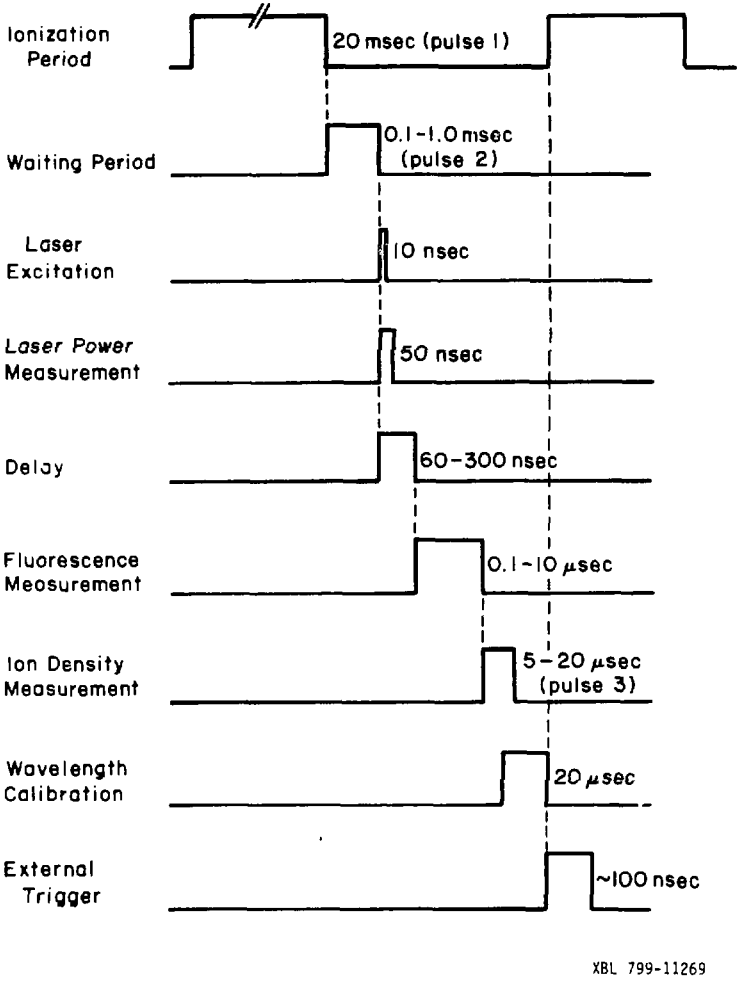

Figure II-23. Experimental Cycle Timing.

calibration is measured. Because this measurement requires a longer period of time than the ion density measurement, its end signals the completion of the experimental cycle. The PDP-8f computer recognizes the end of the cycle and generates a logic pulse (external trigger) to begin a new experimental cycle. Because the ionization period is so long, the computer can start a new cycle and retrieve the experimental data from the previous cycle during this time.

The computer controls only the initiation of an experimental cycle, the scanning of the laser, and the data gathering. The timing control of an experimental cycle is handled by the experimental timing pulse control box (PCB). The PCB contains the logic circuitry which generates 3 ttl logic pulses and two high voltage pulses. The high voltage is actually applied to the PCB from an external power supply, but 2 PCB transistor switching circuits produce the high voltage pulses required in the experiment. The circuit and logic diagram numbers for the PCB are given in Appendix 2.

The first pulse (pulse 1), generated by the PCB, controls the electron gun "on" time (the ionization period). The ttl logic pulse is used in the transistor circuit to produce a high negative voltage pulse to gate the electron gun off. The magnitude of this pulse is controlled by a potentiometer. Another potentiometer controls the time duration of pulse 1. The trailing edge of pulse 1 triggers the second logic pulse, pulse 2.

The length of pulse 2 determines the waiting period between electron gun shut off and laser triggering. The desired length of the waiting period is set by a potentiometer which controls the time duration of this pulse. Unlike the other logic pulses produced by the PCB, there is no high voltage pulse associated with pulse 2. The trailing edge of this logic pulse triggers the laser to fire.

The third pulse produced by the PCB must be triggered externally. As will be seen below, a logic pulse which synchronizes the trailing edge of the fluorescence detection gate with the r.f. phase is usually used to trigger pulse 3. (It should be noted that pulse 2 is used in place of the fluorescence gate to trigger pulse 3 when it is desired to either check the operation of the PCB or to obtain a mass spectrum.) Pulse 3 controls the ion density measurement. It is applied to a transistor circuit to produce a high negative voltage pulse which drives the ions out of the trap. The magnitude and duration of this pulse can be varied by separate potentiometers. The duration of the logic pulse is the same as the duration of the high voltage pulse associated with pulse 3. As mentioned in Section II-C5, the duration of the high voltage pulse has no effect on the resulting ion signal provided it is longer than one r.f. cycle. The length of pulse 3 can then be varied to trigger the detection gate at the correct time for the ion measurement. As was also described in Section II-C5, the ion signal occurs 5 to 10 microseconds after the leading edge of pulse 3

depending on the mass of the ion. Because this time is longer than the time of one r.f. period, 1.6 μsec, the length of pulse 3 can be set to this time and the trailing edge used to trigger the detection gate.

The final aspect of the PCB to consider is the triggering of a new cycle which begins with pulse 1. The PCB is designed to operate in an internal or external triggering mode. In the internal mode, the trailing edge of pulse 3 is used to trigger the beginning of a new cycle. However, the trailing edge of pulse 3 is first applied to a delay circuit. The purpose of the delay circuit is to allow the ion signal measurement to be entirely completed before a new ionization period begins. The internal mode of operation is used whenever the computer is not utilized. The computer is not usually used when obtaining a mass spectrum or when checking the experimental timing circuits.

In the external mode, the beginning of an experimental cycle is triggered by an external source, the computer. In this mode, no delay time is necessary as in the internal mode. All of the components involved in the timing of the experiment when operated in the external mode are described in the next section.

2. Complete Experimental Timing Circuitry

In Figure II-24 the interconnections between the different components involved in the timing of the experiment are displayed. Four Tektronix P.G. 501 pulse generators are used to generate the detection gates for the fluorescence signal, the laser power, the ion signal, and the optogalvanic

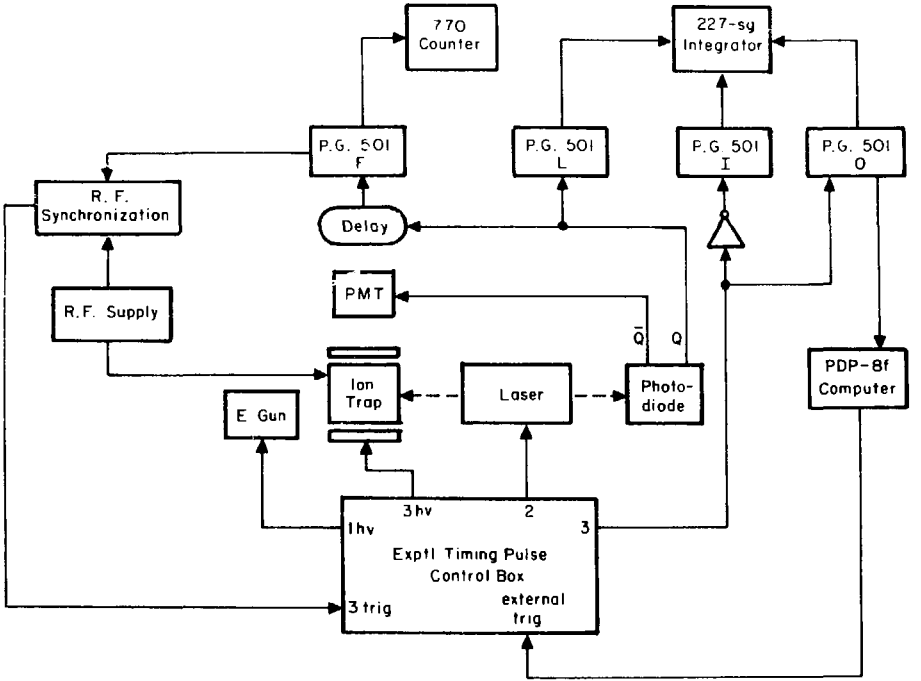

XBL 799-11267

Figure II-24. Complete Experimental Timing Circuitry.

signal (wavelength calibration) and are labeled F, L, I, and O in the figure, respectively. The detection gates are sent either to the 770 counter or the 227-sg integrator where the data signals are measured and stored. These and all of the other components involved in the various measurements have been described in their respective sections. To see how they are synchronized it is best to follow the timing signals through an experimental cycle while referring to Figure II-24. It should be noted that only the timing signal lines are shown in Figure II-24 and no data signal lines are present.

The experiment begins when the PCB receives a signal from the computer at the external trigger input. This initiates pulse 1 turning on the electron gun. After pulse 1, the electron gun is gated off and the waiting period, pulse 2, begins. The PCB uses the compliment of the logic pulse 2 to trigger the laser to fire at the end of the waiting period. This logic pulse is actually sent first through an optical isolater before reaching the laser to isolate the rest of the experiment from the laser's electrical circuits.

After the laser is fired, the timing control is removed from the PCB and is given to the P.G. 501's. Light from the nitrogen laser triggers a photodiode circuit which produces two logic pulses, Q and $\bar{Q}$. Whereas $\bar{Q}$ turns on the PMT for fluorescence detection, Q is used to continue the timing of the experiment. The logic pulse Q is used to trigger the laser power detection gate and is sent through delay cables before triggering the fluorescence signal detection gate.

The trailing edge of the fluorescence detection gate produced by P.G. 501 F signals the end of the measurement and is used to trigger the beginning of the ion measurement. The trailing edge is synchronized with the r.f. phase of the ion trap supply and is sent to trigger pulse 3 in the PCB.

The timing is now returned to the PCB which generates a high voltage pulse to drive the ions out of the trap for measurement. The ttl logic pulse 3 is used to trigger the detection gates for the ion and optogalvanic measurements. Whereas the leading edge of pulse 3 is used to trigger the optogalvanic signal gate at P.G. 501 O, the pulse is inverted so that the trailing edge triggers the ion signal gate at P.G. 501 I.

Because the optogalvanic measurement requires more time than the ion measurement, the trailing edge of its detection gate is used to signal the PDP-8f computer that the experimental cycle is finished. The computer then determines if it is time to change the wavelength. After changing the wavelength or deciding it is not time to do so, the computer sends a logic pulse to the PCB commanding it to begin a new cycle. During the ionization period the computer then gathers the data stored in the 770 counter and 227-sg integrator and awaits the signal for the end of another experimental cycle. This procedure continues until the computer recognizes that the desired wavelength region has been covered.

Thus, it is seen that the timing of an experimental cycle is primarily controlled by the experimental timing

pulse control box. The control of an entire experiment, however, is accomplished by the PDP-8f computer. The interfacing of the computer to the experiment is covered in the next section.

G. The Computer, Computer Interface, and Programming

In Section II-F it was seen that the computer interface must perform the following functions: initiate an experimental cycle, recognize the completion of the cycle, gather data from the 770 counter and the 227-sg integrator, and scan the dye laser wavelength. While the individual functions described above are handled by the interface hardware, the order and timing of their application are accomplished by the software (programming). The interface hardware and logic will first be explained and a section describing the software will follow. To aid in the explanation of the interface, an overview of the computer system which interacts with the experiment is given. A brief description of the PDP-8f computer and the aspects that are pertinent to interfacing are also given.

1. Experimental Computer System

A schematic diagram of the computer system and the experimental components with which it interacts is shown in Figure II-25. The computer in this system is the Digital Equipment Corporation PDP-8f minicomputer. Most communication between the user and the computer is performed through the Tektronix 4010 CRT terminal. The ASR-33 teletype prints

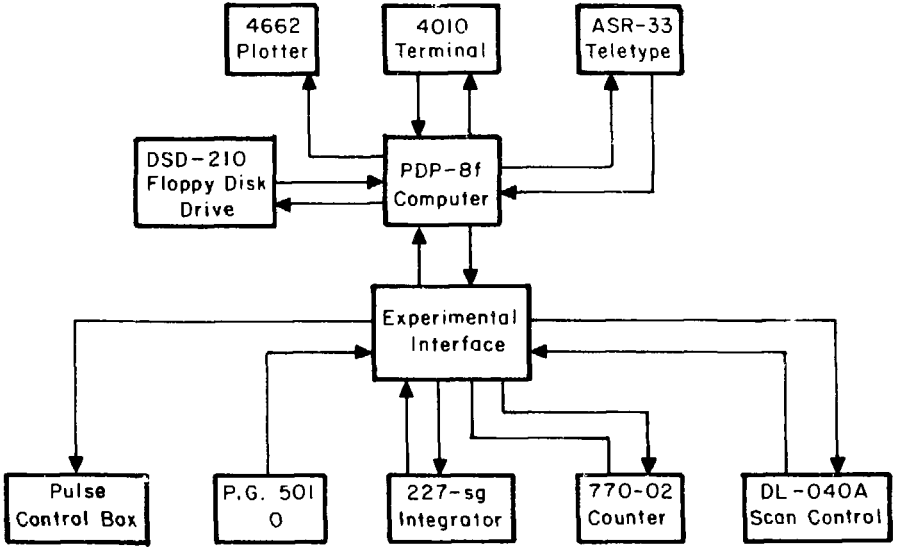

XBL 799-11265

Figure II-25. Computer System Overview.

out programs for hard copy record and the Tektronix 4662 digital plotter is used to plot graphical data. The Data Systems Design DSD-210 triple floppy disk drive system is used for all of the program and mass data storage. The OS-8 operating system used, which is described in Section II-G4a, is stored on a floppy diskette and all programming is developed using this system.

The computer is connected to the various experimental components via the experimental interface. The interface consists of three devices on two different printed circuit boards which interact with the experimental components. Logic and voltage levels are passed between the interface and the components to control the progress of the experiment and to transfer the data for storage in the computer (and later onto floppy diskettes).

An experiment is started by executing one of the ion spectroscopy experimental programs which asks for a variety of inputs including the wavelength region to be scanned, the wavelength increment, and the number of experimental cycles to be run at a particular wavelength. The experiment then begins with the signals being transferred to and from the computer via the interface. During the experiment the data are continuously stored on a floppy diskette and plotted on the 4010 screen. After the experiment is completed, the data can be retrieved and plotted by the 4662.

2. The PDP-8f Computer

The PDP-8f is a 12 bit minicomputer with a 1.2/1.4 microsecond cycle time. A description of the organization and structure of the computer pertinent to the interface is given here. For a complete description of PDP-8 minicomputer, the reader is referred to reference 35. The PDP-8f consists of a central processor, a memory with 32 K addresses (1 K = 1024_{10}), and input/output facilities. All of the above components communicate via a common bus called the "Omnibus". The central processor performs all the logical and arithmetic operations on the contents of the memory. The operations are performed in a logical sequence under the control of a program. Five 12-bit registers are used by the central processor to perform these operations. The most important register as far as the interface is concerned is the accumulator (AC). All of the logical and arithmetic operations are performed in the AC where the result is stored. The result can be transferred to any memory location. The AC is also used for all programmed information input/output transfers (IOT) between I/O devices and the memory. An IOT is defined as any communication between the computer and any peripheral device.

In addition to information storage, the memory also performs the retrieval operations of the contents in the memory locations. The computer memory consists of 32 K addresses (the maximum allowed) which are divided into 8 fields of 4 K. Sixteen K of this memory are core memory (DATARAM DR-118)

and sixteen K are semiconductor memory (Monolithic MSC 3102 and MSC 3201). Eight K of the semiconductor are powered by batteries allowing it to function as core memory for up to thirty days when the computer power is turned off. The entire 32 K memory is contained on four module boards which plug into three slots in the Omnibus.

The Omnibus is a common input/output bus which carries data and control signals. The Omnibus provides 20 connectors (slots) in which the module boards for the central processor, memory, and peripherals are placed. The pin assignments are identical in each connector allowing the modules to be placed in any order without affecting computer operation. (There is a preferred order, however.)[36] Of the 96 signals available on the Omnibus, the following are important regarding the interface. The 12 memory data (MD) lines carry the information of the memory location currently being addressed by the central processor. For an interface the MD lines are used to pass instructions to an interface to perform an Input/Output transfer (IOT) between the computer and an I/O device. These are called an IOT instructions and will be explained in the following paragraphs. The information in the AC is carried on 12 other lines called the DATA lines. These lines are used to pass information from the computer to the experiment and vice versa. Three control signals (C0, C1 and C2) determine the type of transfer between the interface and the processor via the AC. Four other signals: timing pulse 3, skip, interrupt request, and initialize, will be explained in the description of the experimental interface.

To understand how instructions are transferred to the interface, the different machine instruction codes available must be described. The instructions consist of 12 bit words which tell the computer what to do in a single operation. The 12 bit word is commonly written as a 4 digit octal number. The first three bits of the instruction (or the first octal digit) are called the operation code. The operation codes divide into 3 classes: memory reference, housekeeping, and augmented. The memory reference instructions, to which five operation codes belong (0-4), store or retrieve data from the memory while performing their respective functions. There is only one housekeeping instruction (5). It allows interruption of the sequential program operation and transfers control to a different portion of the program.

The augmented instructions divide again into two categories. The first category consists of the operate instructions which begin with the octal number 7. Operate instructions either operate on or test the contents of the AC (and the link[35]). There is a whole repertoire of operate instructions from which the machine language programming code is formed (which is given in reference 35). The final operation code is reserved for input/output transfer instructions, which begin with the octal number 6. This operation code is the one used exclusively when dealing directly with an interface.

Whereas the first octal digit (or the first 3 bits) specifies the operation code, the rest of the word completes

the instruction. For the memory reference and housekeeping instructions, the remaining bits give the memory address involved in the operation. For the operate instructions, they determine the type of operation or test to be performed on the AC or link. When an IOT instruction is being performed, the rest of the instruction selects the peripheral device involved in the IOT and the operation to be performed on that device. The second and third octal digits in the IOT instruction are used for device selection and the fourth digit selects the particular device operation. This allows for 64 different possible device numbers with 8 operations per device. Most of these device numbers are reserved for specific peripherals, but a few are available for user-designed interfaces. An example of an IOT instruction would be 6302 which would cause the device IOT operation 2 to be performed on device 30. The experimental IOT's and how they are used to operate the experiment via the experimental interface are explained in the following Section, II-G3.

3. The Experimental Computer Interface

a. M 1709 Modules

The experimental interface consists of two D.E.C. M 1709 interface modules. The M 1709 makes available all of the Omnibus signals needed for I/O transfers. Each M 1709 board usually functions as one device with eight different device functions. This is accomplished as follows. As described before, when an IOT instruction is executed by the processor, the bits 3 through 8 contain the device number. These bits

are transferred through the MD 03-08 memory data lines. The M 1709 module has the necessary logic (called the device decoder) to convert the binary device code on the MD 03-08 lines into an octal device number. When the M 1709 device number matches the instruction device number, the module is activated to perform an IOT. The particular device number for the module is selected by the user. The last three bits of the instruction, MD 09-11, contain the device operation to be performed. The M 1709 also contains the logic (called the function decoder) to convert this binary device function into an octal-number command available at one of eight wirewrap pins. When a particular device function is made operative, a 100 nanosecond pulse (termed the instruction pulse) is produced at its wirewrap pin. The user develops the logic from this point to accomplish the operation he wishes to perform and to connect the computer with the outside world. For example, if the device number 31 is selected for a M 1709 module and the instruction 6314 is executed, a 100 nanosecond pulse will appear at the fifth pin of the module's function decoder.

The instruction logic pulse generated at the function decoder pin is used to perform every kind of IOT instruction. If a logic pulse is needed simply to initiate the action of some experimental circuit, this pulse is used directly as the input trigger. However, for any communication between the outside world and the computer memory, the DATA lines (which interact with the AC) must be used in conjunction with the

instruction pulse. Information is placed on or received from the data lines via drivers (signal senders) and receivers (signals receivers), respectively. Drivers and receivers are available on the M 1709 board for each of the 12 DATA lines (which correspond to the 12 bits of the AC). The instruction pulse is used to transfer the information from the drivers to the DATA lines and into the AC. In addition to causing the transfer, the pulse is also sent to the 3 control lines C0, C1, and C2 which inform the processor as to what type of transfer is to take place.[37] When information is desired from the AC, it is transferred onto the M 1709 receivers using the instruction pulse. The timing of this information transfer is critical. Timing pulse 3 (one of four timing pulses generated by the computer) is used with the instruction pulse to insure that the transfer occurs at the correct time.

This completes the general description of how interfacing is accomplished via the M 1709 module. The specific experimental IOT's and their logic design using the M 1709 module will be described. First, however, the different types of IOT's available to the user will be discussed.

b. Data Transfers

Any IOT which is performed is described as a data transfer (not to be confused with the transfer of experimental data). In performing an IOT, the user has a choice of three different types of data transfers. The 3 types include programmed data transfers, interrupt facility, and data break

transfers. The data break transfer is the most efficient mode when a large amount of data needs to be transferred as quickly as possible. Because this is not the case in our experiment, only the other two types of transfers are incorporated in the interface. A programmed data transfer is the simplest method of transfer relying on the central processor to occasionally check the status of an experimental I/O component and service it if it is required. The interrupt facility performs the same data transfer, but in a more efficient manner. Rather than the computer occasionally checking the various I/O components to see if they need to be serviced, each device signals the computer only when it needs servicing by grounding the Omnibus interrupt request line. In this manner, no time is wasted checking a device when it is not required.

Most of the IOT operations in our experiment are handled efficiently enough by programmed data transfers to warrant their use. However, once an experimental cycle is begun, at least 20 milliseconds pass before the computer is again needed. With the computer cycle time being ~1 microsecond, a great deal of program run-time can occur in 20 milliseconds. For this reason, the interface is designed to allow the user to select between the interrupt facility and a programmed data transfer to perform the IOT which recognizes the end of an experimental cycle.

If the interrupt mode is selected, the processor can handle two programs simultaneously. The processor performs

the instruction of a background program after a foreground program begins an experimental cycle. When the cycle ends, the background program is interrupted and the processor deals with the experiment via the foreground program. Another cycle is then begun and the processor returns to the background program. If the programmed data transfer mode is selected, the processor must simply wait until the experimental cycle is completed. Thus, no background program can be performed during this wait time.

c. The IOT Instructions

The interfacing of the experiment required two M 1709 modules. One module (the counter interface) deals only with the 770 counter and will be discussed last. The other module (main experimental interface) performs all of the other operations required to run the experiment. On the main experimental interface, 10 device functions are required which exceeds the number available on one M 1709 module. For this reason, the experimental interface module was given two device numbers by duplicating the device decoder logic. The device function decoder logic was also duplicated giving the module a total of sixteen functions. Because of this increase, only one module board is required to perform all but the counter-related experimental functions. Thus, the interface requires only one of the few precious Omnibus slots. In addition, because only ten of the sixteen device functions are utilized, six remain for future expansion. The dual device logic is displayed in a schematic drawing, Figure II-26.

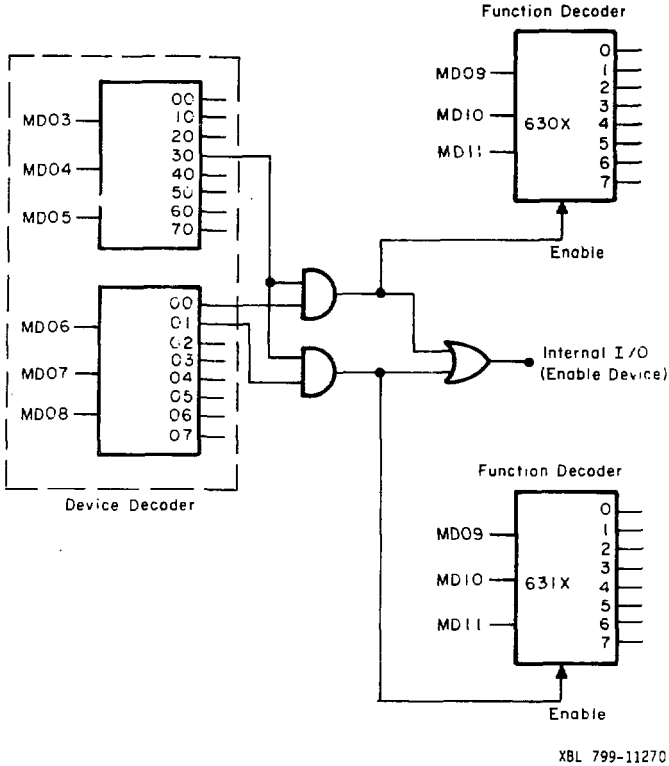

Figure II-26. Dual Device Logic.

The two device numbers chosen were 30 and 31. In this configuration, an IOT instruction of 630X or 631X enables the M 1709 module for an IOT (Internal I/O) and also enables the respective function decoder to initiate function X. (X values range from 0 through 7.)

To complete the discussion of interface design, the individual experimental device functions and the logic which is used to produce them need to be described. All of the IOT instructions are listed in Table II-5. In what follows, the IOT instructions are explained by grouping them into categories dealing with specific experimental components or entities. The two instructions which cannot be categorized as such are explained here.

Flip-flops are used on the interface to store certain logic values. Two different IOT's are used to clear these flip-flops to prepare them for subsequent use. The IOT instruction 6007 generates the initialize pulse which is one of the Omnibus signal lines. This pulse, which is also produced by depressing the "clear" switch of the PDP-8f computer, is used to clear the flip-flops which receive information from the AC via the DATA lines. The user designed IOT instruction 6302 clears the flip-flops which store a logic level indicating the state of various experimental components. This logic level will henceforth be called a "flag". After a flip-flop is cleared (termed clearing the flag), the processor occasionally checks the flip-flop to see if the flag has been set. When it is set, the processor knows that the

TABLE II-5

Experimental IOT Instructions

Instruction	Mnemonic	Function
6300	STADC	Start Analog-to-Digital Conversion
6301	RDSW	Read Status Word
6302	CLRSW	Clear Status Word
6303	SEX	Start Experiment
6304	STPWL	Step Wavelength
6305	SKPWDN	Skip Program Line When Experiment Done
6306	RDAD	Read A/C Value
6307	SETD	Set Direction and/or Enable Interrupt
6310	CLRINT	Clear Integrator
6311	RDINT	Read Integrator Channels
6150	STTWO	Strobe LSB BCD Bits
6151	STONE	Strobe MSB BCD Bits
6152	RSTCNT	Reset Counter
6153	OVRFLW	Check if Overflow has Occurred
6154	RSTOFW	Reset Overflow Flag

device which corresponds to that flip-flop is ready to be serviced.

1) Initiation and Completion of an Experimental Cycle

The initiation of an experimental cycle is performed by execution of the 6303 IOT instruction which simply generates a ttl logic pulse to be applied to the external trigger of the experimental timing pulse control box. This is shown in Figure II-27. The PCB controls the experiment throughout an individual cycle. The recognition of the completion of the cycle is handled either with the interrupt facility or the skip signal line both of which are shown in Figure II-26. As seen in this figure, the end-of-cycle logic pulse, generated by the P.G. 501 O, sets the flag of a flip-flop. The flag will either request an interrupt or enable the skip signal line. The user must choose which IOT mode he desires to handle the end-of-cycle pulse.

The interrupt facility is selected by the IOT 6307. The instruction 6307 transmits the fourth bit of the AC to a flip-flop which stores this value and transmits it, in turn, to the interrupt enable line. Note that the execution of 6307 must be synchronized with timing pulse 3. If the interrupt facility is desired by the user, he sets bit 4 in the AC to the value 1 and executes 6307. Then, the interrupt facility is enabled and an interrupt occurs whenever the end-of-cycle pulse is received by the interface.

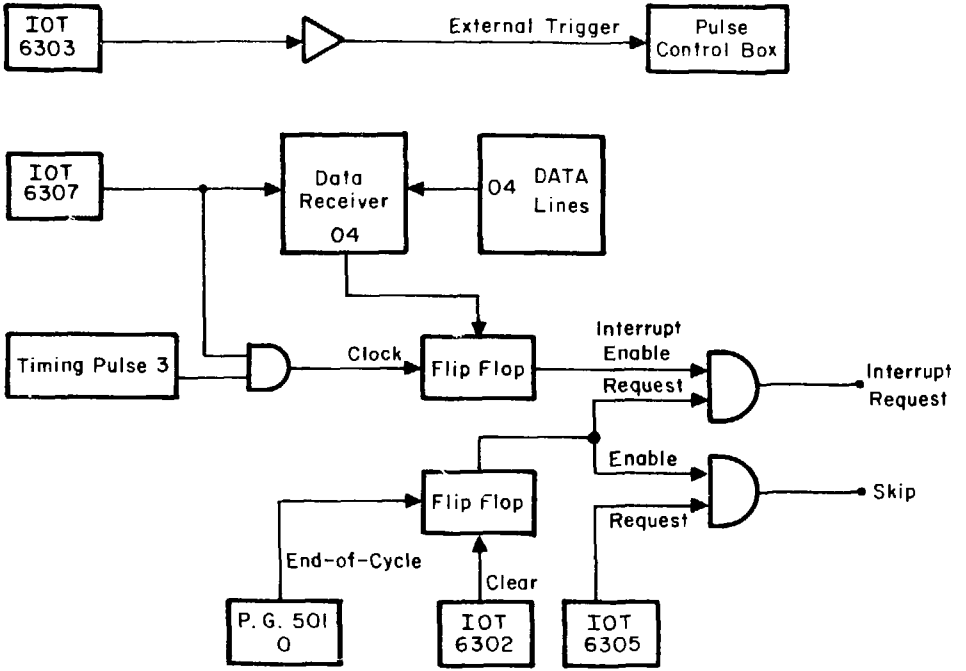

XBL 799-11268

Figure II-27. Start and Finish of Experimental Cycle.

When the interrupt mode is not desired, 6307 must still be executed, but with the AC bit 4 set to 0. The end of cycle flip-flop's flag is then used to enable the skip signal line. In this programmed data transfer mode, the program works as follows. The cycle is started with the execution of 6303. Then, because of the long ionization period, a large number of program instructions are executed. (Note that these instructions belong to the same program that is operating the experiment.) After this execution, the program executes a two line loop. The first line is the IOT 6305 which asks the processor to skip a program line if the skip signal line is enabled. If it is not enabled, the second line is executed which simply jumps the program back one line. Thus, the program continuously asks to skip a program line until the skip line is enabled by the end-of-cycle pulse. When it is enabled, the jump-back program line is skipped and the program continues.

In all of the experiments presented in this thesis, only the skip mode of operation was employed for two reasons. First, the need for running a background program simultaneously with the experimental program never arose. Second, the time waiting for the cycle to end could be put to good use by gathering the experimental data. The program is written in such a manner that after a cycle is started, the data from the previous cycle are retrieved and stored in the computer. The data retrival can be accomplished before the current cycle causes the laser to fire generating its data.

After the cycle ends, the end-of-cycle flag is cleared by the IOT 6302, a new cycle is begun, and the previous cycle's data are gathered.

2) The Status Word

The end-of-cycle pulse occurs at random times with respect to the program timing and is handled by either the interrupt or the skip operation mode. Four other experimental functions occur at random times, but are handled by means of a user-designed status word. The status word consists of four drivers which are given the flags of the various experimental functions indicating their state. When it is desired to check the status of one or more of these functions, the status word is read into the AC and the various flags are checked. In this manner only one IOT instruction is needed to check the status of four different functions. Additional functions can be added to the status word by increasing the number of drivers up to a maximum of twelve.

A schematic diagram of the status word IOT is given in Figure II-28. The four functions handled by the status word belong to the laser scan control and the analog-to-digital converter (A/D) which will be discussed separately later. The two functions, "scan control stepped" and "0.01 nm λ marker" are indicated by logic pulses which require flip-flops to store their status. The IOT 6302 is used to clear these flip-flops when it is so desired. The other two functions are indicated by logic levels and do not require flip-flops. The time at which these different functions come into play

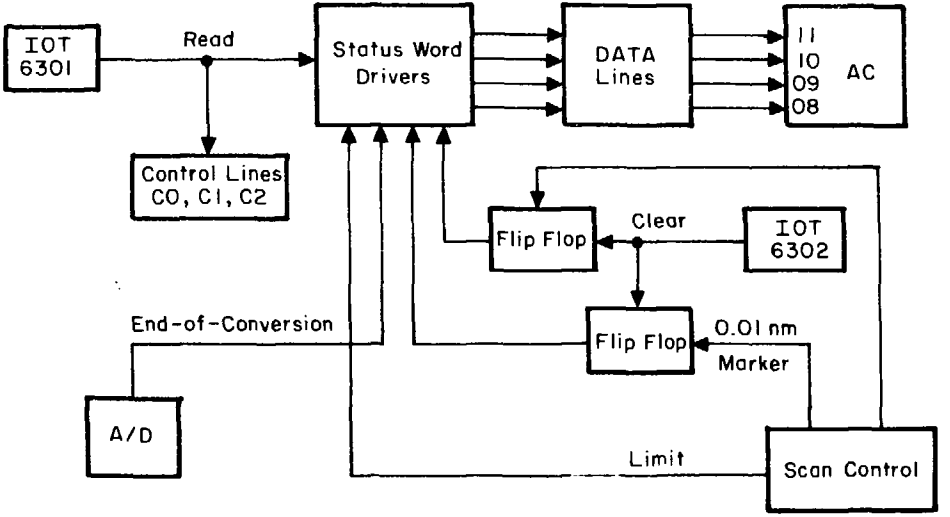

XBL 799-11263

Figure II-28. Status Word.

in the experiment will be discussed in the following sections. What is discussed here is the manipulation of the status word.

When the status of any of the four functions is suspected to have changed, the status word is read into the AC by executing IOT 6301. This instruction pulse places the logic values that have been placed on the drivers onto the DATA lines and into the AC. This pulse is also sent to the control lines (C0, C1, C2) to inform the processor what type of transfer is being made. Because there are four functions to check, AC bits 08 through 11 are used. The program then checks the value of these bits in order to establish the state of their respective functions. For example, to check if the scan control has reached its wavelength limit, the status word is read into the AC and the value of bit 08 is examined. If it is equal to 1,, the scan control has reached its limit and this problem must be handled. It if is equal to 0, no problem exists and the program may continue.

3) Laser Scan Control

A schematic diagram of the interface connections with the laser scan control is given in Figure II-29. All of the connections are made through a printed circuit board connector provided on the scan control. In all, two inputs and two outputs are utilized. The first input sets the direction in which the laser is to be scanned. Bit 05 of the AC is set to 0 (1) to scan in the + (-) direction and the instruction 6307 is executed to set the direction. This instruction sets a flip-flop to the value of bit 05 which stores this value maintaining the direction throughout the experiment.

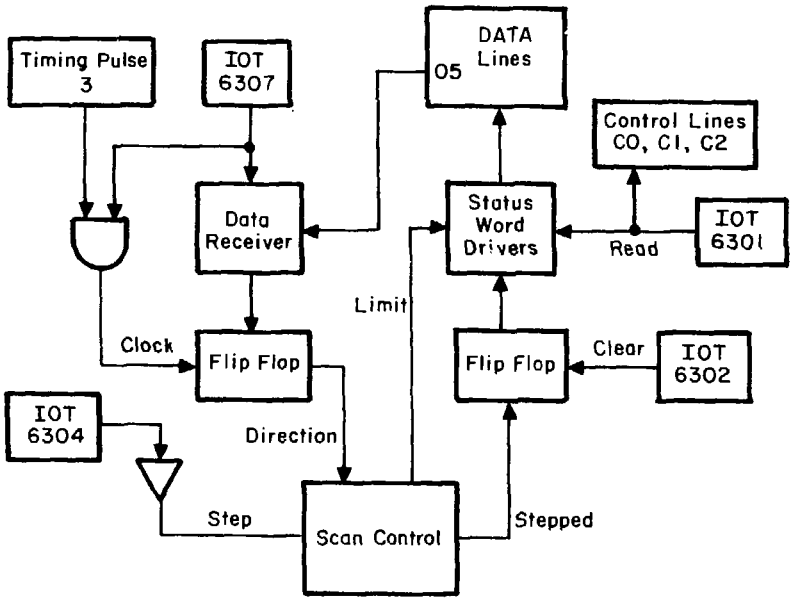

Figure II-29. Scanning Laser Wavelength.

The actual scanning of the laser is accomplished by using one input and one output of the scan control. By applying a ttl logic pulse to the "step" input pin using the IOT 6304, the sine-drive motor rotates the grating a fixed angle increment. The scan control then transmits a logic pulse on the "stepped" output pin to indicate that the wavelength has been moved a fixed step increment. This pulse is stored in a flip-flop whose value is sent to a status word driver. After the IOT 6304 is executed to step the wavelength, the status word is continuously read into the AC and checked by the program until it is determined that the wavelength has been stepped. To advance the wavelength by a certain wavelength increment which is input by the user at the beginning of the experiment, a certain number of wavelength steps must be carried out. This number is calculated from the magnitude of the increment, the size of one step and the order of the grating being used.

The final connection between the interface and the scan control is a protective measure. The dye laser grating can only be rotated to a certain degree. When this point is reached, a sensing device in the dye laser sends a warning signal to the scan control. The scan control transmits the warning to the interface via the "limit" line which is sent to a status word driver. After advancing the wavelength, the program reads the status word and checks to see if the limit has been reached. If it has, a warning is given to the user.

4) The 227-sg Integrator

The 227-sg integrator was discussed in Section II-E3a and a schematic of its interface to the computer is shown in Figure II-30. After the experimental cycle has ended, the values of the measurements made by the 4 different integrating channels are stored by the 227-sg. The value of a particular channel is made available at the multiplexed output by applying a high ttl logic level to the appropriate input pin for that channel. The ttl logic level to be applied is generated by the IOT instruction 6311 synchronized with timing pulse 3. Only one channel may be read at a time. The channel A, B, C, or D is selected by setting the AC bit 11, 10, 09, or 08 respectively to 1 and the other bits to 0. After the AC bit is set and 6311 executed, a flip-flop maintains the proper ttl level so that the signal of the desired channel is held on the multiplexed output until it is measured.

The multiplexed signal is applied to an analog-to-digital converter (A/D). The IOT 6300 is then executed which sends a pulse to the A/D to command it to start the conversion. The program must wait until the A/D completes the conversion before it can continue. When the conversion is completed, the A/D places the digital value on 12 DATA line drivers and sends a logic level to a status word driver indicating its completion. The processor which has been continuously checking the status word recognizes the completion. Instruction 6306 is then executed which places the A/D digital value into the AC. After storing this value in memory, the next

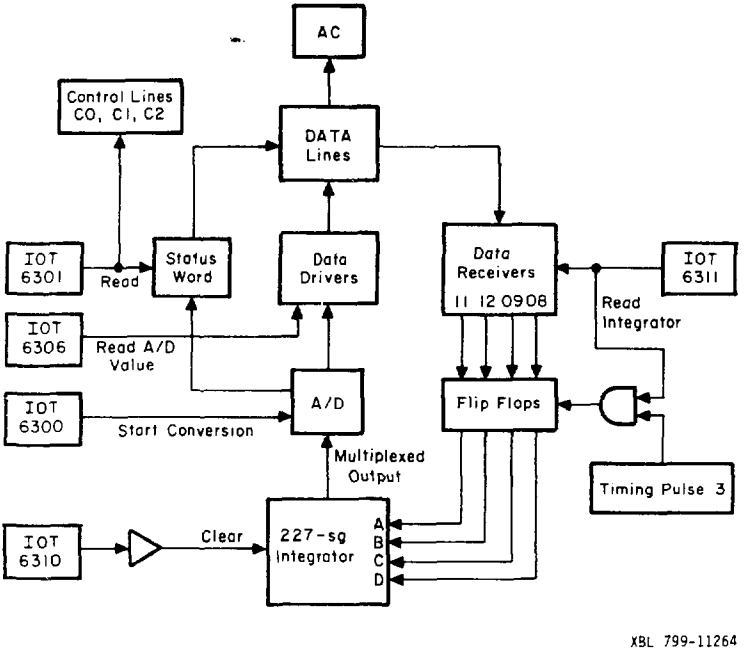

Figure II-30. Retrieving Data from 227-sg Integrator.

channel desired is read. After all the integrator channels that were used in the experiment have been read, the instruction 6310 is executed which sends a logic pulse to the integrator clearing all channels. The integrator is then ready for the next experimental cycle.

The analog-to-digital converter chosen for our experiment is the Datel MA12B-2A successive approximation A/D. It produces a 12 bit binary number at parallel data outputs in a conversion time of 40 microseconds. The A/D is used in the unipolar mode converting analog levels ranging from 0 to +10 volts. A -10 volt amplifier is required to change the 0 to -1 volt signal level from the integrator into the proper range handled by the A/D. Both the A/D and the amplifier are mounted on the M 1709 module printed circuit board. Gain and zero adjustment potentiometers for the A/D are also on this board. Both the gain and zero of the A/D should be checked periodically.

5) The 770-02 Counter

The interface for the Ortec 770 counter consists of its own M 1709 module. The counter was given its own module to allow it to be operated independently from the rest of the experiment. The counter can then be used in other experiments without power being drawn from the computer by the other experimental interface hardware. The counter's interface device number was chosen as 15 resulting in IOT instructions 615X. Five device functions are required to operate the counter.

As described in Section II-E3b, the 770 counter was supplied with the -02 parallel data output (PDO) option. The 6 digit decimal number is stored in 24 binary coded decimal (BCD) bits. The PDO option provides 24 drivers to transmit the BCD bits to the DATA lines. The drivers on the M 1709 module are, therefore, not needed for data transmission. In the original PDO design only one ttl logic pulse was required to transmit all 24 BCD bits. This design was altered so that two logic pulses are required to transmit the 24 bits, 12 at a time. (This is documented in the Ortec 770 counter manual.)

In Figure II-31, it is seen that the IOT instruction 6150 transfers the 12 least significant bits (LSB) and 6151 transfers the 12 most significant bits (MSB) to the data lines. Again, these IOT's set the control lines to the correct state to indicate the type of transfer being performed. If the number count exceeds 999,999, the counter indicates this by sending a logic pulse to its overflow output. This pulse sets a flip-flop which can be checked by IOT 6153. IOT 6153 transfers the overflow flag of the flip-flop through a driver and onto a DATA line (bit 11 of the AC). If an overflow has occurred the program accounts for it and clears the overflow flag with IOT instruction 6154. After the data transmission is complete, the program resets the counter by execution of IOT instruction 6152.

This completes the description of the counter IOT instructions and all of the experimental IOT instructions. In the next section the programming which utilizes these instructions to perform the experiment is discussed.

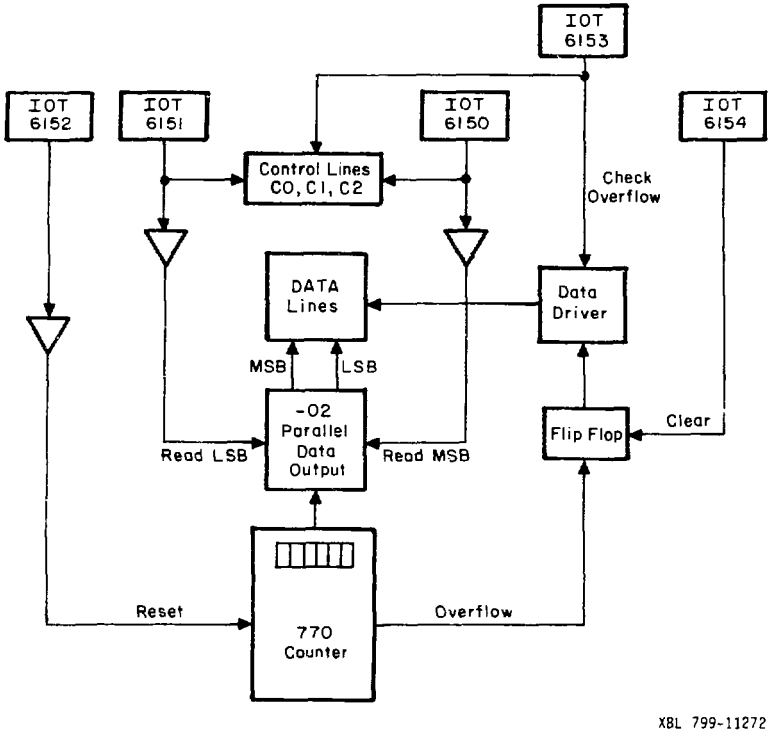

Figure II-31. Retrieving Data from 770-02 Counter.

4. Computer Programming

a. OS-8 Operating System

All program development was accomplished using the OS-8 Version 3D operating system purchased from the Digital Equipment Corporation. The OS-8 system provides a Keyboard Monitor which supervises a large library of system programs. The system includes programs for editing, file manipulation, debugging, PAL8 assembly, and FORTRAN II programming. A list and description of all the programs included in the OS-8 system are given in the OS-8 Handbook. The reader is referred to this handbook for a complete description of the OS-8 system. The OS-8 system programs are kept on a floppy diskette in the first disk drive unit (labeled SYS:) of the triple floppy disk drive system.

Also purchased with the OS-8 system were programs for BASIC, BATCH, TECO, and FORTRAN IV. All of the computer programming for the experiment was performed using the FORTRAN IV system. The machine language routines which operate the interface were written in PAL8 and incorporated into the FORTRAN IV system. A description of this procedure follows a description of the FORTRAN IV system.

b. FORTRAN IV

The FORTRAN IV system offered by the OS-8 is full standard ANSI FORTRAN IV. The FORTRAN IV system consists of the following programs: F4, PASS2, PASS3, PASS3, RALF, LOAD, FRTS, FORLIB, and LIBRA. The function of these programs is best described by stepping through the development of a program.

A source FORTRAN IV program is written by the user usually by using the OS-8 editor. After the source program file is produced, it is compiled by use of the programs F4, PASS2, PASS20 and PASS3. This produces a program file in RALF assembly language. This file is then assembled by the RALF assembly program which produces a relocatable binary program listing. Both the compiling and assembling steps are transparent to the user if he uses the OS-8 COMPILE keyboard command. Using the COMPILE command, an assembled relocatable binary listing is obtained with no intermediate RALF listing being produced. However, the COMPILE command can be executed with an option which halts the procedure after compilation resulting in just a RALF listing. A RALF listing is only desired if some change in the RALF program is necessary before it is assembled.

A main program and each subroutine that it calls must be compiled and assembled separately as described above to produce relocatable binary files. In addition, all of the library subroutines in the FORLIB file are relocatable binary files. All of the relocatable files used in one program are linked together to form a complete binary program (called a loader image) using the LOAD program. This complete binary program is then executed by using the FRTS (FORTRAN run-time system) program.

The FORLIB file mentioned above is the FORTRAN library. The FORLIB library file is usually kept with the OS-8 system on its diskette. The program LIBRA is used to maintain the

library by inserting or deleting relocatable binary files into or from the library. In our actual system, LIBRA was used to form a separate library on its own floppy diskette. In addition to the usual FORTRAN library functions, a whole series of plotting routines are included in the library. These routines were provided by Tektronix and are called the Plot-10 subroutines. These routines are used to control the plotting on the 4010 screen and on the 4662 digital plotter. The routines are described completely in the PLOT-10 manual and will not be discussed further here. When using the LOAD program to link a program which uses library routines, the library diskette is kept in the third disk drive (labeled DX2:).

The last point to be covered about the FORTRAN IV system is the RALF assembly language. RALF is very similar to the PAL8 assembly language. In fact, PAL8 programs can be used in RALF programs as subroutines. This fact leads to the method whereby the machine language IOT instructions are incorporated into the FORTRAN IV system. This method will now be explained.

c. Programming the Experimental IOT Instructions

The memory reference, housekeeping and operate instructions described in Section II-G1 are in machine language code; 4 digit octal numbers. The PAL8 assembly language consists of mnemonic names for these machine language instructions. PAL8 programs are then written in terms of these mnemonic instructions which are converted to machine language code by the PAL8 assembler. The IOT instructions are also in 4 digit

octal machine language code. These instructions are given user-defined mnemonies (as shown in Table II-5) so that they can be used in PAL8 programs. The link between the interface hardware and the programming software is made in this manner. The whole program to run the experiment could have been written in the PAL8 assembly language. However, this is very tedious and the power of the FORTRAN IV programming system would be lost. It is desirable then to incorporate these PAL8 routines into the FORTRAN IV system.

The RALF assembly language being very similar to PAL8 allows PAL8 instruction to be inserted as subroutines into RALF program code. The rules and conditions for this insertion procedure are covered in Chapter 5 of the OS-8 Handbook and the FORTRAN IV Software Support Manual. Then, to handle a particular IOT instruction, the program is first written in PAL8. The PAL8 routine is inserted into a RALF program which calls the PAL8 subroutine (via TRAP3 and TRAP4 program statements). Thus, the PAL8 routine is incorporated into the FORTRAN IV without any source program being written. The RALF programs which handle the different IOT's must be written as a subroutine to be called by a main source program. The experienced RALF programmer can write the RALF subroutine from scratch creating an efficient program.

For the less experienced user, an easier method to produce the subroutine is available. In this method, a source program is written which consists of the beginning SUBROUTINE statement, and RETURN statement, the variables which are to

be passed between the subroutine and the main program, and any other programming which is more easily written in the FORTRAN source language. This source program is compiled to obtain a RALF listing which has all the necessary code for the subroutine operation and for passing variables to the main program. The PAL8 routine and the RALF statements needed to complete the subroutine must then be added. The finished RALF routine is assembled and linked with rest of the program. The experimental routines written in this manner as well as rest of the experimental programming are discussed briefly in the next section.

d. Experimental Programs and Subroutines

All of the programs involved in the operation of the experiment are given in Appendix 3. A main program is used to call a variety subroutines each of which controls a certain aspect of the experiment. Two main programs were written for the two different modes of fluorescence measurement, integration and photon counting. They are listed in Appendix 3 under the names SPINI1.FT and SPCNT1.FT, respectively. The comments supplied with the listings of these programs explain the manner in which they perform the experiment.

There are two types of subroutine listings in Appendix 3. Those subroutines which do not deal with the interface are presented as source listings. The subroutines which perform experimental IOT's via the interface require RALF programming. These subroutines are, therefore, presented as RALF listings. The comments accompaning both of these types of subroutines

explain their function and the manner in which it is accomplished. The reader is referred to the OS-8 handbook for a description of RALF programming.

References, Chapter II

1. For a more complete historical description see references 14 and 27.

2. W. Paul and H. Steinwedel, Z. Naturforsch., 8a, 448 (1953).

3. R. F. Post and L. Henrich, UCRL 2209 (1953).

4. W. Paul and H. Steinwedel, German Patent No. 944,900, June 28 (1956).

5. K. Berkling, "Diplomarbeit", Physik. Inst. Univ. Bonn, Germany (1956).

6. E. Fischer, Z. Physik, 156, 26 (1959).

7. P. H. Dawson, and N. R. Whetton, Dyn. Mass Spec., 2, 1 (1971); P. H. Dawson, Int. J. Mass Spec. Ion Phys., 14, 317 (1974); P. H. Dawson and M. Meunier, Int. J. Mass Spec. Ion Phys., 29, 269 (1979); P. H. Dawson and C. Lambert, J. Vac. Sci. Tech., 12, 941 (1975).

8. G. Lawson and J. F. J. Todd, Chem. in Brit., 8, 373 (1972); J. F. J. Todd, R. M. Waldren, R. E. Mather, and G. Lawson, Int. J. Mass Spec. Ion Phys., 28, 141 (1978); R. E. Mather, G. Lawson, and J. F. J. Todd, Int. J. Mass Spec. Ion Phys., 28, 347 (1978).

9. M. Benalin and Claude Audoin, Int. J. Mass Spec. Ion Phys., 11, 421 (1973).

10. R. F. Bonner, J. E. Fulford, and R. E. March, Int. J. Mass Spec. Ion Phys., 24, 255 (1977).

11. H. G. Dehmelt, Adv. At. Mol. Phys., 3, 53 (1967).

12. L. D. Landau and E. M. Lifschitz, "Mechanics," Pergamon, Oxford (1960).

13. P. H. Dawson and N. R. Whetton, J. Vac. Sci. Tech., 5, 1 (1968).

14. P. H. Dawson (ed.), "Quadrupole Mass Spectrometry and Its Applications," Elsevier Scientific Pub. Co., New York (1976).

15. R. F. Bonner, Int. J. Mass Spec. Ion Phys., 23, 249 (1977).

16. D. B. Langmuir, R. V. Langmuir, and R. F. Wuerker, U. S. Patent 3,065,640 (1962).

17. P. H. Dawson and C. Lambert, Int. J. Mass Spec. Ion Phys., 16, 269 (1975).

18. J. R. Pierce, "Theory and Design of Electron Beams," D. Van Nostrand Co., Inc., New York (1954), Chapter 10.

19. G. Goodrich and W. Wiley, Rev. Sci. Inc., 32, 846 (1961).

20. R. M. Waldren and J. F. J. Todd, Int. J. Mass Spec. Ion Phys., 29, 315 (1979).

21. P. H. Dawson and C. Lambert, Int. J. Mass Spec. Ion Phys., 14, 339 (1974); J. F. J. Todd and R. M. Waldren, Int. J. Mass Spec. Ion Phys., 29, 301-344 (1979); J. E. Fulford and R. E. March, Int. J. Mass Spec. Ion Phys., 30, 39 (1979).

22. H. S. W. Massey, "Electronic and Ionic Impact Phenomena," Volume 2, Oxford, London (1969).

23. G. Lawson, R. F. Bonner, and J. F. J. Todd, J. Phys. E: Sci. Ins., 6, 357 (1973).

24. P. H. Dawson and N. R. Whetton, J. Vac. Sci. Tech., 5, 11 (1968).

25. R. D. Knight and M. H. Prior, J. Appl. Phys., 50, 3044 (1979).

26. P. H. Dawson, J. W. Hedman, and N. R. Whetton, Rev. Sci. Ins., 40, 1444 (1969).

27. P. H. Dawson and N. R. Whetton, Adv. Electron Electron Phys., 27, 59 (1969).

28. J. G. Pruett and R. N. Zare, J. Chem. Phys., 64, 1774 (1976).

29. RCA Photomultiplier Manual PT-61, p. 47.

30. For example: T. F. Johnston Jr., Laser Focus, March (1978) p. 58; R. B. Green, R. A. Keller, G. G. Luther, P. K. Schenck, and J. C. Travis, Applied Phys. Lett., 29, 727 (1976); D. S. King, P. K. Schenck, K. C. Smyth, and J. C. Travis, Appl. Opt., 16, 2617 (1977); R. B. Green, R. A. Keller, G. G. Luther, P. K. Schenck, and J. C. Travis, IEEE J. of Quant. Elec., Feb. (1978) p. 63; R. B. Green, R. A. Keller, P. K. Schenck, J. C. Travis, and G. C. Luther, J.A.C.S., 98, 8517 (1976).

31. D. S. King and P. K. Schenck, Laser Focus, March (1978) p. 50.

32. F. Paschen, Annual. Phys. IV, 60, 27 (1919).

33. G. Herzberg, Spectra of Diatomic Molecules, Van Nostrand Reinhold Co., Princeton, NJ (1966), Chapter II.

34. J. J. Ramirez and L. W. Kruse, Rev. Sci. Instrum. 47, 832 (1976).

35. "PDP-8 Small Computer Handbook," Digital Equipment Corp., 1973.

36. Dataram DR-118 Core Memory System Manual, p. 7.

37. Reference 35, pages 9-12.

APPENDIX 1

List of Apparatus Mechanical Drawings and LBL Numbers*

1. Assembly Drawings

ion trap apparatus	12N7183
baffle arms and main chamber	12N7654
electron gun	12N7661

2. Vacuum Chamber

A. Main Chamber and Ion Apparatus Flange

old main chamber and ion apparatus flange	12M8696
lower chamber	12M8914
main chamber modifications	12N7514
apparatus flange spacer	12N7641
ion gauge fitting	12M8761

B. Baffle System

entry baffle arm flange	12N7523
exit baffle arm flange	12N7531
entry flange	12N7541
1/4" straight baffle	12N7561
3/4" straight baffle	12N7571
1/4" angled baffle	12N7581
metal exit tube	12N7591
locking rings	12N7601

---

* These drawings are filed at the Lawrence Berkeley Laboratory. Copies of the LBL drawings whose numbers are cited here may be obtained by writing to Lawrence Berkeley Laboratory, Technical Information, Building 90, Room 2004, Berkeley, CA 94720.

threaded retainer ring	12N7611
exit flange	12N7622
metal exit tube and Wood's horn	12N7632
Brewster angle window and Wood's horn	12N7841

3. Ion Trap and Mounting Plates

top plate	12N7241
holding plate	12N7901
adjustment plate	12N7911
adjustment plate end	12N7921
adjustment plate side	12N7931
top electrode	12N7251
center electrode	12N7262
bottom electrode	12N7271
cones for $r = \sqrt{2}\ z$	12N7341
cones for $r = z$	12N7351
electrode insulators	12N7201
center electrode insulators	12N7211

4. Ion Detection Plates

ion focusing plate	12N7281
insulation plate	12N7291
collection mirror top bracket	12N7302
collection mirror bottom bracket	12N7311
magnetic plate	12N7322
bottom plate	12N7331
nylon alignment pins	12N7191
copper ion collimating tube	12N7231
magnetic plate insulators	12N7221

5. Electron Gun

light tight shield	12N7381
front plate (base)	12N7391
light tight lava ring	12N74.1
final focusing stage	12N7411
grid	12N7421
pulse plate	12N7431
filament shield	12N7441
filament holder	12N7451
filament pins	12N7461
support rods	12N7471
back plate	12N7481
ceramic top	12N7491
Faraday cup	12N7501

6. Laser Lens Mount

threaded holder plate	12N785
lens holde	12N786
mount plate	12N787
sliding rod plate	12N788
rods	12N789

APPENDIX 2

List of Apparatus Electrical Drawings and LBL Numbers

1.	Vacuum System	
	ion gauge switch	8S2751
	diffusion pump interlock	8S1764 mod 2
	Hasting dual vacuum interlock	6Z4664
2.	Voltage Dividers	
	filament shield, mirror, ion focusing plate	7S1641
	MEM voltage divider	8S6632
3.	Filament Heater Supply	7S1432
4.	External Timing Pulse Control Box	
	circuit diagram	7S1654
	logic diagram	7S2142
5.	Mass Filter Power Supply	8S3234
6.	PDP-8f Interfaces	
	main interface logic diagram	7S1893
	counting interface	928A2*
7.	Gated Dynode Chain	
	PMT dynode chain	820A1*
	gated photomultiplier supply	821A1*

*Chemistry Department Electronic Shop Drawing Number.

APPENDIX 3

Computer Programs

```
LIST SPCNTI.FT

C       SPCNTI.FT
C       MAIN PROGRAM FOR CALLING SUBROUTINES WHICH OPERATE ION
C       SPECTROSCOPY EXPERIMENT.(PLOTTING INCLUDED)
C       NORMALIZED FOR LASER POWER & ION DENSITY; OPTOGALVANIC INCLUDED
C       THIS PROGRAM ASSUMES USE OF 770 COUNTER FOR SIGNAL
C       NO SHOT TO SHOT NORMALIZATION
        CALL GREET
C       INITIALIZATION SECTION
        DIMENSION FILE(3)
        WRITE (4,1)
1       FORMAT (//,' PHOTON COUNTING WITH 770 COUNTER:  ANY # OF SHOTS '

52      IQ=0
57      NLEFT=0
        KK=0
        KKK=0
        M=0
        THC=0
        TM=0
        SUMPWR=0
        SUMION=0
        SUMOPT=0
C       OUTPUT FILE SET UP
14      WRITE(4,11)
11      FORMAT (//,' OUTPUT FILE TO BE CREATED: ',$)
        READ (4,12)FILE
12      FORMAT (3A6)
794     WRITE (4,797)FILE
797     FORMAT (//,' FILE NAME:  ',3A6,' IS THIS CORRECT (Y OR N)? ',$)
        READ (4,94)IQQ
        DATA IYY,INN/1HY,1HN/
        IF (IQQ.EQ.IYY)GOTO 719
        IF (IQQ.EQ.INN)GOTO 14
        GOTO 794
C       USR SUBROUTINE IS IN LIBRARY. IT ALLOWS RUN-TIME
C       DECLARATION OF FILES. SEE DECUS WRITE UP FOR EXPLANATION OF USE.

719     CALL USR (8,FILE,3,EROR)
        IF (EROR)53,53,92
92      WRITE (4,13)EROR
13      FORMAT (' ERROR = ',I3)
        GOTO 14
53      IF (IQ.EQ.1)GOTO 105
        CALL NEWPAG
C       TEXT & INPUT SECTION
150     CALL INITL (B,E,W,NO,NS,IN)
C       CALCULATE # OF STEPS/WAVLTH. INC. AND SET DIRECTION
112     CALL CALC (E,B,W,NO,D,NST)
C       TEST TO SEE IF EVERYTHING'S OKAY & SET -W IF D IS NEGATIVE
        IF (D) 101,150,100
101     W = -W
100     CALL CHNNL (JLPM,JIONM,JOPTM)
C       QPLOT SET TO 1 IN PLOT IF WISH TO GO BACK TO BEGINNING.
C       OTHERWISE QPLOT= 0.
        QPLOT=0.
C       WRITE TITLE IN OUTPUT FILE.
105     WRITE (8,799)IN,B,E,W,NS
799     FORMAT (A6,2G11.5,G11.4,I6)
C       CALCULATE NO. OF POINTS AND PUT ON DISK.
        MX=IFIX((E-B)/W+1.5)
        WRITE (8,798)MX
798     FORMAT(I4)
```

```
      CALL PLOT (B,E,IQ,YMX,YMN,QPLOT)
      IF(QPLOT)102,102,150
C     BF IS WIDTH FOR PLOTTING DURING EXP.
102   BF=B
C     CLEAR INTEGRATOR AND COUNTER FOR START OF EXPERIMENT
      CALL GTDATA (PWR,AION,OPT,JLPM,JIONM,JOPTM)
      CALL PHOTON (SIG)
C     START EXPERIMENT HERE
198   CALL START
C     ONE SHOT EXPERIMENT HANDLED DIFFERENTLY
      IF (NS-1)500,390,199
199   CALL SKPWDN
C     NLEFT IS MARKER FOR # OF SHOTS
      NLEFT = NS-1
200   CALL START
C     GET DATA FROM INTEGRATOR
201   CALL GTDATA (PWR,AION,OPT,JLPM,JIONM,JOPTM)
C     CHECK FOR COUNTER OVERFLOW
      CALL OFLOW(TM)
      IF(TM.GT.0)TMC=TMC+1
C     CHECK TO SEE WHICH NORMALIZATION IS BEING DONE.
C     NO CHECK FOR ZERO PWR OR AION SINCE NO SHOT TO SHOT NORM.
C     CORRECTION FOR PHOTODIODE WAVELENGTH DEPENDENCE (MUST IMPROVE)
      PWR=PWR*(.00215*(BF+W)-.42)
C     NO SHOT TO SHOT NORMALIZATION
      SUMPWR=SUMPWR+PWR
      SUMION=SUMION+AION
      SUMOPT=SUMOPT+OPT
C     TEST IF IT'S TIME TO STORE DATA
300   IF (NLEFT)500,450,390
C     TEST TO SEE IF DONE WITH THIS SAMPLE
390   IF (NLEFT-1) 500,510
392   NLEFT = NLEFT - 1
      CALL SKPWDN
C     LIFT SWITCH 0 ON SWITCH REGISTRAR TO STOP EXP.
393   CALL RSW(0,KK)
      IF (KK.NE.0)GOTO 88
      GOTO 200
C     STORE DATA IN COPE
C     M COUNTS # OF POINTS
450   M=M+1
C     NO CALCULATION OF STANDARD DEVIATION SINCE NO SHOT TO SHOT
C     AVERAGE SIGNALS (COULD DO THIS LATER)
      SMEAN=(SIG*TMC*1000000.)
      PMEAN=SUMPWR/NS/409.6
      AMEAN=SUMION/NS/409.6
      IF (JLPM.EQ.0)PMEAN=1.
      IF (JIONM.EQ.0)AMEAN=1.
      OMEAN=SUMOPT/NS/409.6
      RMEAN=SMEAN/PMEAN/AMEAN
C     PUT EACH INDIVIDUAL POINT IN OUTPUT FILE. RMEAN IS NORMALIZED
C     SIGNAL, SMEAN IS SIGNAL, PMEAN IS LASER POWER, AMEAN IS ION
C     DENSITY, AND OMEAN IS OPTOGALVANIC SIGNAL.
      WRITE (8,31)RMEAN,SMEAN,PMEAN,AMEAN,OMEAN
31    FORMAT (1X,5G14.6)
C     PLOTTING DURING EXP. 1ST POINT IS POINT, ALL OTHERS ARE LINES
      IF (M.GT.1)GO TO 517
      CALL POINTA(B,RMEAN)
      GO TO 599
517   BF=BF+W
      CALL DRAWA(BF,RMEAN)
599   CALL BELL
```

```
C       RESET VARIABLES
        SUMPWR=0
        SUMION=0
        TM=0
        TMC=0
        SUMOPT=0
601     NLEFT=NS
C       PULL UP SWITCH 1 TO STOP EXP.
598     CALL RSW(1,KKK)
        IF (KKK.NE.0)GOTO 88
C       SEE IF DONE WITH EXPERIMENT
        IF (MX.EQ.M)GOTO 600
        GOTO 392
C       GET COUNTS FROM 770 COUNTER & INCREMENT WAVELENGTH
510     CALL SKPWDN
        CALL PHOTON (SIG)
        NLEFT=NLEFT-1
C       TEST TO SEE IF ENDING WAVELENGTH HAS BEEN REACHED
        IF (MX-1.EQ.M)GOTO 201
611     CALL STEPWL (NST,LIMIT)
C       SEE IF SCAN CONTROL LIMIT HAS BEEN REACHED
        IF (LIMIT)520,200,520
C       IQ DETERMINES IF MORE EXPERIMENTS ARE TO BE RUN
600     CALL QDONE(IQ,NLEFT,M)
C       CLOSE FILE AFTER LAST POINT
98      CALL USR(8,FILE,4,ERDR)
        IF(ERDR)9,9,97
97      WRITE (4,96)ERDR
96      FORMAT ('ERROR = ',I3,'FILE WILL NOT CLOSE.WAITING FOR CHARACTE-
     1  & RETURN ')
        READ (4,94)KC
94      FORMAT (A3)
C       AGAIN PULL UP SWITCH 1 TO STOP EXP.
        CALL RSW(1,KKK)
        IF (KKK.NE.0)GOTO 88
        GOTO 98
C       ASK IF ANOTHER EXPERIMENT IS TO BE DONE.
9       GOTO(14,52,99),IQ
500     CALL ERROR (NLEFT)
        GOTO 88
520     CALL ERROR (LIMIT)
        GOTO 88
99      CALL FINITT(512,780)
C       HANDLES OUTCOME IF SWITCH REGISTERS STOP EXP.
88      CALL MOVABS(55,400)
        CALL ANMODE
81      WRITE (4,89)
89      FORMAT(///,' RESET SWITCH REGISTERS!! ',///,' TYPE 1 IF YOU WISH -
0
     1  GO BACK TO BEGINNING WITH INPUTS ',//,' TYPE 2 IF YOU WISH
     1  TO START AT BEGINNING OF EXP. WITHOUT INPUTS. ',//,' TYPE 3 IF
     1  YOU WISH TO START WHERE YOU LEFT OFF OR, ',//,' TYPE 4 IF YOU
     1  WISH TO CLOSE FILE AND FINISH. ')
        READ (4,86)KI
        IF (KI.GT.2)GOTO 83
        WRITE (8,798)M
        M=0
        CALL USR (8,FILE,4,ERDR)
        IF (ERDR)83,83,84
84      WRITE (4,82)ERDR
82      FORMAT (' ERROR = ',I3,'   FILE WILL NOT CLOSE ')
```

```
      GOTO 81
83    IQ=1
      GOTO(52,57,87,600),KI
86    FORMAT (13)
87    CALL MOVEA(BF,RMEAN)
      IF (KK)80,80,393
80    IF (KKK)88,88,598
      END
```

```
LIST SPINT1.FT

C       SPINT1.FT PROGRAM
C       MAIN PROGRAM FOR CALLING SUBROUTINES WHICh OPERATE ION
C       SPECTROSCOPY EXPERIMENT.(PLOTTING INCLUDED)
C       NORMALIZED FOR LASER POWER & ION DENSITY; OPTOGALVANIC INCLUDED
C        ASSUMES USE OF 227*SG INTEGRATOR FOR FLUORESCENCE SIGNAL
C
        COMMON/INTSIG/SIG,JSGM,PWP,JLPM,AION,JIONM,OPT,JOPT
        CALL GREET
C       INITIALIZATION SECTION
        DIMENSION FILE(3)
        WRITE (4,1)
1       FORMAT (/,'  INTEGRATING WITH 227 INTEGRATOR!  ANY # OF SHOTS ',

52      IQ=0
57      NLEFT=0
        KK=0
        KP=0
        K=0
        SUMSIG=0
        SUMPWP=0
        SUMION=0
        SUMOPT=0
C       OUTPUT FILE SET UP
14      WRITE(4,11)
11      FORMAT (/,' OUTPUT FILE TO BE CREATED: ',$)
        READ (4,12)FILE
12      FORMAT (3A6)
794     WRITE (4,797)FILE
797     FORMAT (//,' FILE NAME:  ',3A6,' IS THIS CORRECT (Y OR N)? ',$)
        READ (4,94)IQQ
        DATA IYY,INN/1HY,1HN/
        IF (IQQ.EQ.IYY)GOTO 719
        IF (IQQ.EQ.INN)GOTO 14
        GOTO 794
C       USR SUBROUTINE IS IN LIBRARY. IT ALLOWS RUN-TIME
C       DECLARATION OF FILES. SEE DECUS WRITE UP FOR EXPLANATION OF USE.

719     CALL USR (8,FILE,3,ERROR)
        IF (ERROR)53,53,92
92      WRITE (4,13)ERROR
13      FORMAT (' ERROR = ',I3)
        GOTO 14
53      IF (IQ.EQ.1)GOTO 105
        CALL NEWPAG
C       TEXT & INPUT SECTION
150     CALL INITL (B,E,W,NO,NS,IN)
C       CALCULATE # OF STEPS/WVLTh. INC. AND SET DIRECTION
112     CALL CALC (E,B,W,NO,D,NST)
C       TEST TO SEE IF EVERYTHING'S OKAY & SET -W IF D IS NEGATIVE
        IF (D) 101,150,100
101     W = -W
C       SET UP CHANNELS OF 227 INTEGRATOR WITh RESPECTIVE SIGNALS
100     CALL CHNNL
C       QPLOT SET TO 1 IN PLOT TO GO BACK TO START, OTHERWISE = 0
        QPLOT=0.
C       CALCULATE # OF POINTS. WRITE IT AND TITLE IN OUTPUT FILE.
105     WRITE (8,799)IN,B,E,W,NS
799     FORMAT (A6,2G11.5,G11.4,I6)
        MX=IFIX((E-B)/W+1.5)
        WRITE (8,798)MX
798     FORMAT(I4)
        CALL PLOT (B,E,IC,YMX,YMN,QPLOT)
```

```
      IF(QPLOT)102,102,150
C     BF IS WIDTH FOR PLOTTING DURING EXP.
102   BF=B
C     CLEAR INTEGRATOR FOR START OF EXPERIMENT
      CALL GTDATA
C     START EXPERIMENT HERE
198   CALL START
C     ONE SHOT EXPERIMENT HANDLED DIFFERENTLY
      IF (NS-1)500,390,199
199   CALL SKPWDN
C     NLEFT IS MARKER FOR # OF SHOTS
      NLEFT = NS-1
200   CALL START
C     GET DATA FROM INTEGRATOR
201   CALL GTDATA
C     CORRECTION FOR PHOTODIODE WAVELENGTH DEPENDENCE (MUST IMPROVE)
      PWR=PWR*(.00215*(BF+W)-.42)
      SUMSIG=SUMSIG+SIG
      SUMPWR=SUMPWR+PWR
      SUMION=SUMION+AION
      SUMOPT=SUMOPT+OPT
C     TEST IF IT'S TIME TO STORE DATA
380   IF (NLEFT)500,450,390
C     TEST TO SEE IF DONE WITH THIS SAMPLE
390   IF (NLEFT-1) 500,510
392   NLEFT = NLEFT - 1
      CALL SKPWDN
C     LIFT SWITCH C ON SWITCH REGISTER TO STOP EXP.
393   CALL RSW(C,KK)
      IF (KK.NE.C)GOTO 88
      GOTO 200
C     STORE DATA IN CORE
C     N COUNTS # OF POINTS
450   N=N+1
C     AVERAGE SIGNALS (COULD DO THIS LATER)
      SMEAN=SUMSIG/NS/409.6
      PMEAN=SUMPWR/NS/409.6
      AMEAN=SUMION/NS/409.6
C     CHECK TO SEE WHICH NORMALIZATION IS BEING DONE.
      IF (CLPR.EQ.0)PMEAN=1.
      IF (CIONM.EQ.0)AMEAN=1.
      OMEAN=SUMOPT/NS/409.6
      RMEAN=SMEAN/PMEAN/AMEAN
C     PUT EACH INDIVIDUAL POINT IN OUTPUT FILE. RMEAN IS NORMALIZED
C     SIGNAL, SMEAN IS SIGNAL, PMEAN IS LASER POWER, AMEAN IS ION
C     DENSITY, AND OMEAN IS OPTOGALVANIC SIGNAL.
      WRITE (8,31)RMEAN,SMEAN,PMEAN,AMEAN,OMEAN
31    FORMAT (1X,5G14.6)
C     PLOTTING DURING EXP. 1ST POINT IS POINT, ALL OTHERS ARE LINES
      IF (N.GT.1)GO TO 517
      CALL POINTA(B,RMEAN)
      GO TO 599
517   BF=BF+W
      CALL DRAWA(BF,RMEAN)
599   CALL BELL
C     RESET VARIABLES
      SUMSIG=0
      SUMPWR=0
      SUMION=0
      SUMOPT=0
601   NLEFT=NS
C     PULL UP SWITCH 1 TO STOP EXP.
```

```
598     CALL RSW(1,KKK)
        IF (KKK.NE.0)GOTO 88
C       SEE IF DONE WITH EXPERIMENT
        IF (MX.EQ.M)GOTO 600
        GOTO 392
C       INCREMENT WAVELENGTH
510     CALL SKPWDR
        CALL PHOTON (SIG)
        NLEFT=NLEFT+1
C       TEST TO SEE IF ENDING WAVELENGTH HAS BEEN REACHED
        IF (MY+1.EQ.M)GOTO 201
511     CALL STEPWL (NST,LIMIT)
C       SEE IF SCAN CONTROL LIMIT HAS BEEN REACHED
        IF (LIMIT)520,200,520
C       IS DETERMINES IF MORE EXPERIMENTS ARE TO BE RUN
600     CALL QDONE(IC,NLEFT,M)
C       CLOSE FILE AFTER LAST POINT
98      CALL USR(8,FILE,4,ERR)
        IF(ERR)9,9,97
97      WRITE (4,96)ERR
96      FORMAT ('ERROR = ',I3,'FILE WILL NOT CLOSE.WAITING FOR CHARACTER
     1  & RETURN ')
        READ (4,94)KI
94      FORMAT (A3)
C       AGAIN PULL UP SWITCH 1 TO STOP EXP.
        CALL RSW(1,KKK)
        IF (KKK.NE.0)GOTO 88
        GOTO 98
C       ASK IF ANOTHER EXPERIMENT IS TO BE DONE.
9       GOTO(14,52,99),IC
500     CALL ERROR (NLEFT)
        GOTO 88
520     CALL ERROR (LIMIT)
        GOTO 88
99      CALL FINITT(512,760)
C       HANDLES OUTCOME IF SWITCH REGISTERS STOP EXP.
88      CALL MOVABS(55,400)
        CALL ANMODE
81      WRITE (4,89)
89      FORMAT(///,' RESET SWITCH REGISTERS!! ',///,' TYPE 1 IF YOU WISH
     1  GO BACK TO BEGINNING WITH INPUTS ',//,' TYPE 2 IF YOU WISH
     1  TO START AT BEGINNING OF EXP. WITHOUT INPUTS, ',//,' TYPE 3 IF
     1  YOU WISH TO START WHERE YOU LEFT OFF OR, ',//,' TYPE 4 IF YOU
     1  WISH TO CLOSE FILE AND FINISH. ')
        READ (4,86)KI
        IF (KI.GT.2)GOTO 83
        WRITE (8,798)M
        M=0
        CALL USR (8,FILE,4,ERR)
        IF (ERR)83,83,84
84      WRITE (4,82)ERR
82      FORMAT (' ERROR = ',I3,'   FILE WILL NOT CLOSE ')
        GOTO 81
83      I=1
        GOTO(52,57,87,600),KI
86      FORMAT (I3)
87      CALL MOVEA(BF,RMEAN)
        IF (KK)60,80,393
8       IF (KK)88,88,590
        END
```

SUBROUTINES

```
LIST GREETN.FT

C       SUBROUTINE GREET GIVES OPENING INSTRUCTIONS AND CHECKS COMPUTER
C       SWITCH REGISTER.
        SUBROUTINE GREET
C       INITIALIZE PLOTTING SYSTEM
        CALL INITT(0)
        CALL SETBUF(4)
        CALL TSEND
        WRITE (0,2)
6       WRITE (4,3)
3       FORMAT(//,' MAKE SURE ALL SWITCHES ARE PUSHED DOWN BEFORE
     1  EXPERIMENT STARTS. ')
C       CHECK SWITCH REGISTER
        CALL RSW(0,K3)
        CALL RSW (1,K4)
        IF (K3+K4)6,4,6
4       RETURN
2       FORMAT (/,10X,' ION SPECTROSCOPY EXPERIMENT ',//,' MAKE SURE ALL

     1  COMPUTER CONNECTIONS ARE MADE AND THE EXPERIMENT ',//,' IS READY
     1  TO GO EXCEPT FOR THE LASER. I WILL TELL YOU WHEN TO TURN THE ',//

     1  ' LASER ON. HAVE ALL THE PERTINENT INFO READY! ')
        END
```

```
 LIST INN.FT

C       INITIALIZATION AND INTRODUCTORY TEXT SUBROUTINE
C       INPUTS REQUIRED TO QUESTIONS FROM LINE 18 AND BELOW
        SUBROUTINE INITL (BWL,EWL,WINC,NORDER,NSHOTS,ION)
30      WRITE (0,18)
        READ (0,3)ION
        WRITE (0,4)
        READ (0,5)BWL
        WRITE (0,6)
        READ (0,5)EWL
        WRITE (0,8)
        READ (0,7)WINC
        WRITE (0,12)
        READ (0,9)NORDER
        WRITE (0,14)
        READ (0,11)NSHOTS
        CALL NEWPAG
C       WRITE OUT INPUTS AND ASK USER IF THEY ARE OKAY.
40      WRITE (0,32)ION,BWL,EWL,WINC,NORDER,NSHOTS
        READ (0,3)IQ
        DATA IY,IN/1HY,1HN/
        IF (IQ.EQ.IY)GO TO 20
        IF (IQ.EQ.IN)GO TO 30
        GO TO 40
20      RETURN
C
18      FORMAT (/,' WHAT ION ARE YOU INVESTIGATING?(UP TO 6 SYMBOLS) ',.
)
3       FORMAT (A6)
4       FORMAT (/,' WHAT WAVELENGTH ARE YOU STARTING AT? (PUT ANSWER II
*
     1  /,' NANOMETERS AND INCLUDE THE DECIMAL POINT.) ',$)
5       FORMAT (G11.5)
6       FORMAT (/,' WHAT WAVELENGTH WILL YOU END AT? (PUT ANSWER IN '
     1  /,' NANOMETERS AND INCLUDE DECIMAL POINT.) ',$)
7       FORMAT (G11.4)
8       FORMAT (/,' WHAT IS THE WAVELENGTH INCREMENT (PUT ANSWER IN ',/
     1  ' NANOMETERS AND INCLUDE THE DECIMAL POINT)? ',$)
9       FORMAT (I1)
11      FORMAT (I4)
12      FORMAT (/,' WHAT IS THE DYE ORDER (INTEGER)? ',$)
14      FORMAT (/,' HOW MANY SHOTS AT EACH WAVELENGTH (INTEGER)? ',$)
32      FORMAT (///,' THESE ARE YOUR INPUTS: ',///,' THE ION IS: ',A6,//
     1  ' THE BEGINNING WAVELENGTH IS: ',G11.5,' NM ',//,' THE ENDING WA'

     1  LENGTH IS:  ',G11.5,' NM ',//,' THE WAVELENGTH INCREMENT IS:  ',
     1  G11.4,' NM ',//,' THE DYE ORDER IS:  ',I1,//,' THE NUMBER OF SHOTS

     1  IS:  ',I4,///,' ARE ALL THE INPUTS CORRECT (Y OR N) ',$)
        END
```

```
 LIST CHNNLC.FT

C       SUBROUTINE CHNNL.FT
C         SETS UP INTEGRATOR CHANNELS WITH THEIR RESPECTIVE
C         SIGNAL INPUTS. NO REVISION OF RALF FILE.
C         USES 3 CHNNLS. COUNT FLUORESCENCE SIGNAL.
C
        SUBROUTINE CHNNL (JLP,JION,JOPT)
        CALL NEWPAG
C       ASK FOR CHANNEL NUMBERS
        WRITE (4,549)
549     FORMAT(//,' NOW INPUT THE SIGNAL CHANNELS OF THE INTEGRATOR. ',///
     *
     1  ' IF YOU ARE NOT NORMALIZING FOR LASER POWER OR FOR ION SIGNAL,
     1  ',//,' ENTER C FOR THAT RESPECTIVE CHANNEL. ')
573     WRITE (0,551)
        READ (0,552)JLP
        WRITE (0,553)
        READ (0,552)JION
        WRITE (0,555)
        READ (0,552)JOPT
        DATA IYM,INM/1HY,1HN/
C       WRITE OUT CHANNEL ASSIGNMENTS AND ASK IF THEY ARE OKAY
577     WRITE (0,557)JLP,JION,JOPT
        READ (0,563)ION
        IF (ION.EQ.IYM)GO TO 571
        IF (ION.EQ.INM)GO TO 573
        GO TO 577
C       ROUTINE TO SET UP JLP,JION, & JOPT SO THAT CORRECT CHANNEL VALUE

C       IS STORED IN THEIR RESPECTIVE EXPONENT
C       EXPONENT OF 1 IS 1, 2 IS 2, 8 IS 3, & 128 IS 4 IN FLOATING POINT

571     IF (JLP-2)521,521
        IF (JLP.EQ.4)GO TO 523
        JLP=8
        GO TO 521
523     JLP=128
521     IF (JION-2)531,531
        IF (JION.EQ.4)GO TO 533
        JION=8
        GO TO 531
533     JION=128
531     IF (JOPT-2)541,541
        IF (JOPT.EQ.4)GO TO 543
        JOPT=8
        GO TO 541
543     JOPT=128
541     RETURN
C
551     FORMAT(///,' WHICH CHANNEL OF THE INTEGRATOR HAS THE LASER POWER
     *
     1  ,//,' INPUT  (0,1,2,3,OR 4)? ',$)
553     FORMAT(//,' WHICH CHANNEL HAS THE ION SIGNAL INPUT (0,1,2,3,
     1  OR 4)? ',$)
555     FORMAT (//,' WHICH CHANNEL HAS THE OPTOGALVANIC SIGNAL
     1  (1,2,3, OR 4) ',$)
557     FORMAT (///,' THE INTEGRATOR SET UP IS AS FOLLOWS: ',//,
     1  ' THE LASER POWER IS IN CHANNEL:              ',I2,//,
     1  ' THE ION SIGNAL IS IN CHANNEL:               ',I2,//,
     1  ' THE OPTOGALVANIC SIGNAL IS IN CHANNEL:      ',I2,///,
     1  ' IS THIS CORRECT (Y OR N)?? ',$)
563     FORMAT (I3)
```

```
563     FORMAT (A1)
        END
```

```
LIST CHNNL1.FT

C       SUBROUTINE CHNNL.FT
C         SETS UP THE INTEGRATOR CHANNELS WITH THEIR RESPECTIVE
C         SIGNAL INPUTS. NO REVISION OF HALF FILE.
C         ASKS FOR ALL 4 CHNNLS. INTEGRATION OF FLUORESCENCE SIGNAL.
C
        SUBROUTINE CHNNL
        COMMON/INTSIG/SIG,JSG,PWR,JLP,AION,JION,OFT,JOFT
        CALL NEWFAG
C       ASK FOR CHANNEL NUMBERS
        WRITE (4,549)
549     FORMAT(//,' NOW INPUT THE SIGNAL CHANNELS OF THE INTEGRATOR. ',///
     1  ' IF YOU ARE NOT NORMALIZING FOR LASER POWER AND/OR ION DENSITY,
     1  ',//,' ENTER 0 FOR THAT RESPECTIVE CHANNEL. ')
570     WRITE (4,547)
        READ (4,552)JSG
        WRITE (0,551)
        READ (0,552)JLP
        WRITE (0,553)
        READ (0,552)JION
        WRITE (0,555)
        READ (0,552)JOFT
        DATA INN,INM/1HY,1HN/
C       WRITE OUT CHANNEL ASSIGNMENTS AND ASK IF THEY ARE OKAY
580     WRITE (0,557)JSG,JLP,JION,JOFT
        READ (0,560)IOK
        IF (IOK.EQ.INN)GO TO 571
        IF (IOK.EQ.INM)GO TO 573
        GO TO 580
C       ROUTINE TO SET UP JSG,JLP,JION, & JOFT SO THAT CORRECT CHANNEL
C       VALUE IS STORED IN THEIR RESPECTIVE EXPONENT
C       EXPONENT OF 1 IS 1, 2 IS 2, 8 IS 3, & 128 IS 4 IN FLOATING POINT
571     IF (JLP-2)521,521
        IF (JLP.EQ.4)GO TO 523
        JLP=8
        GO TO 521
523     JLP=128
521     IF (JION-2)521,531
        IF (JION.EQ.4)GO TO 533
        JION=8
        GO TO 531
533     JION=128
531     IF (JOFT-2)541,541
        IF (JOFT.EQ.4)GO TO 543
        JOFT=8
        GO TO 541
543     JOFT=128
541     IF (JSG-2)544,544
        IF (JSG.EQ.4)GOTO 539
        JSG=8
        GOTO 544
539     JSG=128
544     RETURN
C
547     FORMAT(//,' WHICH CHANNEL OF THE INTEGRATOR HAS THE '
     1  ,/,'       FLUORESCENCE SIGNAL (1,2,3, OR 4)? ',$)
551     FORMAT(//,' WHICH CHANNEL HAS THE LASER POWER '
     1  ,/,' INPUT  (0,1,2,3,OR 4)? ',$)
552     FORMAT(//,' WHICH CHANNEL HAS THE ION SIGNAL INPUT (0,1,2,3,
     1  OR 4)? ',$)
```

```
555     FORMAT (///,' WHICH CHANNEL HAS THE OPTOGALVANIC SIGNAL
     1  (1,2,3, OR 4) ',$)
557     FORMAT (///,' THE INTEGRATOR SETUP IS AS FOLLOWS: ',//,
     1  ' THE FLUORESCENCE SIGNAL IS IN CHANNEL:   ',I2,//,
     1  ' THE LASER POWER IS IN CHANNEL:           ',I2,//,
     1  ' THE ION SIGNAL IS IN CHANNEL:            ',I2,//,
     1  ' THE OPTOGALVANIC SIGNAL IS IN CHANNEL:   ',I2,///,
     1  ' IS THIS CORRECT (Y OR N)? ',$)
562     FORMAT (I3)
563     FORMAT (A1)
        END
```

```
 LIST PLOTN.FT

C       SUBROUTINE PLOT.FT
C         DRAWS AXES FOR PLOT OF DATA DURING EXPERIMENT.
        SUBROUTINE PLOT(BP,EP,QP,YMAX,YMIN,QPL)
C       CHECK IF SCALE CHANGE IS DESIRED.
        IF(1.+QP)717,717,332
717     WRITE(R,334)
        READ(4,336)IT
        DATA IY,IN/1HY,1HN/
        IF (IT.EQ.IY)GO TO 332
        IF (IT.EQ.IN)GO TO 337
        GO TO 717
332     CALL NEWPAG
C        READ IN AXES VALUES.
        WRITE(4,333)
        READ (4,444)YMAX
        WRITE(4,377)
        READ (4,444)YMIN
        DATA NY,NN/1HY,1HN/
C       CHECK IF USER THINKS EVERYTHING IS OKAY.
140     WRITE (0,24)
        READ (0,13)NW
        IF (NW.EQ.NY)GO TO 337
        IF (NW.EQ.NN)GO TO 130
        GO TO 140
C       THINGS NOT OKAY, JUMP OUT OF SUBROUTINE.
130     QPL=1.
        GO TO 996
C       THINGS OKAY, CONTINUE.
337     BPC=BP
        EPC=EP
        IF (EP.GT.BP)GO TO 55
        E=EPC
        EPC=BPC
        BPC=E
55      BP=EPC
C       PLOT AXES.
        CALL INITT(0)
        CALL SETBUF(4)
        CALL TWINDO (120,980,90,715)
        CALL DWINDO (BPC,EPC,YMIN,YMAX)
        CALL MOVEA(EPC,YMIN)
        CALL DRAWA(BPC,YMIN)
        CALL DRAWA(BPC,YMAX)
        WD=BPC+.15*(EPC-BPC)/1023
        Y = YMAX
C       DRAWIY AXIS TIC MARKS.
447     CALL DRAWA(WD,Y)
        Y=Y-(YMAX-YMIN)/10
        CALL MOVEA(BPC,Y)
        IF (Y-YMIN)448,448,447
448     HG=15*(YMAX-YMIN)/780 + YMIN
        BD=BPC
C       DECIDE HOW MANY X AXIS TIC MARKS.
        NG=INT((EPC-BPC+6)/10.)
        IF (NG.NE.0)GO TO 310
        GRASS=.1
        GO TO 300
310     GRASS=FLOAT(NG)
C       DRAW X AXIS TIC MARKS.
300     BD =BD + GRASS
        IF (BD.GT.EPC)GO TO 301
        CALL MOVEA (BD,HG)
```

```
      CALL DRAWA (BD,YMI
      GO TO 300
C     LABEL AXES.
301   CALL MOVABS(35,50)
500   CALL ANMODE
      WRITE (4,40)BPC
      CALL MOVABS (950,50)
      CALL ANMODE
      WRITE (4,40)EPC
      CALL MOVABS (0,90)
      CALL ANMODE
      WRITE(4,449)YMIN
      CALL MOVABS(0,775)
      CALL ANMODE
      WRITE(4,445)YMAX
996   RETURN
444   FORMAT (G15.6)
449   FORMAT (F7.2)
445   FORMAT (F6.2)
40    FORMAT (G11.4)
336   FORMAT(A2)
334   FORMAT (//,' DO YOU WANT TO CHANGE THE YMAX? (Y OR N) ',$)
333   FORMAT (//,' FOR PLOTTING, INPUT YMAX (NORMALIZED)
     1  AND INCLUDE ',//,' DECIMAL POINT. ',$)
337   FORMAT(//,' INPUT YMIN (LOWER LIMIT 0.) INCLUDING DECIMAL PT. ',
$)
24    FORMAT (//,' START UP THE LASER NOW AND IF EVERYTHING IS OKAY ',
/
     1  ' TYPE Y AND RETURN (AFTER TURNING ON THE LASER). ',//
     1  /,' IF THINGS ARE NOT OKAY YOU CAN TYPE N AND RETURN. ',//
     1  ' THIS WILL START YOU COMPLETELY OVER WITH INPUTS. ')
13    FORMAT (A1)
      END
```

```
LIST START.RA

/       SUBROUTINE START (RALF ASSEMBLY LANGUAGE)
/         STARTS EXPERIMENTAL CYCLE
        SECT    START
        JA      #ST
#XR,    ORG     .+10
        TEXT    +START+
#RET,   SETX    #XR
        SETB    #BASE
        JA      .+3
#BASE,  ORG     .+6
        ORG     #BASE+30
        FNCT
        JA      #RET
        FNCT
#GOBAL, DEC
#ABCS,  ORG     .+3
#TMP,   ORG     .+0011
#LIT,   0001
        2000
        0000
        0001
        3001
        0000
        0003
        3001
        0000
        #LBL*.
        ORG     #LBL
#RTN,   BASE    #BASE
        JA      #GOBAL
#ST,    START
        0811
        FSTM    #GOBAL,0
        0200
        SETX    #XR
        SETB    #BASE
        STARTF
        TRAP4 STEXP     /JUMP TO RALB SBRTNE WHICH STARTS EXP. CYCLE
        LDX     0002,0
        LDX     0003,0
        EXTERN  #NE
        JA      #RTN
        LDX     0004,0
        EXTERN  #NE
        JA      #RTN
        SECTE SEXP      /RAL B ROUTINE
        SEX=6302        /START EXP CYCLE IOT
        CLRSW=6302      /CLEAR STATUS WORD FLAGS IOT
*TEXP,  0
        CLRSW           /CLEAR FLAGS FOR BEGINNING OF CYCLE
        SEX             /START EXP CYCLE
        CDF CIF 0
        JMP* STEXP      /RETURN TO RALF PROGRAM
```

```
 LIST GET3C.RA

/       GTDATA SUBROUTINE (RALF ASSEMBLY LANGUAGE)
/         ROUTINE READS THREE CHANNELS OF THE INTEGRATOR
/         AND ALSO CLEARS THE INTEGRATOR
        SECT    GTDATA
        JA      #ST
#XR,    ORG     .+10
        TEXT    *GTDATA*
#RET,   SETX    #XR
        SETB    #BASE
        JA      .+3
#BASE,  ORG     .+6
/       DATA VARIABLES
ONE,    ORG     .+3
TWO,    ORG     .+3
THREE,  ORG     .+3
/       DATA CHANNEL VARIABLES
JONE,   ORG     .+3
JTWO,   ORG     .+3
JTHRE,  ORG     .+3
        ORG     #BASE+30
        FNCP
        JA      #RET
        FNCP
#GOBAK, OCO
#ARGS,  ORG     .+3
/       DUMMY VARIABLES FOR PASSING DATA & CHANNEL #
DUMMY,  ORG     .+0003
JS,     ORG     .+0003
#TMP,   ORG     .+0011
#LIT,   0001
        2000
        000C
        0002
        3000
        0000
        0003
        3000
        0000
        #LBL=.
        OPG     #LBL
#RTN,   BASE    #BASE
        JA      #GOBAK
#ST,    STARTD
        0210
        FSTA    #GOBAK,0
        0200
        SETX    #XR
        SETB    #BASE
        LDX     0,1
        FSTA    #BASE
        FSTA    #ARGS
        FLDA%   #BASE,1+
        FSTA    ONE
        FLDA%   #BASE,1+
        FSTA    TWO
        FLDA%   #BASE,1+
        FSTA    THREE
        FLDA%   #BASE,1+
        FSTA    JONE
        FLDA%   #BASE,1+
        FSTA    JTWO
        FLDA%   #BASE,1+
```

```
        FSTA    JTHRE
        STARTF
        LDX     0002,0
        LDX     0003,C
/       INPUT LASER CHANNEL
        FLDA#   JONE
        FSTA    JS
        FLDA    JS
        FSTA    JSUB
/       JUMP TO PDP-8 ROUTINE TO GET DATA
        TRAP4   READ
/       PREPARE FOR PASS BACK TO MAIN PROGRAM
        FLDA    DUM
        FNORM
        FSTA    DUMMY
        FLDA    DUMMY
/       LASER POWER STORED IN ONE FOR PASS BACK
        FSTA#   ONE
        LDX     0004,0
/       NOW SIGNAL CHANNEL
        FLDA#   JTWO
        FSTA    JS
        FLDA    JS
        FSTA    JSUB
/       GET SIGNAL
        TRAP4   READ
        FLDA    DUM
        FNORM
        FSTA    DUMMY
        FLDA    DUMMY
/       STORE IN TWO FOR PASS BACK
        FSTA#   TWO
        LDX     0005,0
/       NOW ION CHANNEL
        FLDA#   JTHRE
        FSTA    JS
        FLDA    JS
        FSTA    JSUB
/       GET ION SIGNAL
        TRAP4   READ
        FLDA    DUM
        FNORM
        FSTA    DUMMY
        FLDA    DUMMY
/       STORE IN THREE
        FSTA#   THREE
/       JUMP TO PDP-8 ROUTINE TO CLEAR INTEGRATOR
        TRAP4   CLEAR
        LDX     0006,0
        EXTERN  #NE
        JA      #RTN
        LDX     0007,0
        EXTERN  #NE
        JA      #RTN
        SECT6 GTDTAB        /PALB ROUTINE
        STADC=6300          /START AD CONVERSION IOT
        RDSW=6301           /READ STATUS WORD FLAGS IOT
        CLRSW=6302          /CLEAR STATUS WORD FLAGS IOT
        RDAD=6306           /READ AD DIGITAL VALUE IOT
        CLRINT=6310         /CLEAR INTEGRATOR IOT
        RDINT=6311          /READ INTEGRATOR CHANNEL IOT
JSUB,   0;0;0
```

```
DUM,    27?0?0          /DUMMY VARIABLE FOR PASS BACK OF INTEGRATOR
/                         CHANNEL SIGNAL. EXPONENT OF 27?NEEDED FOR PRT

MSC,    -100
MSCA,   -100
MICC,   -100
MICCA,  -100
ADBIT,  2               /BIT TO CHECK IF A/D IS DONE
WAIT,   0               /WAIT 50 USEC BEFORE GETTING DATA
        ISZ MSC
        JMP .-1
        CLA
        TAD MSCA
        DCA MSC
        CDF CIF 0
        JMP* WAIT       /JUMP BACK TO RALF
READ,   0               /READ INT.,CONVERT TO DIGITAL,& PASS BACK AS
        CLA             /FLOATING POINT NUMBER
        TAD JSUB+2      /CHECK IF NOT USING THIS CHNNL (I.E. JSUB+2=0)
        SNA             /IS JSUB+2 = 0?
        JMP DON         /YES, JUMP OUT OF ROUTINE
        DCA DUM+1       /NO, CONTINUE WITH ROUTINE
        TAD JSUB        /EXPONENT OF JSUB GIVES RIGHT CHANNEL
        RDINT           /READ INTEGRATOR
        TAD MICCA
        DCA MICC
        ISZ MICC        /WAIT FOR INTEGRATOR TO SETTLE
        JMP .-1
        STADC           /START A/D CONVERSION
        RDSW            /CHECK TO SEE WHEN A/D IS DONE
        AND ADBIT
        SNA
        JMP .-3
        RDAD            /VALUE NOW IN AC
        DCA DUM+2       /PUT DATA IN FLOATING PT NUMBER
DON,    CDF CIF 0
        JMP* READ       /JUMP BACK TO RALF
/
CLEAR,  0
        CLRINT          /CLEAR INTEGRATOR
        CDF CIF 0
        JMP* CLEAR      /JUMP BACK TO RALF

 LIST GET3?.FT

C       SUBROUTINE GETS DATA FROM INTEGRATOR, CONVERTS IT TO DIGITAL
C       AND RETURNS IT AS FLOATING POINT NUMBER.
C       ONE=SIGNAL FROM CHANNEL JONE, TWO = SIGNAL FROM CHANNEL JTWO,
C       THREE=SIGNAL FROM CHANNEL JTHRE
C       INTEGRATOR CHANNEL #'S:  JONE IS FIRST CHNNL IN CALL SBRTN STATE
-
C         MENT OF MAIN PROG., JTWO IS 2ND IN CALL SBRTN STATEMENT, ETC.
        SUBROUTINE GTDATA (ONE,TWO,THREE,JONE,JTWO,JTHRE)
        JS=JONE
        JS=JTWO
        JS=JTHRE
        RETURN
        END
C       NOTE THAT GTDATA.RA HAS BEEN CHANGED EXTENSIVELY.
```

```
LIST GET41.RA

/       GTDATA SUBROUTINE (RALF ASSEMBLY LANGUAGE)
/         ROUTINE READS THREE CHANNELS OF THE INTEGRATOR
/         AND ALSO CLEARS THE INTEGRATOR
/         VARIABLES PASSED BY MEANS OF A COMMON STATEMENT.
        SECT    GTDATA
        UR      #ST
#XR,    ORG     .+10
        TEXT    +GTDATA+
#RET,   SETX    #XR
        SETB    #BASE
        UA      .+3
#BASE,  ORG     .+6
        ORG     #BASE+30
        FNOP
        UA      #RET
        FNOP
#GOBAK, ORG
#ARGC,  ORG     .+3
DUMMY,  ORG     .+0003
JSR,    ORG     .+0003
#TMP,   ORG     .+0011
#LBL,   0001
        2000
        0000
        0007
        3007
        0006
        0003
        3000
        0000
        #LBL+.
        COMMON  INTSIG
ONE,    ORG     .+0003
JONE,   ORG     .+0003
TWO,    ORG     .+0003
JTWO,   ORG     .+0003
THREE,  ORG     .+0003
JTHRE,  ORG     .+0003
FOUR,   ORG     .+0003
JFOUR,  ORG     .+0003
        ORG     #LBL
#RTN,   BASE    #BASE
        UR      #GOBAK
#ST,    START
        0210
        FSTA    #GOBAK,0
        0200
        SETX    #XR
        SETB    #BASE
        START
        LDX     0002,0
        LDX     0003,0
        LDX     0004,0
        FLDA    JONE            /INPUT FLUORESCENCE SIGNAL CHANNEL
        FSTA    JS
        FLDA    JS
        FSTA    JSUB
        LDX     0005,0
        TRAP4   READ            /JUMP TO READ ROUTINE
        FLDA    DUM             /PASS SIGNAL TO COMMON VARIABLE SIG
        FLOAT
        FSTA    DUMMY
```

```
        FLDA    DUMMY
        FSTA    ONE
        LDX     0006,0
        FLDA    JTYO            /INPUT LASER CHANNEL
        FSTA    JS
        FLDA    JF
        FSTA    JSUB
        TRAP4   READ            /JUMP TO PALB ROUTINE
        FLDA    DUM             /PASS SIGNAL TO COMMON VARIABLE PVT
        FNORM
        FSTA    DUMMY
        FLDA    DUMMY
        FSTA    TWO
        LDX     0007,0
        LDX     0010,0
        FLDA    JTHRE           /INPUT ION DENSITY CHANNEL
        FSTA    JS
        FLDA    JF
        FSTA    JSUB
        TRAP4   READ            /JUMP TO PALB ROUTINE
        FLDA    DUM             /PASS TO COMMON VARIABLE AION
        FNORM
        FSTA    DUMMY
        FLDA    DUMMY
        FSTA    THREE
        LDX     0011,0
        LDX     0012,0
        FLDA    JFOUR           /INPUT OPTOGALVANIC CHANNEL
        FSTA    JS
        FLDA    JF
        FSTA    JSUB
        LDX     0013,0
        TRAP4   READ            /JUMP TO PALB ROUTINE
        FLDA    DUM             /PASS SIGNAL TO COMMON VARIABLE OPT
        FNORM
        FSTA    DUMMY
        FLDA    DUMMY
        FSTA    FOUR
        TRAP4   CLEAR   /JUMP TO PALB ROUTINE TO CLEAR INTEGRATOR
        LDX     0014,0
        EXTERN  #NE
        JA      #RTN
        LDX     0015,0
        EXTERN  #NE
        JA      #RTN
        SECT8 GTDTA8    /PALB ROUTINE
        STADC=6300      /START AD CONVERSION IOT
        RDSW=6301       /READ STATUS WORD FLAGS IOT
        CLRSW=6302      /CLEAR STATUS WORD FLAGS IOT
        RDAD=6306       /READ AD DIGITAL VALUE IOT
        CLRINT=6310     /CLEAR INTEGRATOR IOT
        RDINT=6311      /READ INTEGRATOR CHANNEL IOT
JSUB,   0,0,0
DUM,    27,0,0          /DUMMY VARIABLE FOR PASS BACK OF INTEGRATOR
/                         CHANNEL SIGNAL. EXPONENT OF 27 NEEDED FOR FPTN

M50,    -100
M50A,   -100
M100,   -100
M100A,  -100
ADBIT,  2               /BIT TO CHECK IF A/D IS DONE
WAIT,   C               /WAIT 50 USEC BEFORE GETTING DATA
```

```
        ISZ MSC
        JMP .-1
        CLA
        TAD MSCA
        DCA MSC
        CDF CIF 0
        JMP# WAIT       /JUMP BACK TO RALF
READ,   0               /READ INT.,CONVERT TO DIGITAL,& PASSIBACK AS
        CLA             /FLOATING POINT NUMBER
        TAD JSUB+2      /CHECK IF NOT USING THIS CHNNL (I.E. JSUB+2=0)
        SNA             /IS JSUB+2 = 0?
        JMP DON         /YES, JUMP OUT OF ROUTINE
        DCA DUM+1       /NO, CONTINUE WITH ROUTINE
        TAD JSUB        /EXPONENT OF JSUB GIVES RIGHT CHANNEL
        RDINT           /READ INTEGRATOR
        TAD MIOCA
        DCA MIOC
        ISZ MIOC        /WAIT FOR INTEGRATOR TO SETTLE
        JMP .-1
        STADC           /START A/D CONVERSION
        RDSW            /CHECK TO SEE WHEN A/D IS DONE
        AND ADBIT
        SNA
        JMP .-3
        RDAC            /VALUE NOW IN AC
        DCA DUM+2       /PUT DATA IN FLOATING PT NUMBER
DON,    CDF CIF 0
        JMP# READ       /JUMP BACK TO RALF
/
CLEAR,  0
        CLRINT          /CLEAR INTEGRATOR
        CDF CIF 0
        JMP# CLEAR      /JUMP BACK TO RALF
```

```
LIST GETAT.FT

C       SUBROUTINE GETS DATA FROM INTEGRATOR, CONVERTS IT TO DIGITAL
C       AND RETURNS IT AS FLOATING POINT NUMBER.
C       ONE=SIGNAL FROM CHANNEL JONE, TWO = SIGNAL FROM CHANNEL JTWO,
C       THREE=SIGNAL FROM CHANNEL JTHRE, FOUR=SIGNAL FROM CHANNEL JFOUR
C       INTEGRATOR CHANNEL #'S:  JONE IS FIRST CHNNL IN CALL SBRTN STATE
C
C         MENT OF MAIN PROG., JTWO IS 2ND IN CALL SBRTN STATEMENT, ETC.
C
        SUBROUTINE GTDATA
        COMMON/INTSIG/ONE,JONE,TWO,JTWO,THREE,JTHRE,FOUR,JFOUR
        JS=JONE
        ONE=DUMMY
        JS=JTWO
        TWO=DUMMY
        JS=JTHRE
        THREE=DUMMY
        JS=JFOUR
        FOUR=DUMMY
        RETURN
        END
C       NOTE THAT GTDATA.RA HAS BEEN CHANGED EXTENSIVELY.
```

```
LIST OFLOW.RA

/       SUBROUTINE OFLOW.RA (RALF ASSEMBLY LANGUAGE)
/         CHECKS TO SEE IF COUNTER OVERFLOW HAS OCCURED.
        SECT    OFLOW
        JA      #ET
#XR,    ORG     .+10
        TEXT    *OFLOW*
#RET,   SETX    #XR
        SETB    #BASE
        JA      .+3
#BASE,  ORG     .+6
TMS,    ORG     .+3     /TMS PASSES OVERFLOW INFO TO MAIN PROG.
        ORG     #BASE+3C
        FNOP
        JA      #RET
        FNOP
#GOBAK, CLC
#ARGS,  ORG     .+3
DUM2,   ORG     .+0003
#TMP,   ORG     .+0011
#LIT,   0001
        2000
        0000
        0002
        3000
        0004
        0003
        3000
        0000
        #LBL=.
        ORG     #LBL
#RTN,   BASE    #BASE
        JA      #GOBAK
#ET,    START
        0210
        FSTA    #GOBAK,0
        0200
        SETX    #XR
        SETB    #BASE
        LDX     0,1
        FSTA    #BASE
        FSTA    #ARGS
        FLDA%   #BASE,1*
        FSTA    TMS
        START
        LDX     0002,0
        LDX     0003,0
        TRAP4   FLOW            /JUMP TO ROUTINE TO CHECK OVERFLOW
        FLDA    DUM3            /OVERFLOW INFO PASSED FROM DUM3--
        FNORM
        FSTA    DUM2            /  TO DUM2--
        FLDA    DUM2            /  TO TMS.
        FSTA%   TMS     /TMS = 0 IF NO OVERFLOW, = 1 IF OVERFLOW
        LDX     0004,0
        EXTERN  #NE
        JA      #RTN
        LDX     0005,0
        EXTERN  #NE
        JA      #RTN

        SECT6 FLOWE             /PAL8 ROUTINE
        OVRFLW=6153             /CHECK FOR OVERFLOW IOT
        RSTOFW=6154             /RESET OVERFLOW STATUS (FLIP FLOP) IOT
```

```
DUM3,   27?C?C
FLOW,   0
        CLA
        OVRFLW                  /READ OVERFLOW STATUS
        DCA DUM3+2              /PUT OVERFLOW STATUS IN DUM3
        RSTOFW                  /RESET OVERFLOW STATUS FLAG
        CDF CIF 0
        JMP% FLOW               /BACK TO RALF


 LIST OFLOW.FT

C       SUBROUTINE FINDS IF OVERFLOW HAS OCCURED AT COUNTER. TMS VALUE
C       INDICATES OVERFLOW IF EQUAL TO ONE.
C       SUBSTANCIAL REVISION OF RALF FILE.
        SUBROUTINE OFLOW(TMS)
        TMS=DUM2
        RETURN
        END
```

```
 LIST SKPWDN.RA

/       SUBROUTINE SKPWDN (RALF ASSEMBLY LANGUAGE)
/         RECOGNIZES END OF EXP CYCLE
        SECT    SKPWDN
        DA      #ST
#YR.    ORG     .+10
        TEXT    +SKPWDN.+
#RET.   SETX    #XR
        SETB    #BASE
        DA      .+3
#BASE.  ORG     .+6
        ORG     #BASE+30
        FNOP
        DA      #RET
        FNOP
#GOBAK. ORG
#ARGS.  ORG     .+2
#TRP.   ORG     .+0011
#LIT.   0001
        2000
        0000
        0002
        3000
        0000
        0003
        3000
        0000
        #LBL=.
        ORG     #LBL
#PTR.   BASE    #BASE
        DA      #GOBAK
#ST.    START
        0210
        FETA    #GOBAK,0
        0200
        SETX    #XR
        SETB    #BASE
        START
        TRAP4   SKIPDN  /JUMP TO RALF SBRTN.
        LDX     0002,0
        LDX     0003,0
        EXTERN  #NE
        DA      #RTN
        LDX     0004,0
        EXTERN  #NE
        DA      #RTN

        SECTE SKPDNE    /RALF ROUTINE
        SKPEDN=6305     /SKIP PROGRAM LINE IF SKIP LINE ENABLED IOT
SKIPDN. 0
        SKPEDN          /SKIP NEXT PROGRAM LINE IF SKIP ENABLED.
        JMP .-1
        CDF CIF 0       /END OF CYCLE PULSE ENABLED SKIP LINE
        JMP* SKIPDN     /JUMP BACK TO RALF PROGRAM
```

```
LIST PHOTON.RA

/       SUBROUTINE PHOTON.RA (RALF ASSEMBLY LANGUAGE)
/         RETRIEVES COUNT FROM 770 COUNTER, CONVERTS IT FROM
/           BCD TO FRTN FLOATING PT., AND PASSES IT TO MAIN PROG.
        SECT    PHOTON
        JA      #ST
#XR,    ORG     .+10
        TEXT    +PHOTON+
#RET,   SETX    #XR
        SETB    #BASE
        JA      .+3
#BASE,  ORG     .+6
SIGS,   ORG     .+3             /VARIABLE FOR PASSING COUNT TO MAIN
        ORG     #BASE+30
        FNCF
        JA      #RET
        FNCF
#GOBAK, OIC
#ARGS,  ORG     .+3
DUMMY,  ORG     .+0003
#TMP,   ORG     .+0011
#LIT,   0001
        2000
        0000
        0002
        3000
        0000
        0003
        3000
        0000
        #LBL=.
        ORG     #LBL
#RTN,   BASE    #BASE
        JA      #GOBAK
#ST,    STARTF
        0210
        FSTA    #GOBAK,0
        0200
        SETX    #XR
        SETB    #BASE
        LDX     0,1
        FSTA    #BASE
        FSTA    #ARGS
        FLDA*   #BASE,1+
        FSTA    SIGS
        STARTF
        LDX     0002,0
        LDX     0003,0
        TRAP4   CONV8           /JUMP TO RALF ROUTINE
        FLDA    DUM             /PASS FLTNG PT. COUNT FROM DUM--
        FNORM
        FSTA    DUMMY           /  TO DUMMY--
        FLDA    DUMMY
        FSTA*   SIGS            /  TO SIGS.
        LDX     0004,0
        EXTERN  #NE
        JA      #RTN
        LDX     0005,0
        EXTERN  #NE
        JA      #RTN

        SECT8   CONV8           /RALF ROUTINE
        STONE=6151              /STROBE MSB FROM 770 COUNTER IOT
```

```
        STTWO=6150              /STROBE LSB FROM 77C COUNTER IOT
        RSTCNT=6152             /RESET COUNTER IOT
DUM,    27;0;0
CONV,   0
        CLA CLL
        STONE                   /GET 12 MSB FROM 24 BCD BITS
        DCA HOLD
        STTWO                   /GET 12 LSB FROM 24 BCD BITS
        DCA HOLD+1
/       USE SLIGHTLY ALTERED DECUS PROGRAM CHEW TO CONVERT BCD INTO
/           FRTN FLOATING POINT
                        /CHEW-CONVERT ANY BCD TO BINARY-
                        /DOUBLE PRECISION PAL 00021 A
                        /THEN TO FLOATING POINT
        TAD NEG24
        DCA CHK1        /SET COUNTER I#-30 OCTAL
        TAD M4
        DCA CHK2
        TAD M6          /-6 IN AC
        DCA CHK3        /SET L#-6
        DCA CHK4        /SET M#0
        DCA DUM+1       /NOW CLEAR THESE TWO LOCATIONS FOR
        DCA DUM+2       /SUMMATION OF ANSWER
        TAD HOLD        /MOST SIG. OF BCD NO. IN AC
MID,    DCA TEMPY       /VALUE IN AC TO COMMON STORAGE
DO,     CLA CLL         /STORE IT + GET IT BACK
        TAD TEMPY
        RAL
        DCA TEMPY       /STORE ROTATED #
        SNL             /IS THERE A BIT
        JMP INCJ        /NO INCREMENT COUNTERS
        TAD TABLE       /YES ADD ONE OF THE BIT VALUES
        DCA CUM+1       /PUT IT IN LEAST SIG OF MULTIPLICATIONS
AGN,    ISZ CHK4        /M#M+1
        TAD CHK4        /GETM
        TAD CHK3        /M+(-L)
        SZA             /IS M#L
        JMP MLTPY       /NOW GO MULTIPLY
        CLL CLA
        TAD CUM+1       /YES GET LEAST SIG RESULT OF MULTIPLY
        TAD DUM+2       /ADD IT TO LEAST SIG. OF BINARY NO.
        DCA DUM+2       /STORE RESULT IN BINARY NO. LOCATION
        RAL             /ADD
        TAD CUM         /MOST SIG
        TAD DUM+1       /HALVES
        DCA DUM+1       /STORE FOR POSSIBLE EXIT
        DCA CUM         /CLEAR FOR RESULT OF NEXT MULTIPLY
        DCA CHK4        /SET M#0
        JMP INCJ        /GO INCREMENT COUNTERS
MLTPY,  JMS MULT        /GO TO MULTIPLY BY 12 SUBROUTINE
        JMP AGN
INCJ,   CLA             /SET TABLE TO NEXT BCD BIT VALUE
        TAD TABLE
        RAR
        DCA TABLE
        ISZ CHK2        /J#J+1%C
        JMP INCI        /NO INCREMENT I
        TAD M4
        DCA CHK2
        CLA CLL         /YES, RESET TABLE TO 8 OCTAL
        TAD RESET
        DCA TABLE       /PUT TABLE BACK TO INITIAL VALUE OF 10
```

```
          IAC               /+1 IN AC
          TAD CHK3          /L+1
          DCA CHK3          /L@L+1
INCI,     ISZ CHK1          /I@I+1@0
          JMP NOT           /NO. TO SEE IF I EQUALS -14 OCTAL
          RSTCNT            /PREPARE TO LEAVE, RESET COUNTER
          CLL
          CDF CIF 0
          JMP% CONV         /LEAVE
NOT,      TAD CHK1          /ADD 1 TP AC
          TAD FRTN          /ADD +14 OCTAL TO AC
          SZA CLA           /DOES I@=12
          JMP II            /NO, GO BACK AND LOOP FOR ANOTHER BIT
          TAD HOLD+1        /YES, GET LEAST SIG. BCD NO. IN AC
          JMP MID           /PUT LEAST SIG OF BCD# IN TEMP
SUBPR,    0                 /SUBPOUTINE TO MULTIPLY THE VALUE
          CLA CLL           /IN CUM BY 12 OCTAL
          TAD NEG12         /SET COUNTER TO---
          DCA COUNT         /MINUS 12 OCTAL.
          TAD CUM+1         /RESTORE STARTING VALUE SO IT CAN---
          DCA NOW+1         /BE ADDED TO ITSELF 12 TIMES (OCTAL)--
          TAD CUM           /AND STILL RETAIN THE RUNNING TOTAL--
          DCA NOW           /IN CUM AND CUM+1.
REPEAT,   CLL
          TAD CUM+1         /ADD LEAST---
          TAD NOW+1         /SIG. PARTS.
          DCA CUM+1
          RAL               /ADD ANY OVERFLOW IN LINK---
          TAD CUM           /TO THE SUM OF THE MOST SIGS.
          TAD NOW
          DCA CUM
          ISZ COUNT         /IF ZERO, NO. HAS BEEN ADDED TO ITSELF---
          JMP REPEAT        /12 OCTAL TIMES.
          CLL
          JMP% MULT         /EXIT TO MAIN PROGRAM
NO,       -4
NS,       -6
NBCD84,   -30               /OCTAL NO.
CHK1,     0                 /COUNTER I-SEE FLOWCHART
CHK2,     0                 /COUNTER J
CHK3,     0                 /COUNTER L
CHK4,     0                 /COUNTER M
TENPS,    0
ADDR,     0                 /LOCATION OF BCD#
NOW,      0
          0
NEG11,    7765
COUNT,    0
CUM,      0                 /HOLDS RESULTS F MULTIPLYIN.12'S
          0                 /WHERE X#5,4,2, OR 1 W#ITHINS
TABLE,    10                /8 IN OCTAL
RESET,    17                /RESETS TABLE TO 8 OCTAL
FRTN,     14                /OCTAL NO.
HOLD,     0
          0

 LIST PHOTON.FT

C         SUBROUTINE PHOTON TRANSFERS COUNT FROM 77C TO MAIN PROGRAM
C         SUBSTANCIAL REVISION OF RALF FILE
          SUBROUTINE PHOTON (SIGS)
          DUMMY=SIGS
          RETURN
```

```
 LIST STEPWL.RA

/       SUBROUTINE STEPWL
/         STEPS LASER GRATING ONE STEP INCREMENT AND CHECKS
/         SCAN CONTROL LIMIT LINE
        SECT    STEPWL
        JA      #ST
#XR,    ORG     .+10
        TEXT    +5TEPWL+
#RET,   SETX    #XR
        SETB    #BASE
        JA      .+3
#BASE,  ORG     .+6
NOSTPS, ORG     .+3
LIM,    ORG     .+3
        ORG     #BASE+30
        FNOP
        JA      #RET
        FNOP
#GOBAK, DIO
#ARGS,  ORG     .+3
NOSE,   ORG     .+0003
#TMP,   ORG     .+0011
#LIT,   C000
        0000
        0003
        C001
        2000
        0000
        0002
        3000
        0000
        0003
        3000
        0000
        #LBL=.
        ORG     #LBL
#RTN,   BASE    #BASE
        JA      #GOBAK
#ST,    START2
        0210
        FSTA    #GOBAK,0
        0200
        SETX    #XR
        SETB    #BASE
        LDX     0,1
        FSTA    #BASE
        FSTA    #ARGS
        FLDA*   #BASE,1+
        FSTA    NOSTPS
        FLDA*   #BASE,1+
        FSTA    LIM
        START2
        LDX     0002,0
        LDX     0003,0
        FLDA    #LIT+0003
        FSTA    NOSE
        FLDA*   NOSTPS
        FSTA    #DOTMP+0000

#GOOD1, LDX     0004,0
        TRAP4   STEP    /JUMP TO PAL8 SUBROUTINE
        FLDA    #LIT+0000
        PASS BACK LIMIT WARNING INFORMATION
```

```
        FSTA%   LIM
        FLDA    LM
        FNOP%
        FSTA%   LIM
        LDX     0005,0
        FLDA%   LIM
        CLT     #955
        JER     #950
        JA      #955
        LDI     0006,0

#955,   FLDA%   NOSTP%
        FADD    #LIT+0003
        FSTA    NOSE
        LDX     0007,0

#950,   FLDA    NOSE
        FADD    #LIT+0003
        FSTA    NOSE
        FSUB    #DOTMP+0000
        JLE     #0001
        LDX     0010,0
        ENTER1  #NE
        JA      #RTN
        LDX     0011,0
        ENTER1  #NE
        JA      #RTN
#DOTMP, DPO     .+0003
        SECTS STEPE             /FALE ROUTINES
        RDSW=6301               /READ STATUS WORD FLAGS IOT
        CLRSW=6302              /CLEAR STATUSWORD FLAGS IOT
        STPWL=6304              /STEP LASER ONE STEP INCR. IOT
STBIT,  10                      /CHECK STEPPED BIT, BIT 8 OF AC
LIMBIT, 1                       /CHECK LIMIT BIT, BIT 11 OF AC
LM,     0000
EXPCT,  27
/
STEP,   0
        CLRSW                   /CLEAR STEPPED FLAG OF SCAN CONTROL
        STPWL                   /STEP WAVELENGTH
        RDSW                    /CHECK STATUS WORD
        AND STBIT               /SEE IF STEPPED FLAG HAS BEEN SET
        SNA                     /HAS IT BEEN SET?
        JMP .-3                 /NO, CHECK AGAIN
        RDSW                    /YES, READ STATUS WORD AGAIN
        AND LIMBIT              /CHECK IF SCAN CONTROL LIMIT REACHED
        DCA LM+2                /PUT VALUE OF AC IN LM
        TAD EXPCT
        DCA LM
        DCA LM+1
        CDF CIF 0
        JMP* STEP
```

```
 LIST QDONEN.FT

C       SUBROUTINE QDONE HAS MESSAGES ONCE EXPERIMENT HAS ENDED. IT ALSO

C       PRINTS THE # OF DATA POINTS ACTUALLY TAKEN IN THE OUTPUT FILE.
        SUBROUTINE QDONE(IW,NL,MK)
C       PRINT # OF POINTS IN OUTPUT FILE.
        WRITE (8,899)MK
899     FORMAT (I4)
        MM=0
C       RING BELL TO INDICATE END OF EXPERIMENT.
        DO 898 IJK=1,20
        CALL BELL
898     CONTINUE
        CALL MOVABS(55,740)
        CALL ANMODE
210     WRITE(4,211)
211     FORMAT(' DECISION TIME!! ',///,' TYPE 1 TO REPEAT SAME EXPERIMENT
     ,
     1   ',//,' TYPE 2 TO RUN EXPERIMENT WITH SOME CHANGES OR ',//,
     1  ' TYPE 3 IF YOU ARE DONE AND RETURN TO KEYBOARD MONITOR. ')
        READ (4,218)IW
218     FORMAT (I2)
        IF (IW.GT.3)GOTO 210
        IF (IW.LT.1)GOTO 210
        GOTO(214,217,217),IW
214     NL=0
        MK=0
        WRITE(4,221)
        READ(4,212)IP
        DATA IY,IN/1HY,1HN/
        IF(IP.EQ.IN)GO TO 210
217     RETURN
221     FORMAT (//,' YOU MUST SET THE SCAN CONTROL BACK TO
     1  THE ORIGINAL ',//,' WAVELENGTH BEFORE WE CAN START. TYPE Y WHE
     1  RETURN WHEN ',//,' THE EXPERIMENT IS READY TO RUN AGAIN. ',///,
     1  ' IF YOU WISH TO START OVER WITH THE PRECEDING ?, TYPE N. ')
212     FORMAT (A3)
        END
```

```
LIST ERROR.FT

C       SUBROUTINE HANDLES ALL ERROR MESSAGES
C
        SUBROUTINE ERROR(ERR)
        IF (ERR+1)475,485,555
475     WRITE (0,495)ERR
        GO TO 555
485     WRITE (0,515)ERR
555     RETURN
495     FORMAT (' ERROR: NLEFT IS NEGATIVE!? NLEFT = ',I10)
515     FORMAT (' ERROR: INDICATION IS YOU HAVE REACHED THE LIMIT OF
     1  THE SCAN CONTROL RANGE. CHECK SCAN CONTROL. LIMIT = ',G12.6)
        END
```

CHAPTER III

THE FIRST SPECTRA: N_2^+ AND CO^+

The purpose of this chapter is to present the first successful attempts at obtaining spectra of molecular ions with our experimental apparatus. In addition to serving as the initial test of our apparatus, the resulting spectra provided some information about different aspects of our experimental technique.

Because the (v'=0, v''=0) band of the $\tilde{B}\ ^2\Sigma_u^+ - \tilde{X}\ ^2\Sigma_g^+$ transition of N_2^+ is so intense, it was chosen as the first spectrum to be attempted. The large oscillator strength for this transition implies a very short radiative lifetime for the $^2\Sigma_u^+$ state (~60 nanoseconds). This short lifetime required the fluorescence detection gate (described in Section II-D) to be placed very close to the time of the laser pulse, and thereby tested our system in the nanosecond time regime.

After the success of the N_2^+ experiments, the ability of our apparatus to obtain spectra for weaker transitions needed to be examined. The (2,0) band of the $\tilde{A}\ ^2\Pi_i - \tilde{X}\ ^2\Sigma^+$ transition of CO^+ was chosen. The radiative lifetime of the state is on the order of 3 microseconds which indicates a lower transition probability than that of the N_2^+ $\tilde{B}$-$\tilde{X}$ transition. The low signal level of this $\tilde{A}$-$\tilde{X}$ transition required the use of the photon counting system described in Section II-D to obtain a reasonable spectrum. Both the N_2^+ and CO^+ spectra are presented in the following sections.

A. The (0,0) Band of the N_2^+ $\tilde{B}$-$\tilde{X}$ Transition

For these experiments, very low mass resolution was used to maximize the number of N_2^+ ions in the trap. The N_2 pressure was kept at 5×10^{-5} torr (uncorrected ionization gauge). A 20 millisecond ionization period was used with the laser being fired 150 microseconds after the electron gun was gated off. A fluorescence detection gate, 200 nanoseconds in duration, was placed 50 nanoseconds after the laser pulse. The detection gate could not be placed any closer to the laser pulse because of the radio frequency interference (RFI) generated by the firing of the nitrogen laser.

The resulting fluorescence was so intense that the spectrum could be easily obtained by either the integration detection scheme or the photon counting system described previously in Chapter II. The spectrum shown in Figure III-1 was taken using the photon counting system with the laser being fired 500 times at each wavelength point. A wavelength increment of 0.1 Å was used which is smaller than the laser's nominal bandwidth (~0.2 Å) in this wavelength region.

Because the transition is between two Σ electronic states, only a P and R branch are observed, as can be seen in Figure III-1. The difference in rotational constants in the two states results in a very strong P branch band head. The R branch assignments are shown in the figure labeled by the rotational quantum number N'' where it is seen that the rotational structure is easily resolved. Two remaining features in the spectrum should be mentioned. The alteration

Figure III-1. The Fluorescence Excitation Spectrum of the (0,0) $\tilde{B}\ ^2\Sigma_u^+ - \tilde{X}\ ^2\Sigma_g^+$ Band System of N_2^+.

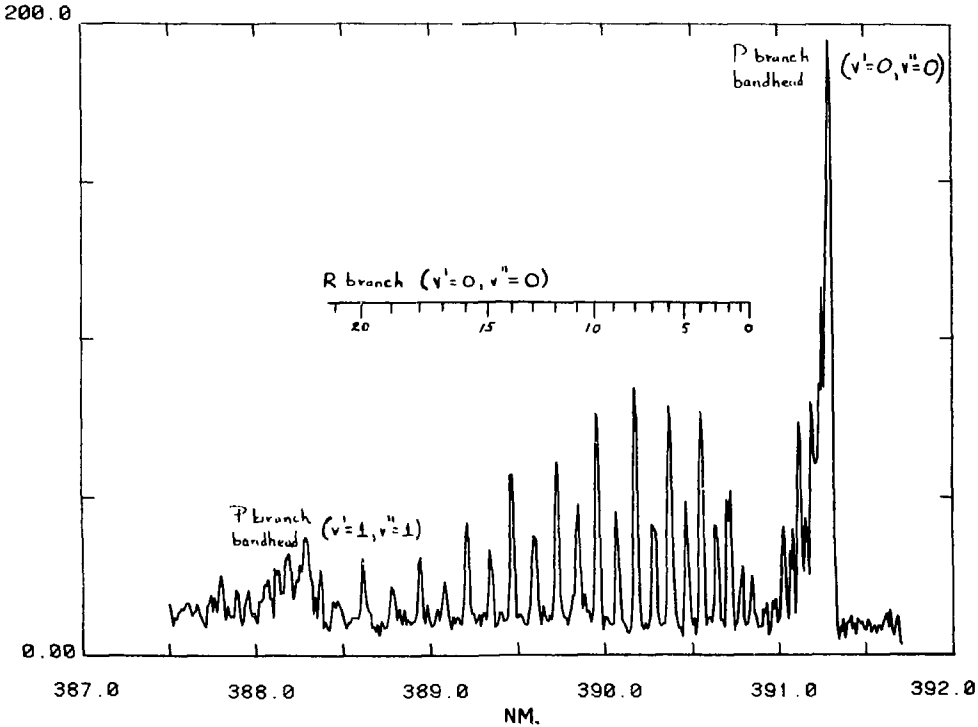

XBL 799-11273

in the intensities is due to the nuclear-spin statistics which results in the odd N" having half as many nuclear-spin states as even N" levels. The second feature to be noted is the (1,1) band head near 3882.5 Å. At room temperature, this band head is usually 70,000 times less intense than the (0,0) band head.[1] The increased population of the second vibrational level of the $\tilde{X}$ state observed in our spectrum is a direct result of the "collision-free" conditions in our experiment: the population in the v'=1 level of the $\tilde{X}$ state, created by electron impact, does not have time to collisionally relax before being interrogated by the laser.

The R branch can be used to derive a rotational temperature of the N_2^+ ions in our trap by plotting the logarithm of $I_{N',N''}/(N'+N''+1)$ versus N"(N"+1) where I is the intensity of the transition between the N" rotational level of the $\tilde{X}$ state and the N' rotational level of the $\tilde{B}$ state.[2] Only the even rotational levels were used to produce such a plot shown in Figure III-2 where a rotational temperature of 360 ± 25°K is derived. This temperature compares well with the results obtained by Zare et al.[3] in their experiments on the N_2^+ rotational temperature versus electron energy.

B. The (2,0) Band of the CO^+ $\tilde{A}\ ^2\Pi_i$ - $\tilde{X}\ ^2\Sigma^+$ Transition

To obtain the spectra of CO^+ molecular ions, the ions were again trapped under low mass resolution. The longer lifetime allowed the fluorescence detection gate to be moved out to 200 nanoseconds after the laser pulse reducing the problem of RFI produced by the laser. The detection gate was

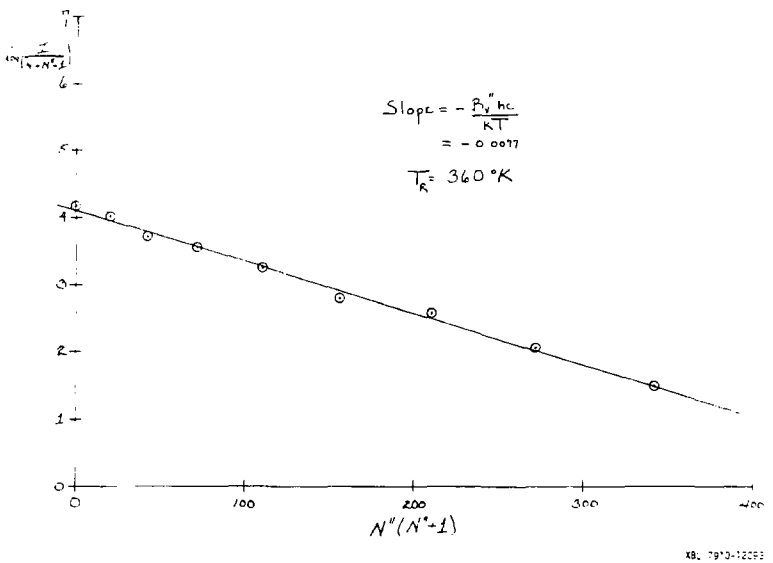

Figure III-2. Rotational Temperature Determination from N_2^+ Spectrum.

set to 6 microseconds in duration. All other conditions were the same as those in the N_2^+ experiments.

While attempts to observe the (2,0) band with the integration detection system failed, the spectrum shown in Figure III-3 was observed with the photon counting system. Good signal-to-noise was obtained by firing the laser 1000 times at each wavelength point. The spectrum for this band system is a good deal more complicated than that of the N_2^+ band system just described. The complications arise from the unit of orbital angular momentum about the internuclear axis in the Π electronic state. In addition to P and R rotational branches, Q branches are now also allowed. The interaction between the non-zero spin and the electronic angular momentum (spin-orbit coupling) splits each of these branches which results in two P, two Q and two R branches. The doublet splitting of the $^2\Sigma^+$ ground state again splits each of these branches yielding a total of 12 overlapping rotational branches observed in Figure III-3.

The spin-orbit splitting is large enough to separate the branches into two manifolds, $^2\Pi_{3/2}$ and $^2\Pi_{1/2}$, each containing 6 branches. In Figure III-3, the $^2\Pi_{1/2} - {}^2\Sigma^+$ branches are seen to begin at 4248 Å and extend throughout the spectrum overlapping with the $^2\Pi_{3/2} - {}^2\Sigma^+$ bands which begin at ~4272 Å. Only the band heads are labeled in the interest of clarity. The subscripts on the labels represent the two doublet components of the $^2\Sigma^+$ state. The lines in the Q_2 and R_1 branches in both spin-orbit manifolds lie so close together that they cannot be resolved (even in high resolution emission

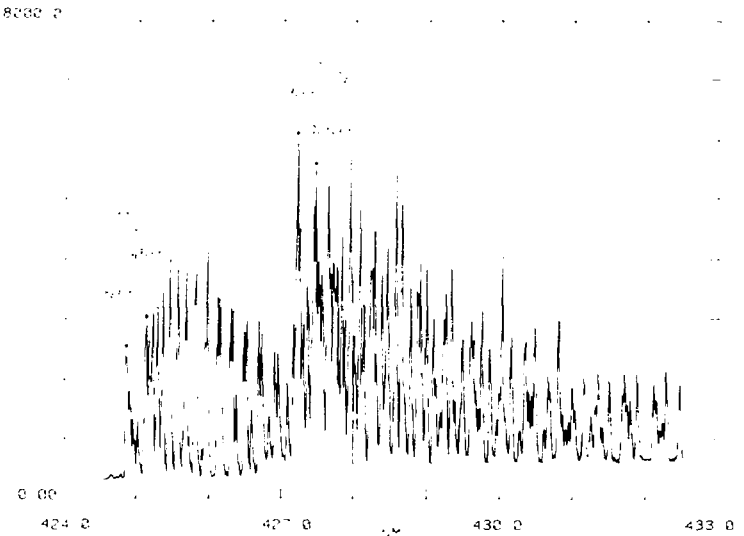

Figure III-3. Fluorescence Excitation Spectrum of the (2,0) $\tilde{B}\ ^2\Pi - \tilde{X}\ ^2\Sigma^+$ Band System of CO^+.

spectroscopy) and are, therefore, labeled together. All of the lines observed in the spectrum can be matched with the assignments in Reference 4.

From the frequencies of some of the nearly overlapping lines, an indication of our resolving power can be obtained. As was mentioned before in Chapter II, our resolution is limited by the bandwidth of the laser (1 cm^{-1}) and the Doppler width of our ions. The part of the $^2\Sigma_{1/2} - {}^2\Sigma^+$ subband which does not overlap with the $^2\Pi_{3/2}$ band is reproduced in Figure III-4 where it is now plotted on a frequency scale. The frequencies for three pairs of closely spaced lines are given in this figure. The center pair of lines being the least well resolved is separated by 1.52 cm^{-1}. The pair of lines at higher frequencies are slightly more resolved and are separated by 1.57 cm^{-1}. The pair at lowest energy which differ in frequency by 2.76 cm^{-1} are well resolved (although not completely). The FWHM of several non-overlapped rotational lines (indicated by the narrow arrows in Figure III-4) is 1.7 cm^{-1}. This linewidth agrees with that observed for lines in the N_2^+ spectrum. Assuming the width to be totally due to the Doppler effect, a velocity of 1.1×10^6 cm/sec is obtained. This value agrees well with that derived in Section II-B.

In summary, the spectra observed for N_2^+ and CO^+ proved that our experiment would work. They also tested the performance of our apparatus under conditions of fast time scale detection and low signal intensity. Although no new spectroscopic

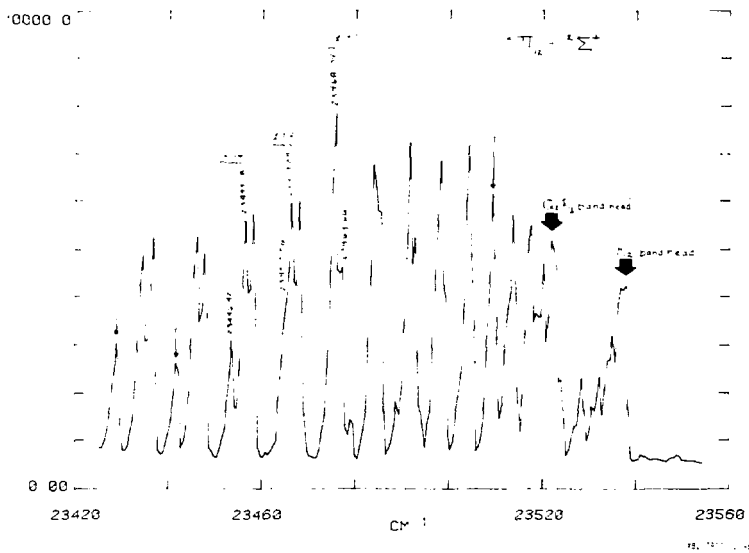

Figure III-4. Part of (2,0) $\tilde{B}\ ^2\Pi_{1/2} - \tilde{X}\ ^2\Sigma^+$ Band System of CO^+.

information could be derived for these ions, the rotational structure resolved allowed the determination of some of the characteristics of our apparatus. In the next two chapters, the spectra we obtained for the 1,3,5-trifluorobenzene cation and the BrCN cation are described. New information derived from these spectra concerning the vibrational states of these molecules is also presented.

References, Chapter III

1. K. Lofthus, J. Phys. Chem. Ref. Data, 6, 113 (1977).

2. G. Herzberg, Spectra of Diatomic Molecules, Van Nostrand Reinhold Co., Princeton, NJ (1950) p. 206.

3. J. Allison, T. Kondow, and R. N. Zare, Chem. Phys. Lett., 64, 202 (1979).

4. D. Coster, H. H. Brons, and H. Bulthuis, Z. Physik, 79, 787 (1928).

CHAPTER IV

THE $\tilde{B}\ A_2''$ - $\tilde{X}\ E''$ BAND SYSTEM OF 1,3,5-TRIFLUOROBENZENE CATION

In an attempt to resolve the controversy concerning the number of bands in the photoelectron (PE) spectrum of benzene and the ordering of its molecular orbitals, the PE spectra of many of the fluoro-substituted benzenes have been obtained by several groups.[1-5] From these spectra, the $\tilde{B}$-$\tilde{X}$ transition of the fluorobenzene cations is found to lie in the visible wavelength region. Using th nformation, Maier and co-workers[6,7] proceeded to obtain the emission spectra of several of these cations by a controlled electron impact technique. In all of their spectra, they observed a strong 0_0^0 (vibrationless) band accompanied by less intense bands at longer wavelengths. These longer wavelength bands provided information about the vibrational levels of the ground state ion.

Very few bands at wavelengths shorter than the 0_0^0 band which would provide information about the excited electronic state, were observed. This prompted our investigation of the 1,3,5-trifluorobenzene cation. From the fluorescence excitation spectrum that we would observe, transitions to excited vibrational levels of the upper electronic state would most likely occur. Thus, we should be able to provide data concerning the vibrational levels of the upper electronic state of this cation and thereby, supplement the information obtained from emission spectroscopy.

During the time of our investigations of this molecular ion, several other groups were also studying the fluorobenzene cations. Leach et al.[8,9] completed a very in-depth analysis of the high resolution emission spectra of several of these cations. Miller, Bondybey, and co-workers carried out a very thorough investigation on many halo-substituted benzenes in the gas phase[10,12,15] and in condensed phases[11,13,15] using a laser induced fluorescence technique very similar to ours. The purpose of this chapter is to present the spectrum we have observed for the 1,3,5-trifluorobenzene cation and to compare our results with those obtained by other researchers.

A. Experimental Conditions

Because of the large molecular weight (132 a.m.u.), we were unable to use high mass resolution in trapping these ions. Although difficult to determine, the FWHM mass range obtained in these experiments appeared to be about $\pm$ 15 a.m.u. The only interference encountered by other research groups was the transitions of the neutral species CH ($\tilde{A}\ ^2\Delta$ - $\tilde{X}\ ^2\Pi$) and H (Balmer lines). These will not appear in our spectra. Thus, the mass resolution we obtained was sufficient for our purposes. A pressure of 5×10^{-5} torr was maintained throughout these experiments.

The lifetime of the $\tilde{B}$ state of 1,3,5-tribluorobenzene cation (referred to hereafter as sym-TFB) was measured to be ~60 nanoseconds with a quantum yield approaching unity.[7] We, therefore, used a fluorescence detection gate of 200 nanoseconds

duration, and the large quantum yield allowed us to place the detection gate 150 nanoseconds after the laser pulse. The laser fired 150 microseconds after the electron gun was gated off. It should be noted here that, unlike the laser induced fluorescence experiments of other research groups,[10-15] we did not need to place a filter in front of our photomultiplier tube to block scattered laser light.

The rotational structure could not be resolved by the 1 cm^{-1} bandwidth of our laser, so a 1 Å wavelength increment was used in scanning the laser. The laser was fired 750 times at each wavelength point. The 400 nm to 500 nm region required the use of 8 laser dyes whose spectra were overlapped with the use of our minicomputer.

B. The Fluorescence Excitation Spectra of the 1,3,5-Trifluorobenzene Cation

From the photoelectron work,[1-5] the $\tilde{B}$-$\tilde{X}$ transition of sym-TFB is found to be a π-π transition. The molecule is assumed to be a regular planar hexagon in both states. The electronic ground state of the ion is $^2E''$, being formed by the removal of an electron from a doubly degenerate π-molecular orbital of e" symmetry. The $\tilde{B}$ state of the ion is formed by the removal of an electron from an a_2'' π-orbital resulting in a $^2A''$ state. Thus, the $\tilde{X}$ state is doubly degenerate while the $\tilde{B}$ state is not. The transition is then $\tilde{B}\ ^2A'' - \tilde{X}\ ^2E''$ and is fully allowed as will be shown later.

The spectrum we observed for this transition is reproduced in Figure IV-1. What we observe is a series of bands

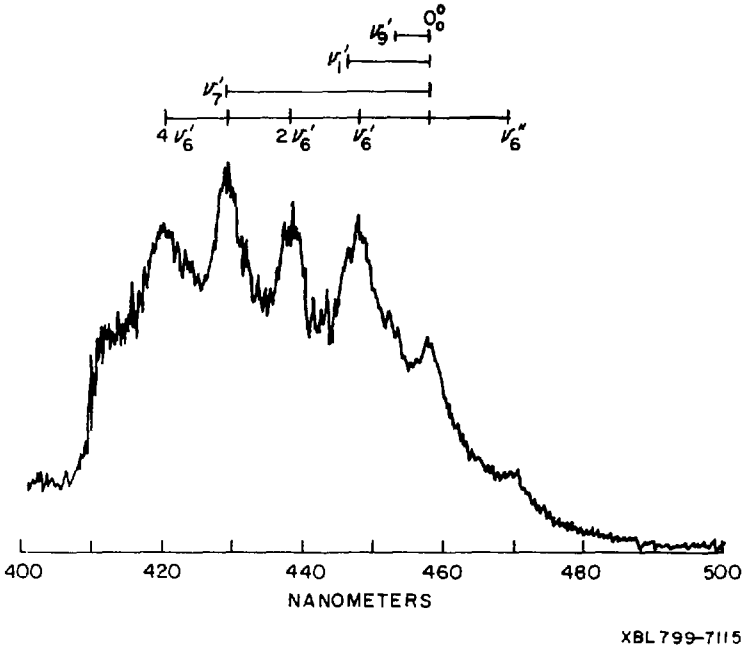

Figure IV-1. Fluorescence Excitation Spectrum of the $\tilde{B}\ ^2A'' - \tilde{X}\ ^2E''$ Band System of the 1,3,5-Trifluorobenzene Cation.

on top of a pseudocontinuum. This appearance is similar to what was observed by Maier et al.,[6,7] but is unlike that of Miller and Bondybey.[10,12,15] In their work, less of a pseudocontinuum is observed which indicates that our ions are more vibrationally "hot" than theirs. This is reasonable because we work under almost collisionless conditions where as Miller and Bondybey's ions are contained in a bath of noble gas molecules.

The vibrationless transition, denoted 0_0^0 in Figure IV-1, is assigned by comparison with the PES work and the emission spectrum. As was anticipated, several bands are observed at shorter wavelengths while only one band appears at longer wavelengths. The frequencies of these bands are given in the first column of Table IV-1. These values are center-band frequencies and are uncertain to about ± 10 cm^{-1}. The last band and those observed with weak intensity are more uncertain, ± 20 cm^{-1}.

In the second column, the 0_0^0 band is given as the origin (0) and the separation of each band from 0_0^0 is listed. It is seen from these values and from Figure IV-1 that the very strong vibrational bands observed are separated by slightly less than 500 cm^{-1}. The one hot band peak is separated by a larger value, 535 cm^{-1}. Three weaker bands are also observed at 245 cm^{-1}, 579 cm^{-1}, and 769 cm^{-1}. The assignment of these bands to the various vibrational modes requires a consideration of selection rules, the molecular orbitals, and the spectra obtained by other researchers.

Table IV-1

1,3,5-Trifluorobenzene Cation Band Positions

$\tilde{\nu}_{vac}(cm^{-1})$	$\Delta\nu(cm^{-1})$	Intensities
21288	-535	m
21823	0	m
22068	245	vw
22307	484	vs
22402	579	w
22592	769	w
22811	988	vs
23319	1496	vs
23831	2008	m

C. Vibrational Analysis

1. Considerations

The molecular cation sym-TFB contains 12 atoms and has 30 vibrations. We clearly are not observing all of these vibrational modes in our spectrum. We, therefore, need some criteria on the basis of which we can decide the vibrational modes involved in the $\tilde{B}$-$\tilde{X}$ transition.

The first of these criteria stems from the fact that the neutral parent molecule has 18 bonding electrons. One would not expect a dramatic change in the molecule when one of these electrons is removed to form either the $\tilde{B}$ or $\tilde{X}$ ionic states. Thus, the vibrational frequencies in the molecular ion would be expected to be very similar to those of the neutral molecule. The thirty vibrations for the neutral molecule are listed in Table IV-2. They are grouped by their symmetry class and numbered in the same manner as Wilson (reference 9 and references therein). The vibrations are seen to consist of 10 non-degenerate modes and 10 doubly degenerate modes. Many of the modes have frequencies similar to those observed in our spectrum. To further decide between these, the selection rules for this electronic transition need to be considered. This will further restrict the vibrations we can observe due to their symmetry.

The transition probability depends on the square of the transition moment. For an electronic transition, the transition moment is given by[16]

Table IV-2

Parent Ground State Vibrational Frequencies[9]

Vibrational Mode	Frequency (cm^{-1})	Symmetry Class	Vibration Type
ν_1	578	A_1'	C
ν_{12}	1010	A_1'	C
ν_{13}	1350	A_1'	F(s)
ν_2	3082	A_1'	H(s)
ν_9	326	E'	F(b)
ν_6	500	F'	C
ν_{18}	993	E'	-
ν_{19}	1122	E'	-
ν_8	1475	E'	F(s)
ν_7	1624	E'	-
ν_{20}	3109	E'	H(s)
ν_{11}	214	A_2''	-
ν_4	664	A_2''	C
ν_5	847	A_2''	H(b)
ν_{16}	253	E''	C
ν_{10}	595	E''	F
ν_{17}	858	E''	H
ν_{15}	564	A_2'	-
ν_3	1126	A_2'	-
ν_{14}	1294	A_2'	-

$$R_{e'v'e''v''} = \int \psi'^{*}_{ev} M \psi''_{ev} d\tau_{ev} \qquad \text{(IV-1)}$$

where e denotes electronic, v denotes vibrational, single prime labels the upper state, double prime labels the lower state, ψ_{ev} is the vibronic wave function, and M is the electric dipole moment. In the Born-Oppenheimer approximation (where vibronic interaction is neglected) the vibronic wavefunction can be resolved into the product $\psi_e\psi_v$. The transition moment then becomes

$$R_{e'v'e''v''} = \int \psi'^{*}_{e} M_e \psi''_{e} d\tau_e \int \psi'^{*}_{v} \psi''_{v} d\tau_v \qquad \text{(IV-2)}$$

where M_e is the dipole moment due to the electrons. The first integral in this expression is the electronic transition moment. In the approximation that ψ_e varies slowly with respect to the nuclear coordinates, this integral forms the general selection rule; when it is different from zero, the transition is said to be allowed. For the $^2A_2'' - {}^2E''$ transition we are considering, the electronic transition moment is non-zero for the M_x and M_y components of the dipole moment.[17] The transition is, therefore, allowed.

The transition probability then depends on the value of the second integral in Eq. IV-2, the overlap integral. In order for this integral to be non-zero, the direct product of the ψ''_v and ψ'_v symmetry species must contain the totally symmetric representation A_1'; i.e., $\psi'^{*}_v \psi''_v$ must be symmetric. In addition, if sym-TFB is assumed to have the same symmetry in

both the $\tilde{X}$ and $\tilde{B}$ electronic states, the symmetry species listed in Table IV-2 can be used to determine the value of the overlap integral because both electronic states would belong to the same point group, D_{3h}.

The vibrational wavefunction ψ_v' represents the combination of all the normal mode wavefunctions. Its symmetry is then the direct product of the symmetry species of all these vibrational wavefunctions. It is important to note that any unexcited mode (0 quantum) is totally symmetric, singly excited modes have the symmetry given in Table IV-2, a doubly excited mode has the symmetry contained in the direct product of its symmetry with itself, etc.

The transitions we observe in our spectrum would primarily be from the vibrationless ground electronic state. The symmetry of ψ_v'' for this state is totally symmetric, A_1' Then, on the basis of the overlap integral, the only vibrations we should observe to singly excited vibrations are those with the symmetry A_1'. ($\Delta v' = 2,4,...$for any mode are allowed.) This amounts to just the first four vibrations listed in Table IV-2. These vibrations might explain the bands we observe, however, there are some difficulties. For example, the large band 484 cm^{-1} from the 0_0^0 band would have to be explained by the 578 cm^{-1} neutral vibration. This is a rather large change in frequency. Also, there are no vibrations corresponding to the weak bands we observe in our spectrum.

The above analysis was performed assuming no vibronic interaction. It should be remembered that the ground electronic state is doubly degenerate. According to the Jahn-Teller theorem for a non-linear molecule,[18] there exists at least one non-totally symmetric vibration which will split this degeneracy. For a molecule of D_{3h} symmetry the only vibrational symmetry which is Jahn-Teller active is E'.[19] Thus, the E' vibrations are involved in a vibronic interaction. The question that remains is to what magnitude.

The selection rules for this transition must be reviewed again beginning with Eq. IV-1. We start by writing the $\tilde{X}$ state vibronic wavefunction as the sum

$$\psi''_{e,v} = \psi''_e\psi''_v + \chi''_{e,v} \qquad \text{(IV-3)}$$

where the first term to the right of the equals sign is the product used previously and the second term contains all the vibronic interaction. The symmetry of $\chi''_{e,v}$ is the same as the direct product of the ψ''_e and ψ''_v symmetry species. The transition moment then becomes

$$R_{e''e'v''v'} = R_{n.v.} + \int \psi'_e\psi'^*_v M \chi''_{e,v}\, d\tau_{e,v} \qquad \text{(IV-4)}$$

where $R_{n.v.}$ is the transition moment with no vibronic interaction obtained before (Eq. IV-2).

In order for a non-totally symmetric vibration to be allowed, the direct product of the symmetry species of all the terms in the integral appearing in Eq. IV-4 must contain

the A_1' representation. For E' vibrations, this is indeed the case for the M_x and M_y components of the dipole moment.[17] Therefore, E' type vibrations are allowed to occur vibronically and are expected to occur because of the Jahn-Teller vibronic interaction. Because it is difficult to predict which term, vibronic or non-vibronic, will be the larger in the transition probability of non-diagonal transitions, the first ten vibrations listed in Table IV-2 should all be considered.

One last consideration which will aid in the vibrational assignments concerns the molecular orbitals. In a simple Hückel approximation the transition involves removing an electron from a ring π-molecular orbital which is totally bonding between all the carbon atoms and placing it in one that has some antibonding character between these atoms. The vibrations involved in non-diagonal transitions would then be expected to be those that alter the C-C bonds. Vibrations involving the C-F bonds might also be expected to appear depending on the degree of mixing between the F p-orbitals and the ring π-orbitals. In the last column in Table IV-2 the vibration type is listed for each mode. A "C" denotes a vibration which involves primarily the C-C bonds. The "F" and "H" denote vibrations which involve the C-F and C-H bonds, respectively. The letter "s" signifies a stretch, whereas the letter "b" signifies a bend. These vibration types were obtained from an infrared analysis performed by Nielsen et al.[20]

2. Assignments

Considering the criteria presented in the previous section we can proceed with the vibrational assignments. The positions of the bands we observed relative to the 0_0^0 peak are given again in Table IV-3. It is important to remember that the bands observed at wavelengths shorter than the 0_0^0 band provide vibrational information about the excited B electronic state. This state is not degenerate and no direct evidence related to the Jahn-Teller effect can be derived from these bands.

The intense band at 484 cm^{-1} has been assigned to the ν_6' E' vibrational mode. The ν_6'' mode was observed to be very active in the emission spectrum[9] where a very irregular progression was found. This irregularity was attributed to the Jahn-Teller interaction. Although all the E' vibrations were found to be Jahn-Teller active in the emission spectrum, ν_6'' was found to be by far the most active. Also, ν_6' is a trigonal ring-distortion vibration and therefore satisfies all the criteria presented previously.

The only other mode that could possibly account for this band is the ν_1' totally symmetric ring-breathing mode. This has been assigned to the weak band at 579 cm^{-1} which matches the neutral $\bar{\nu}_1$ frequency of 578 cm^{-1}. The other weak bands were assigned as $\bar{\nu}_9' = 245$ cm^{-1} and $\bar{\nu}_6' + \bar{\nu}_9' = 769$ cm^{-1}. Whereas the $\bar{\nu}_9'$ assignment agrees well with that of Miller and Bondybey,[12] the 769 cm^{-1} assignment is somewhat doubtful. While in their gas phase work[12] Bondybey and Miller found a

Table IV-3

1,3,5-Trifluorobenzene Cation Vibrational Assignments

$\Delta\nu(cm^{-1})$	Assignment	Symmetry Class
- 535	ν_6'' (hot band)	E'
0	0_0^0	A_1'
245	ν_9'	E'
484	ν_6'	E'
579	ν_1'	A_1'
769	$\nu_9' + \nu_6'$(?)	A_1' & E'
988	$2\nu_6'$ (ν_{12}')	A_1' & E' (A_1')
1496	ν_7' (ν_8'?)	E' (E')
2008	$2\nu_{12}'$ ($4\nu_6'$)	A_1' (A_1' + E')

frequency of 722 cm^{-1}, they found a frequency of 811 cm^{-1} in their condensed phase experiments.[15] This assignment is, therefore, tentative.

The second intense band we see is 988 cm^{-1} from 0_0^0 and is assigned to $2\nu_6'$. Our value differs somewhat from that of Bondybey and Miller (966 cm^{-1}).[12] There are two possible reasons for this discrepancy. The first is that our ions are believed to be considerably more vibrationally hot than their ions which can result in slight band shifts due to band overlap. The second reason is that they observe another band in their condensed phase work[15] at 1005 cm^{-1}. This was attributed to the totally symmetric ν_{12}' vibrational mode. The band we observe is then most likely the overlap of the $2\nu_6'$ and ν_{12}' bands. It should be noted that a Fermi resonance would most likely occur between these two levels.

The next intense band occurs at 1496 cm^{-1} which agrees well with the frequency of 1490 cm^{-1} found by Bondybey and Miller.[12] They assign this transition to the ν_7' E' vibrational mode on the basis of isotopic shifts[15] and the neutral vibrational frequency of 1624 cm^{-1}. However, the ν_8' E' vibrational mode has a frequency of 1475 cm^{-1} and is, therefore, a possible candidate. The ν_3 frequency would have to increase in going from the neutral to the $\tilde{B}$ ionic state which was not found to occur for any of the other vibrational modes. The assignment is then given to ν_7', but is tentative. It should also be noted that $3\nu_6'$ would appear in this region.

The frequency is expected to be somewhat lower than 1496 cm^{-1} (~1450 cm^{-1}).[15]

The last band observed is 2008 cm^{-1} from the 0_o^o band and has an uncertainty of $\pm$20 cm^{-1}. This band is most likely attributed to an overlapping of the $4\nu_6$ and $2\nu_{12}$ bands.

The final band left to assign is the only hot band we observed at -535 cm^{-1} from the 0_o^o band. This value agrees well with that observed by Bondybey et al.[15] at -544 cm^{-1}. This is assigned to the ν_6'' vibrational mode. However, as Leach has shown,[9] this does not represent the vibrational frequency for ν_6'' because the Jahn-Teller interaction causes a shift in this peak position. The assignment of this band along with all the others is listed in Table IV-3. The assignments are also indicated in Figure IV-1.

D. Conclusion

The vibrational bands we observed in our fluorescence excitation spectrum of the $\tilde{B}\ ^2A_2''$ - $\tilde{X}\ ^2E''$ transition of the 1,3,5-trifluorobenzene cation were all assigned on the basis of the criteria set forth in Section IV-C1 and by comparison with spectra obtained by other research groups. The assignment of such a spectrum offers information primarily about the excited state of the molecular ion. The pseudocontinuum observed in our spectrum and the fact that our vibrational bandwidths of ~100 cm^{-1} are considerably larger than those obtained from other LIF techniques (60-70 cm^{-1}) indicate that our ions are most likely vibrationally (and perhaps rotationally)

hot in comparison. The explanation for this, of course, is our "collisionless" conditions. This higher vibrational temperature offers an advantage in that the appearance of hot bands allows information about the ground state ion to be obtained. It also allows for easier comparison with results from emission spectroscopy. There are disadvantages, however, including poorer signal-to-noise and band shifts both of which are due to band overlap.

References, Chapter IV

1. B. Narayan and J. N. Murrel, Mol. Phys., 19, 169 (1970).
2. C. R. Brundle, M. B. Robin, and N. A. Kruebler, J. Am. Chem. Soc., 94, 1466 (1972).
3. A. W. Potts, W. C. Price, D. G. Streets, and T. A. Williams, Disc. Fara. Soc., 54, 168 (1972).
4. R. Gilbert, P. Sauvageau, and C. Sandorfy, Chem. Phys. Lett., 17, 465 (1972).
5. D. G. Streets and G. P. Ceasar, Mol. Phys., 26, 1037 (1973).
6. M. Allan and J. P. Maier, Chem. Phys. Lett., 34, 442 (1975).
7. M. Allan, J. P. Maier, and O. Marthaler, Chem. Phys., 26, 131 (1977).
8. C. Cossart-Magos, D. Cossart, and S. Leach, J. Chem. Phys., 69, 4313 (1978).
9. C. Cossart-Magos, D. Cossart, and S. Leach, Mol. Phys., 37, 793 (1979).
10. T. A. Miller and V. E. Bondybey, Chem. Phys. Lett., 58, 454 (1978).
11. V. E. Bondybey, J. H. English, and T. A. Miller, J. Am. Chem. Soc. 160, 5251 (1978).
12. V. E. Bondybey and T. A. Miller, J. Chem. Phys., 70, 138 (1979).
13. V. E. Bondybey, T. A. Miller, and J. H, English, J. Am. Chem. Soc., 101, 1248 (1979).
14. T. A. Miller, V. E. Bondybey, and J. H. English, J. Chem. Phys., 70, 2919 (1979).
15. V. E. Bondybey, T. A. Miller, and J. H. English, J. Chem. Phys., 71, 1088 (1979).
16. G. Herzberg, Electronic Spectra of Polyatomic Molecules, Van Nostrand Reinhold Co., Princeton, NJ (1966), Chapter II.

17. Reference 16, p. 132.

18. H. A. Jahn and E. Teller, Proc. Roy Soc., 161A, 220 (1937).

19. Reference 16, p. 50.

20. J. R. Nielsen, C. Liang, and D. C. Smith, Disc. Fara. Soc., 9, 177 (1950).

CHAPTER V

THE $\tilde{B}\ ^2\Pi_{3/2,1/2}$ - $\tilde{X}\ ^2\Pi_{3/2,1/2}$ BAND SYSTEM OF $BrCN^+$

From the band separation in the photoelectron spectrum of BrCN obtained in 1970,[2] the $\tilde{B}$-$\tilde{X}$ and $\tilde{A}$-$\tilde{X}$ electronic transitions of the molecular ion $BrCN^+$ were found to lie in the visible wavelength region. Using this information Allan and Maier[4a] successfully obtained the emission spectra of both of these transitions. They proceeded to tentatively assign vibrational bands in the $\tilde{A}$-$\tilde{X}$ transition, but were unable to assign any of the $\tilde{B}$-$\tilde{X}$ transition. We, therefore, undertook the study of the $\tilde{B}$-$\tilde{X}$ band system by laser induced fluorescence in order to help in the vibrational assignment of this electronic transition.

In order to anticipate the appearance of our fluorescence excitation spectrum, the results obtained from photoelectron spectroscopy concerning the molecular orbitals of BrCN are first described, followed by what was learned from Allan and Maier's work. The fluorescence excitation spectrum we observed is then presented in which many complications are seen to exist. In order to understand the phenomena that occur in the spectrum, a description of the perturbations believed to be occurring and the rules governing them are given. Finally, the assignments and information which can be determined in spite of these complications are presented.

A. Electronic Configuration, Molecular Orbitals, and the Photoelectron Spectrum

The neutral molecule BrCN contains 16 valence electrons. The last three orbitals in the electron configuration of these valence electrons are the σ_N, π_1, and π_2-orbitals.[1] The "N" subscript refers to the nitrogen lone pair electrons and the π-orbitals are formed from linear combinations of the atomic p-orbitals. The actual ordering of these orbitals was determined from the photoelectron spectrum obtained by Lake et al.[2] in which three bands were observed in the 11-15 eV region.

The first band observed in the PE spectrum corresponds to the $\tilde{X}$ state of $BrCN^+$. Two short vibrational progressions were observed which were attributed to the C-Br stretching vibration (ν_1'') and the C-N stretching vibration (ν_3''). The frequencies obtained for these vibrations were 580 cm^{-1} and 1835 cm^{-1}, respectively, and were assigned by comparison with vibrational frequencies in the neutral molecule ($\bar{\nu}_1$ = 575 cm^{-1}, $\bar{\nu}_3$ = 2200 cm^{-1}).[3] In addition, each peak observed in the $\tilde{X}$ band was found to split into two subbands implying the existence of two closely spaced levels. These two levels were assigned to the spin-orbit doublet pair $^2\Pi_{3/2}$, $^2\Pi_{1/2}$ which indicates that an electron is removed from a π-orbital of the neutral molecule to form the $\tilde{X}$ state of the ion.

The next band observed in the PE spectrum, associated with the $\tilde{A}$ state of the ion, has the appearance of a transition involving a non-bonding electron. A strong vibrationless

transition (denoted as 0_0^0) is observed and no splitting of the peaks into subbands occurs. The $\tilde{A}$ state is produced by removal of an electron from the σ_N-molecular orbital. The only vibrational progression they observe in this band, however, corresponds to the C-Br stretch with a frequency of $\bar{\nu}_1 = 580\ cm^{-1}$.

The third band in the PE spectrum, corresponding to the $\tilde{B}$ state of $BrCN^+$, consists of a long progression in the ν_1 stretching mode with a mean frequency of about 516 cm^{-1}. No progression involving the ν_3 stretching mode was observed. Unlike the $\tilde{X}$ and $\tilde{A}$ bands, the most intense transition is not the 0_0^0 band, but involves the transition to the fifth ν_1 vibrational level of the $\tilde{B}$ state. Splitting of each of the peaks due to spin-orbit coupling is again observed indicating that the $\tilde{B}$ state is formed by removal of an electron from the π_1-molecular orbital.

From the relative position of these bands, the ordering of the last three molecular orbitals in BrCN is found to be $(\pi_1)^4\ (\sigma_N)^2\ (\pi_2)^4$. The electronic states of the molecular ion $BrCN^+$ are: $\tilde{X}\ ^2\Pi$, $\tilde{A}\ ^2\Sigma$, and $\tilde{B}\ ^2\Pi$.

The photoelectron study performed by Lake and co-workers also included the isovalent molecules ClCN and ICN where results similar to those described for BrCN were obtained. From a comparison of the results for these molecules, information regarding the nature of the π_1 and π_2-molecular orbitals was derived. The important results are summarized here.

Because both vibrational stretching frequencies were found to be excited in the $\tilde{X}$ band, the electrons in the π_2-molecular orbital are believed to be delocalized over the entire molecule. Further evidence for this delocalization is obtained from the comparison of spin-orbit splitting values. The magnitude of the spin-orbit splitting increases with increasing unpaired-electron density on the halogen atom. The spin-orbit splitting of the XCN^+ molecules (X = Cl, Br, I) was found to be smaller than that of the corresponding XH^+ molecule. This indicates a delocalization of the unpaired-electron density (i.e., the electron hole) over the entire molecule.

The π_1 and π_2 molecular orbitals are then considered to result from a mixing of the halogen p-orbitals and the CN π-orbitals. The two molecular orbitals derived from linear combinations of these orbitals are shown in Figure V-1. In this figure the π_2 molecular orbital is seen to have anti-bonding character between the Br atom and the C atom, where as the π_1 orbital is seen to have bonding character. Both orbitals, of course, have bonding character between the C and N atoms. Lake has inferred from his PES results that the extent to which these p-orbitals and π-orbitals mix decreases from ClCN to ICN.

One last point in considering the PES results concerns the resolution under which the spectra were obtained. The resolving power quoted by Lake was about 20 mV ($\sim$160 cm^{-1}). This poor resolution provided one of the reasons for pursuing the optical spectra of $BrCN^+$.

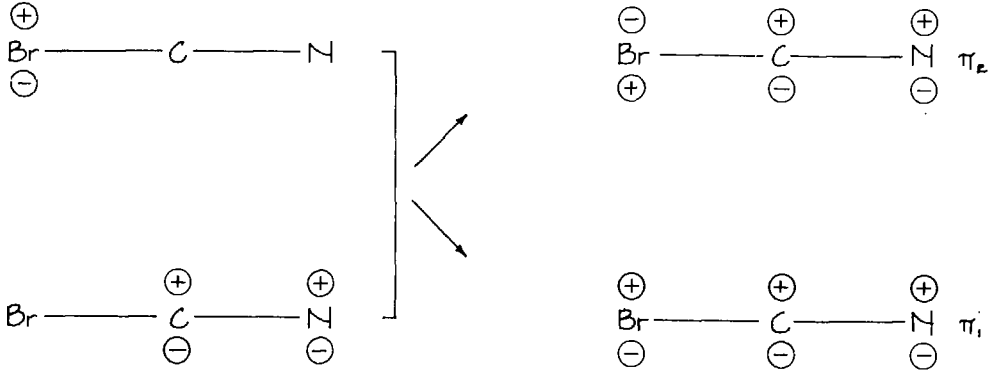

Figure V-1. The π_1 and π_2-Molecular Orbitals Formed from the Atomic p-orbitals.

B. Emission Spectra, $\tilde{A}\ ^2\Sigma$ - $\tilde{X}\ ^2\Pi$ and $\tilde{B}\ ^2\Pi$ - $\tilde{X}\ ^2\Pi$ Band Systems

Allan and Maier have obtained the emission spectra for both the $\tilde{A}$-$\tilde{X}$ and $\tilde{B}$-$\tilde{X}$ band systems of $BrCN^+$ by a controlled electron impact fluorescence technique.[4a] Because they have not assigned the spectrum they have obtained for the $\tilde{B}$-$\tilde{X}$ band system, it is of little help to us. They have, however, given tentative assignments in their $\tilde{A}$-$\tilde{X}$ spectrum.

From these assignments, an approximate $\bar{\nu}_2$ bending frequency of 290 cm^{-1} can be measured.[5] The spin-orbit splitting constant was also determined to be -1470 $\pm$ 10 cm^{-1}. (The minus sign indicates an inverted doublet, $^2\Pi_{3/2}$ is lower in energy than $^2\Pi_{1/2}$.) The spin-orbit splitting of the $\tilde{B}$ band is approximated to be about ~-1200 cm^{-1}. This value was obtained from PES results given by Allan and Maier and is very approximate because the adiabatic ionization energy of the $\tilde{B}\ ^2\Pi_{1/2}$ state must be inferred from the spin-orbit sum rule.[4a]

C. Predicted Appearance of LIF Spectrum

From the discussion in Section V-A of the π-orbitals in the $BrCN^+$ molecular ion and the PES results, the general appearance of the optical spectrum can be predicted. The transition involves removing an electron from the π_1-molecular orbital and placing it in the π_2-molecular orbital, both of which are shown in Figure V-1. The degree of mixing between the Br p-orbital and the CN π-orbital will determine the ultimate appearance of the spectrum.

In the absence of any mixing (a first approximation) the transition would correspond to moving an electron from the CN π-orbital to the Br p-orbital, both of which are shown on the left hand side of Figure V-1. This certainly would be expected to affect the CN bond distance leading to a vibrational progression in the spectrum involving the ν_3 mode. The electron's placement in the non-bonding p-orbital (in this approximation) would most likely affect the C-Br bond distance only slightly.

Another interesting effect would involve the splitting due to spin-orbit coupling. As mentioned before, the magnitude of the spin-orbit splitting is primarily determined by the unpaired-electron density on the Br atom. In the approximation of no mixing, the $\tilde{B}$-$\tilde{X}$ transition would pair all the electrons on the Br atom which would decrease the spin-orbit splitting dramatically. The evidence from PES and the emission spectrum is in contrast to this; the spin-orbit splitting constant was found to decrease from -1475 cm^{-1} in the $\tilde{X}$ state to only ~-1200 cm^{11} in the $\tilde{B}$ state. It appears then that in the π_1-molecular orbital, just as in the π_2-molecular orbital, a good deal of mixing occurs among the p-orbitals in the molecule.

If there is sufficient mixing between the orbitals, the transition would involve moving an electron from an orbital which has bonding character between the Br atom and the CN group to one with antibonding character. In the optical spectra, we would then expect a vibrational progression in the ν_1 C-Br stretching mode. In either extreme, no mixing or

large mixing, the frequencies of the ν_1 and ν_3 modes would not be expected to change dramatically in either electronic state. The progressions in either mode should, therefore, be easily identified.

Because our ions are not thermalized, some population is expected in the $\tilde{X}\ ^2\Pi_{1/2}$ state, even though it is much higher in energy than the $\tilde{X}\ ^2\Pi_{3/2}$ ground state. (Collisional relaxation of the $^2\Pi_{1/2}$ state is probably very slow.) We then expect transitions from both of these states splitting each vibronic band into spin-orbit subbands. Because the spin-orbit splitting is so large, both the $\tilde{X}$ and $\tilde{B}$ states belong to Hund's case (a).[6] The $\Delta\Sigma = 0$ selection rule for transitions between $^2\Pi$ states belonging to this case permits only the $^2\Pi_{3/2} - {}^2\Pi_{3/2}$ and $^2\Pi_{1/2} - {}^2\Pi_{1/2}$ transitions. In the optical spectrum each vibronic band would then split into two spin-orbit subbands, the separation of which would be an approximation to the difference in the spin-orbit coupling constants in $\tilde{X}$ and $\tilde{B}$ states, $\Delta A = A''-A'$.

D. Fluorescence Excitation Spectrum of the $\tilde{B}\ ^2\Pi - \tilde{X}\ ^2\Pi$ Band System of $BrCN^+$

1. Experimental Conditions

The BrCN sample was obtained from the Eastman-Kodak company and was used without further purification. The pressure was kept as 3-5 x 10^{-5} torr (uncorrected ionization gauge). Because no interfering ions were found to exist, a mass resolution of $\pm$10 a.m.u. was used.

The radiative lifetime of the $\tilde{B}$ state of $BrCN^+$ is on the order of 300 nanoseconds and the quantum yield is close to unity. The laser fired 150 microseconds after the electron beam was gated off eliminating any interference from electron impact fluorescence. Because of the high quantum yield, the fluorescence detection gate used was 2 microseconds in duration and set 200 nanoseconds after the laser pulse. Because the rotational spacing for $BrCN^+$ is too small ($\sim 0.2\ cm^{-1}$) to be resolved by the $1\ cm^{-1}$ bandwidth of our laser, a 0.5 Å wavelength increment was used in scanning the laser. At each particular wavelength, the laser was fired 750-1000 times. The 4000 Å - 5000 Å region covered required the use of five different laser dyes. Each laser dye wavelength region was scanned several times to insure the reproducibility of the features observed. Because each dye region overlapped well with successive dye regions, the overall spectrum was easily produced from the spectra obtained in the various wavelength regions. The computer was used for the matching of these different wavelength regions.

2. The Observed Spectrum

The fluorescence excitation spectrum we obtained for the $\tilde{B}\ ^2\Pi - \tilde{X}\ ^2\Pi$ band system of $BrCN^+$ is shown in Figure V-2. The result of the interrogation of our non-thermalized $BrCN^+$ ions is series of peaks on top of a pseudocontinuum. Most of the bands are degraded to the red as has also been observed for the $^2\Pi - {}^2\Pi$ transition of the isovalent molecules SCN[7] and OCN.[8] A long vibrational progression which at first glance can be attributed to the ν_1 stretching mode is observed. No

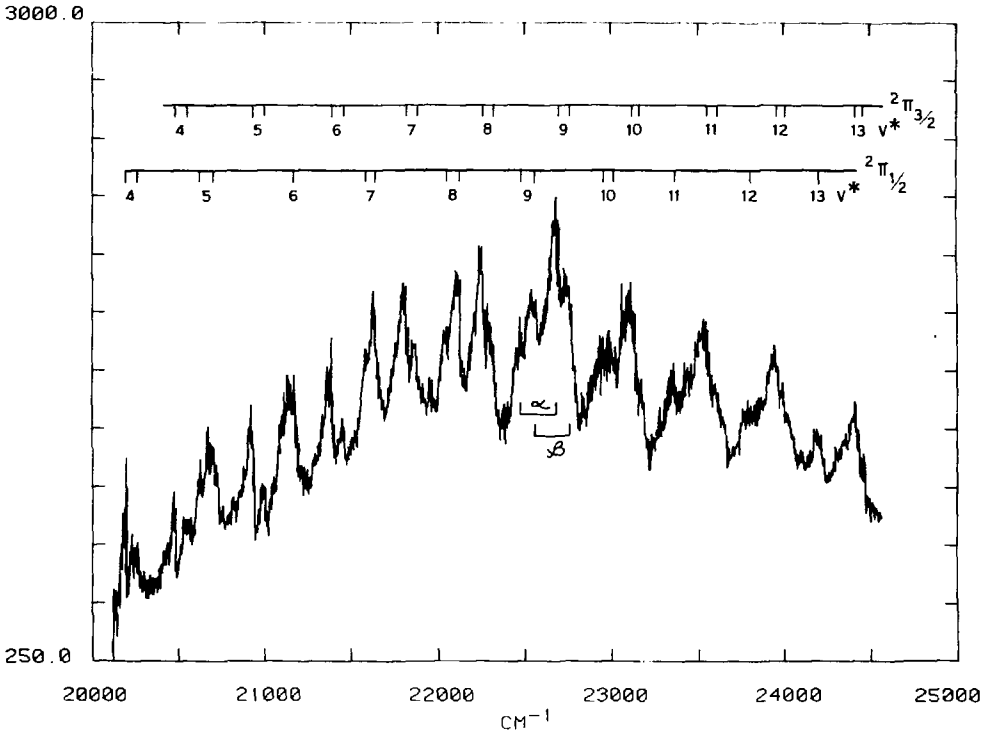

Figure V-2. Fluorescence Excitation Spectrum of $BrCN^+$: $\tilde{B}\ ^2\Pi - \tilde{X}\ ^2\Pi$ Band System.

XBL 7910-12095

evidence for the ν_3 mode is seen indicating that a good deal of mixing, as previously described, occurs in the π_1 and π_2-molecular orbitals. The vibrational interval of this progression, however, is found to be very irregular varying between 402 cm^{-1} and 481 cm^{-1}.

A spin-orbit doublet structure occurs as was expected, splitting each vibronic band into a $^2\Pi_{3/2}$ and a $^2\Pi_{1/2}$ subband. But again, a nonsystematic spacing between these subbands is found varying between -176 cm^{-1} and -306 cm^{-1}. The spacing usually represents a good approximation to ΔA and should not vary greatly from band to band.

Upon closer examination of the spectrum, another important feature is observed. Each subband is found to consist of two band heads rather than one as would be expected in a $^2\Pi_\Omega$- $^2\Pi_\Omega$ transition. This behavior along with the irregular progression and spin-orbit splitting has been observed in other linear triatomics[3,9-13] including the isovalent species SCN[7] and OCN[8] and has been attributed to a Fermi resonance effect. In all of the cases referenced, a Fermi resonance between the vibrational levels (v_1,v_2,v_3) and (v_1,v_2+2, v_3-1) which are of the same symmetry is believed to occur.[14] To explain Fermi resonance and to determine its effect on the $\tilde{B}\ ^2\Pi$ - $\tilde{X}\ ^2\Pi$ transition, the selection rules involved need to be considered.

3. Selection Rules, Fermi Resonance and Its Plausibility in $BrCN^+$

In order to assign the spectrum given in Figure V-2, the selection rules for electronic transitions need to be considered.

The transition moment in the absence of vibronic interaction was previously discussed in Section C of Chapter IV. For the $\tilde{B}\ ^2\Pi$ - $\tilde{X}\ ^2\Pi$ transition, the electronic transition moment

$$R_{e'e''} = \int \psi_e'^{*}\, M_e \psi_e''\, d\tau_e \qquad \text{(V-1)}$$

does not vanish for the M_z component of the dipole moment; the transition is, therefore, allowed. (The $\Delta\Sigma = 0$ selection rule for $^2\Pi$ states belonging to Hund's case (a) which restricts the electronic transition to $^2\Pi_{3/2}$ - $^2\Pi_{3/2}$ and $^2\Pi_{1/2}$ - $^2\Pi_{1/2}$ subbands was previously mentioned.)

The transitions to various vibrational levels of the $\tilde{B}$ electronic state is then governed by the overlap integral

$$\int \psi_v'^{*}\, \psi_v''\, d\tau_v \qquad \text{(V-2)}$$

where ψ_v' and ψ_v'' are the vibrational wavefunctions of the $\tilde{B}$ and $\tilde{X}$ states of $BrCN^+$, respectively. The square of this integral is termed the Franck-Condon (FC) factor. To determine when this overlap integral vanishes, the symmetry species of the three different vibrations in $BrCN^+$ must be known. According to the Walsh diagram[15] for triatomic molecules, $BrCN^+$ is linear in both the $\tilde{B}$ and $\tilde{X}$ electronic states. Hence, both states belong to the same symmetry point group, $C_{\infty v}$. This result is important because it permits the overlap integral to be nonzero only if the direct product of the ψ_v' and ψ_v'' symmetry species contains the totally symmetric representation, Σ^+ (or A_1).

The three vibrations involved in $BrCN^+$ and their symmetry species are given in Figure V-3. Both the ν_1 and ν_3 vibrations are of Σ^+ symmetry and are described as the C-Br stretch and the C-N stretch, respectively. Transitions between any of these levels are allowed with their intensity being governed by their FC factors. The ν_2 vibrational mode, on the other hand, is doubly degenerate being of Π symmetry.[16] The transition probability involving odd quanta of this mode is identically zero according to the overlap integral. However, even quanta ($\Delta v_2 = \pm 2, \pm 4, \pm 6...$) are allowed, but expected to occur only weakly in the spectrum because of the FC principle. That is, because $BrCN^+$ is linear in both electronic states, the potential minimum of the bending vibration will occur at the same angle, 180°, in both states. Thus, the most intense bands will involve $\Delta v_2 = 0$ transitions. (It should also be noted that the symmetry of ν_2 is Σ^+ when $v_2 = 0$.)

According to the selection rules (when vibronic interaction is neglected) only ν_1 and ν_3 vibrational progressions should occur strongly in our optical spectrum, their intensities being dependent upon FC factors. Transitions involving even quanta of ν_2, however, can "borrow" intensity from strongly allowed ν_1 and ν_3 transitions in favorable cases through Fermi resonance. A Fermi resonance[17] arises when two different vibrational levels have nearly the same energy. This accidental degeneracy results in a mixing of the eigenfunctions of the two different states by the anharmonic terms

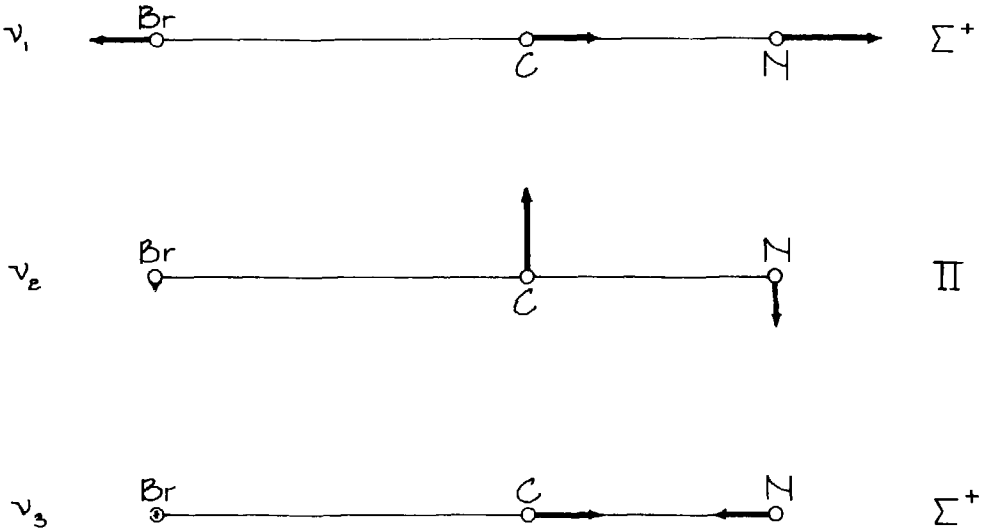

Figure V-3. The Three Vibrational Modes in $BrCN^+$ and Their Symmetries.

in the potential, W. For example, the anharmonic term which leads to a Fermi resonance[18] between the levels (v_1, v_2, v_3) and (v_1-1, v_2+2, v_3) is $f_{1rr} Q_1 r^2$, where f is the coefficient, Q_1 is the normal coordinate for the C-Br stretch and r is the polar coordinate for the amplitude of the BrCN bending vibration. The magnitude of the perturbation,[17] derived from second order perturbation theory, is found to depend inversely on the energy difference of the two unperturbed levels and on the matrix element

$$W_{ni} = \int \psi_n^{\circ} W \psi_i^{\circ *} \, d\tau \qquad (V-3)$$

where W is given by the anharmonic terms in the potential energy and ψ_n° and ψ_i° are the eigenfunctions of the unperturbed vibrational levels. The important point here is that W has the full symmetry of the molecule, that is, it is totally symmetric. Therefore, a Fermi resonance can only occur between vibrational levels that are of the same symmetry species.

In the case of linear triatomics these two conditions (same symmetry species and nearly the same energy) are usually observed between the ν_1 stretching frequency and even quanta of the degenerate ν_2 bending frequency which for nonsymmetric linear triatomics (such as $BrCN^+$) contain the same symmetry species, Σ^+. To prove that a Fermi resonance is definitely occurring, a rotational analysis of several bands is required. Because we did not resolve the rotational structure of $BrCN^+$ in our spectrum, a Fermi resonance effect cannot be proven in this manner.

The plausibility of such a resonance can be demonstrated, however, if it can be shown that $2\bar{\nu}_2' \cong \bar{\nu}_1'$. But here again, we run into difficulty; $\bar{\nu}_2$ has never been measured for the $\tilde{X}$ or the $\tilde{B}$ state of $BrCN^+$. This frequency can be estimated for the $\tilde{X}$ state from the tentative assignments of the $\tilde{A}\ ^2\Sigma - \tilde{X}\ ^2\Pi$ emission spectrum given by Maier et al.[4,5] to be about ~290 cm^{-1}. This bending frequency would not be expected to change dramatically in going to the $\tilde{B}$ state. Comparing this frequency with the ν_1 frequency of about ~500 cm^{-1} suggests that Fermi resonance is indeed plausible.

Additional evidence can be found by considering the ground state of the neutral BrCN molecule. Both $\bar{\nu}_2$ and $\bar{\nu}_1$ for this molecule are known to be 342.5 cm^{-1} and 575 cm^{-1}, respectively, and a Fermi resonance was found to occur between the (0,0,1) band and the (0,2,0) vibrational levels.[3] From these observations it appears likely that $\bar{\nu}_1 \cong 2\bar{\nu}_2$ for both the $\tilde{X}$ and $\tilde{B}$ states of the ion and that Fermi resonance is probably the best explanation for the irregularities observed in our spectrum.

The vibrational progression we observe in our spectrum (given in Figure V-2) is very long, involving high vibrational quantum number (v_1' = 4-13). It is important to realize then, that even though we are observing only two Fermi components in each subband, several vibrational levels are involved in each Fermi resonance interaction. For example, for v_1' = 5, six levels, (5,0,0), (4,2,0), (3,4,0), 2,6,0), (1,8,0) and (0,10,0) take part in the resonance interaction. (The number

of levels involved increases by one for each unit increase in v_1'). We believe that in our spectrum only the two most intense transitions in each Fermi multiplet are observed. This was also found to be the case in the spectrum of the $\tilde{A}\ ^2\Pi - \tilde{B}\ ^2\Pi$ transition of CS_2^+ treated by Balfour.[11] These two intense bands will be referred to, hereafter, as a Fermi couplet.

Although in a few cases[10,12] the center lines of each Fermi multiplet were found to be the most intense, it is difficult to predict which components will appear in our spectrum. The extent to which the various vibrational levels mix, which, in turn, determines how much intensity borrowing will occur, is dependent on how resonant these levels are. The determination of the resonance condition requires knowledge of the v_1 and v_2 vibrational frequencies and their anharmonicities. Because no bands unaffected by Fermi resonance have been observed, none of these quantities can be obtained. The end result is that identification of the v_1 and v_2 quantum numbers for each band in our spectrum cannot be made. Therefore, vibrational frequencies for these individual normal modes cannot be determined.

One additional complication must also be discussed. With the excitation of the bending vibrational mode, a vibrational angular momentum is generated along the symmetry axis of the molecule.[19] This angular momentum can couple with the electronic angular momentum (Renner-Teller interaction) causing further splitting of the vibrational levels. (A complete description of this interaction is given in reference

20. Only the points pertinent to our analysis are given here.) The magnitude of the vibrational angular momentum along the molecular axis is $\ell h/2\pi$ where $\ell = v_2, v_2-2, \ldots, 1$ or 0 and h is Planck's constant. These different ℓ levels couple with the electronic angular momentum Λ ($\Lambda = 1$ for a Π electronic state) to give the resultant $K = |\pm\Lambda\pm\ell|$. All of the K levels in a Π electronic state except $K = |v_2+\Lambda|$ occur in pairs. The Renner-Teller interaction causes the splitting of each of these pairs.

We would then expect each Fermi component with $v_2 \neq 0$ to split again into more bands. However, Johns[10] states and Hougen[18] has shown that only the $\ell = 0$ levels will interact strongly with the $(v_1,0,0)$ Fermi resonance level. Therefore, the same number of intense Fermi components would be observed as if no Renner-Teller interaction had occurred. The position of these bands, however, would be altered by this interaction.

The magnitude of this band shift cannot be predicted, but must be determined from the rotational analysis of an unperturbed band. The splitting due to this interaction has been found to be quite variable depending on the molecule and the particular electronic state of the molecule involved. The splitting was observed to be very large in a few cases.[7,10] Another important point is that the splitting increases approximately linearly with v_2. Because the Fermi components which are the most intense can vary from band to band, the v_2 quantum numbers of these components can also vary. This will

result in a variance in the relative positions of each band which could account for some of the irregular vibrational and spin-orbit spacing observed.

4. Assignment of the Spectrum

In the previous section, the plausibility of a Fermi resonance between levels of the form (v_1,v_2,v_3) and (v_1-1, v_2+2, v_3) was presented. The spectrum will be discussed assuming that this is indeed the case. The bands in the $^2\Sigma_{3/2}$ and $^2\Sigma_{1/2}$ manifolds are labeled using two different horizontal lines in Figure V-2. The splitting due to the difference in spin-orbit coupling constants of the two electronic states is clearly observed. A pair of closely shaped vertical lines identifies the Fermi couplet in each subband. A number next to each Fermi couplet labels the different vibrational levels of the $\tilde{B}$ state.

Two points need to be made to make these assignments clear. First, we do not believe that any hot bands are observed in our spectrum (other than in contribution to the pseudocontinuum). This seems reasonable because most of the ions are probably produced with no vibrational excitation in the ν_1 or ν_2 modes of the $\tilde{X}$ state due to FC factors. No evidence for combination bands involving ν_3 was observed. Then, all of the transitions take place from the (0,0,0) level of the $\tilde{X}$ state and the assignments derived will apply to the $\tilde{B}$ state of $BrCN^+$.

The second point of clarification involves the identification of the different Fermi couplet components. As described

in the previous section, which components of the Fermi multiplet will be the most intense cannot be determined. In fact, because the magnitudes of ν_2 bending frequency and the ν_1 stretching frequency in the $\tilde{B}$ state are not known, assignment of the relative position of the (v_1,v_2,v_3) component versus the (v_1-1,v_2+2,v_3) component cannot be made. Because there exists no means to definitely distinguish the two Fermi components we are observing in each vibronic band, a common vibrational quantum number is used to label them both. This number is $v^* = v_1 + 1/2\ v_2$ (following Balfour[11]) and is given in Figure V-2 and in Table V-I for the various vibrational levels.

In Table V-I, the frequencies of the various band heads we observed are also given. The actual v^* numbers labeling the various bands were determined by comparison of the band head frequencies with the approximate position of the 0_0^0 band of the $^2\Pi_{3/2}$ manifold at 18601 cm^{-1} given by Maier et al.[4] and should, therefore, be considered tentative.

In contrast to the photoelectron results, the most intense transitions in our spectrum are seen to be to the eighth and ninth v^* vibrational levels. Because of the similar ν_1 frequencies in the $\tilde{X}$ states of BrCN (575 cm^{-1}) the $BrCN^+$ (580 cm^{-1}), this change in the Franck-Condon profile to higher v_1 (or v^*) quantum numbers indicates that the Br-C bond distance in the $\tilde{X}$ state of $BrCN^+$ is shorter than that in the $\tilde{X}$ state of BrCN. This bond length change is expected when the π-orbitals described previously are considered; the ground state ion is formed from the neutral molecule by removal of an electron from a π-orbital which has antibonding character

Table V-1

$\tilde{B}\ ^2\Pi$-$\tilde{X}\ ^2\Pi$ Subband Heads for $BrCN^+$. All Transitions are from the (0,0,0) Level of the $\tilde{X}$ State. $v^* = (v_3' + 1/2\ v_2')$. The Different Fermi Resonance Components are Represented by α and β

	$^2\Pi_{1/2} - {}^2\Pi_{1/2}$ $\bar{\nu}(cm^{-1})$		$^2\Pi_{3/2} - {}^2\Pi_{3/2}$ $\bar{\nu}(cm^{-1})$		
v^*	α	β	α	β	
4	20205 (426)	20275 (449)	20482 (455)	20537 (463)	Δv^*
5	20631	20724 (450)	20937 (450)	21000 (466)	Δv^*
6	---	21174 (466)	21387 (421)	21466 (402)	Δv^*
7	21592† (449)	21640 (481)	21808 (442)	21868 (454)	Δv^*
8	22041† (443)	22121 (447)	22250 (433)	22322† (431)	Δv^*
9	22484 (438)	22568 (447)	22683 (424)	22753 (434)	Δv^*
10	22922† (441)	23015†	23107 (441)	23187	Δv^*
11	23363† (407)	---	23548† (416)	---	Δv^*
12	23770† (432)	---	23964 (443)	---	Δv^*
13	24202	---	24407	---	

†The uncertainty in these frequencies is ± 20 cm^{-1}. All of the others are ≤ ± 10 cm^{-1}. Note that these frequencies have not been corrected to vacuum.

between the Br atom and the CN group. The Franck-Condon profiles also indicate, of course, that C-Br bond distance is longer in the $\tilde{B}$ state of $BrCN^+$ than in either the $\tilde{X}$ state of $BrCN^+$ or BrCN which is again expected upon considering the π-molecular orbitals involved. The magnitude of these changes cannot be ascertained, however.

The separation of successive v* bands determines a frequency which can be compared with photoelectron spectroscopic results.[2] From the values given in Table V-I a mean frequency of 441 $\pm$ 18 cm^{-1} is obtained. (The uncertainty is one standard deviation.) This value is smaller than that obtained in PES, 516 cm^{-1}. Because we are observing transitions to higher vibrational levels, some of this discrepancy can be explained by anharmonicity. The uncertainty in both of these values offers another source of explanation. The poor resolution (~160 cm^{-1}) resulting in the Fermi components not being resolved contributes to the uncertainty in the PES value. The uncertainty in our value stems from the shift in levels due to Fermi resonance (and therefore Renner-Teller coupling) and the inability to identify the different Fermi components.

Because no bands unaffected by Fermi resonance were observed, no estimate of magnitude of this effect can be determined. The transitions involved in these perturbed bands are to states with a great deal of mixing between ν_1 and ν_2 vibrational levels. The ν_1 and ν_2 frequencies cannot then be determined separately and the mean frequency of 441 cm^{-1} only represents an approximation to both the ν_1 and $2\nu_2$ frequencies. The difference between these two quantities cannot be determined.

The last quantity that needs to be considered is the spin-orbit splitting of the vibronic bands. Although the different Fermi components cannot be distinguished, it can be reasonably assumed that the same ones are involved in each subband of a particular v* vibronic band. The relative position should also remain the same in each subband. In Figure V-2 the two different Fermi components involved in the most intense v* vibronic band are labeled α and β. A small horizontal line connects the spin-orbit doublet pair belonging to each Fermi component. The frequency difference between the subbands of a spin-orbit doublet pair is an approximation to the difference in spin-orbit coupling constants ΔA.

The ΔA values for the α and β components of each vibronic band are given in Table V-II. Because of the resonance perturbation, the ΔA values are found to vary between -176 cm^{-1} and -306 cm^{-1} as can be seen in Table V-II. Although the ΔA values vary widely, some trends in the values given in Table V-II are seen. The ΔA_α values of all v* levels except one are larger than the corresponding ΔA_β value. There also appears to be a decrease in ΔA with increasing v*. The change in ΔA is quite large in going from the v* = 6 to the v* = 7 vibrational level.

A possible explanation for these observations is found when examining the expression for the band splitting when the Renner-Teller interaction is included. The spin-orbit splitting of vibronic subbands is increased by the Renner-Teller interaction and is determined by the effective spin-orbit splitting constant[21]

between the Br atom and the CN group. The Franck-Condon profiles also indicate, of course, that C-Br bond distance is longer in the $\tilde{B}$ state of $BrCN^+$ than in either the $\tilde{X}$ state of $BrCN^+$ or BrCN which is again expected upon considering the π-molecular orbitals involved. The magnitude of these changes cannot be ascertained, however.

The separation of successive v* bands determines a frequency which can be compared with photoelectron spectroscopic results.[2] From the values given in Table V-I a mean frequency of 441 $\pm$ 18 cm^{-1} is obtained. (The uncertainty is one standard deviation.) This value is smaller than that obtained in PES, 516 cm^{-1}. Because we are observing transitions to higher vibrational levels, some of this discrepancy can be explained by anharmonicity. The uncertainty in both of these values offers another source of explanation. The poor resolution (~160 cm^{-1}) resulting in the Fermi components not being resolved contributes to the uncertainty in the PES value. The uncertainty in our value stems from the shift in levels due to Fermi resonance (and therefore Renner-Teller coupling) and the inability to identify the different Fermi components.

Because no bands unaffected by Fermi resonance were observed, no estimate of magnitude of this effect can be determined. The transitions involved in these perturbed bands are to states with a great deal of mixing between ν_1 and ν_2 vibrational levels. The ν_1 and ν_2 frequencies cannot then be determined separately and the mean frequency of 441 cm^{-1} only represents an approximation to both the ν_1 and $2\nu_2$ frequencies. The difference between these two quantities cannot be determined.

The last quantity that needs to be considered is the spin-orbit splitting of the vibronic bands. Although the different Fermi components cannot be distinguished, it can be reasonably assumed that the same ones are involved in each subband of a particular v* vibronic band. The relative position should also remain the same in each subband. In Figure V-2 the two different Fermi components involved in the most intense v* vibronic band are labeled α and β. A small horizontal line connects the spin-orbit doublet pair belonging to each Fermi component. The frequency difference between the subbands of a spin-orbit doublet pair is an approximation to the difference in spin-orbit coupling constants ΔA.

The ΔA values for the α and β components of each vibronic band are given in Table V-II. Because of the resonance perturbation, the ΔA values are found to vary between -176 cm^{-1} and -306 cm^{-1} as can be seen in Table V-II. Although the ΔA values vary widely, some trends in the values given in Table V-II are seen. The ΔA_{α} values of all v* levels except one are larger than the corresponding ΔA_{β} value. There also appears to be a decrease in ΔA with increasing v*. The change in ΔA is quite large in going from the v* = 6 to the v* = 7 vibrational level.

A possible explanation for these observations is found when examining the expression for the band splitting when the Renner-Teller interaction is included. The spin-orbit splitting of vibronic subbands is increased by the Renner-Teller interaction and is determined by the effective spin-orbit splitting constant[21]

Table V-2

Approximate Spin-orbit Splitting Determined From Separation of the Subbands of Similar Fermi Components, α or β

v*	ΔA_α (cm^{-1})	ΔA_β (cm^{-1})
4	-277	-262
5	-306	-276
6	----	-292
7	-210	-228
8	-209	-201
9	-199	-185
10	-185	-1/2
11	-185	----
12	-194	----
13	-205	----

$$A^{*}_{v_2,K} = \sqrt{(A')^2 + \varepsilon^2 \bar{\nu}_2^2 [(v_2+1)^2 - K^2]} \qquad (V\text{-}4)$$

where ε is the Renner parameter which is a measure of the interaction. All the other variables have been previously defined. As explained before, we believe that we are observing only transitions where $\ell = 0$. Therefore, $K = \Lambda + \ell = 1$ in our case. The subband spacing we are observing in our spectrum is then

$$\Delta A = A'' - A^{*} = A'' - \sqrt{(A')^2 + \varepsilon^2 \bar{\nu}_2^2 [(v_2+1)^2 - 1]}. \qquad (V\text{-}5)$$

What is important to notice in this expression is that as v_2 increases, ΔA should decrease, the magnitude of the decrease depending on $\varepsilon^2 \bar{\nu}_2^2$.

Using this expression and the fact that $\Delta A_{\alpha} > \Delta A_{\beta}$, the α Fermi components would have a larger v_2 quantum number than their β counterparts. The β components should then be tentatively assigned to the (v_1, v_2, v_3) levels and the α components to the (v_1-1, v_2+2, v_3). (The absolute values of these quantum numbers still cannot be determined.) Because the α components occur at lower frequencies than the β components, this assignment would indicate that $\bar{\nu}_1$ is slightly greater than $2\bar{\nu}_2$.

Because the v_2 quantum number of the intense components of the Fermi multiplet is expected to increase as v* increases, the trend toward lower ΔA with increasing v* is also explained by Eq. V-5. This trend was also found to occur in the $^2\Pi$ - $^2\Pi$ transition of BO_2 and was interpreted in terms of Eq. V-5.[10] The reverse trend observed in ΔA for v* = 4 to 6 and the large

change in ΔA going from $v^* = 6$ to $v^* = 7$ are difficult to explain. Equation V-5 would seem to indicate that ν_2 decreases as v^* increases in these levels. It would also indicate a large change in ν_2 occurs in going from $v^* = 6$ to $v^* = 7$. No explanation can be given for these observations at this time.

Equation V-5 can also be used to compare our values of ΔA with the work of Allan and Maier.[4] They have obtained a value of -1470 ± 10 cm^{-1} for A'' and a value of ~ -1200 cm^{-1} for A'. Their A' value is very uncertain. The perturbations in our spectrum prevent a direct comparison of our ΔA value with the difference in the A values they have obtained (~ -270 cm^{-1}). However, neglecting the shift due to Fermi resonance, Eq. V-5 indicates that the best approximation for ΔA we have are the larger values in Table V-II. These values of ΔA are for $v^* = 4$-6 and average about ~ -280 cm^{-1} which agrees well with Allan and Maier's value of ~ -270 cm^{-1}. The most accurate value for ΔA that we could obtain would result from the observation of the 0_0^0 band of the $\tilde{B}$-$\tilde{X}$ transition in which no Fermi resonance would occur. However, by examining Figure V-2, the Franck-Condon factor for this band is seen to be very small. Because of the resulting low signal level, we were unable to observe this band.

In conclusion, the complications arising in the $\tilde{B}\ ^2\Pi$ - $\tilde{X}\ ^2\Pi$ transition of $BrCN^+$ diminish the information content of the spectrum. Only approximate values for the vibrational interval and spin-orbit splitting can be derived. On the other hand, the variance in these values presents strong

evidence for the occurrence of a Fermi resonance interaction in the $\tilde{B}$ electronic state which, in turn, supports the hypothesis that $2\bar{\nu}_2 \cong \bar{\nu}_1'$. With the assumption that Renner-Teller coupling dictates the trends found in the variance in spin-orbit coupling values, it can be further concluded that $\bar{\nu}_1$ is slightly greater than $2\bar{\nu}_2$. The assumption also allowed the selection of our best approximation to the spin-orbit coupling constant of the $\tilde{B}$ state.

References, Chapter V

1. G. Herzberg, Electronic Spectra of Polyatomic Molecules, Van Nostrand Reinhold Co., Princeton, NJ (1966), p. 345.

2. R. F. Lake and Sir H. Thompson, Proc. Roy. Soc. Lond. A., 317, 187 (1970).

3. W. O. Freitag and E. R. Nixon, J. Chem. Phys. 24, 109 (1956).

4. a) M. Allan and J. P. Maier, Chem. Phys. Lett., 41, 231 (1976).

   b) C. Cossart-Magos, D. Cossart, and S. Leach, Mol. Phys., 37, 793 (1979).

5. J. P. Maier, private communication.

6. G. Herzberg, Spectra of Diatomic Molecules, Van Nostrand Reinhold Co., Princeton, NJ (1966), p. 242.

7. R. N. Dixon and D. A. Ramsay, Can. J. Phys., 46, 2619 (1968).

8. R. N. Dixon, Can. J. Phys., 38, 11 (1960).

9. E. Fermi, Z. Physik, 71, 250 (1931).

10. J. W. C. Johns, Can. J. Phys., 39, 1738 (1961).

11. W. J. Balfour, Can. J. Phys., 54, 1969 (1976).

12. V. E. Bondybey, J. H. English, and T. A. Miller, J. Chem. Phys., 70, 1621 (1979).

13. V. E. Bondybey and J. H. English, J. Chem. Phys., 67, 2868 (1977).

14. In some papers, the labeling ν_1 and ν_3 is reversed. We label the vibrations as in Herzberg (Ref. 17) with ν_3 labeling the C-N stretch.

15. Reference 1, p. 319.

16. C. S. Johnson, Jr. and L. G. Pederson, Quantum Chemistry and Physics, Addison-Wesley Co., Reading, MA (1974), p. 334.

17. G. Herzberg, Infrared and Raman Spectra of Polyatomic Molecules, Van Nostrand Reinhold Co., Princeton, NJ (1945), p. 215.

18. J. T. Hougen, J. Chem. Phys., 37, 403 (1962).

19. Reference 17 page 75 and Reference 1 page 24.

20. Reference 1, p. 26.

21. Reference 1, p. 36.

U.S. GPO: 1979-689-169/F-87